The Thesis Committee for Miguel Mejia
Certifies that this is the approved version of the following Thesis

Experimental Investigation of Surfactant Flooding in Fractured Limestones

APPROVED BY
SUPERVISING COMMITTEE:

Matthew T. Balhoff, Supervisor

Gary A. Pope, Co-Supervisor

Experimental Investigation of Surfactant Flooding in Fractured Limestones

by

Miguel Mejia

Thesis

Presented to the Faculty of the Graduate School of

The University of Texas at Austin

in Partial Fulfillment

of the Requirements

for the Degree of

Master of Science in Engineering

The University of Texas at Austin

December 2018

Dedication

To my parents, brother, and sister.

Acknowledgements

I would like to thank my supervisors, Dr. Matthew T. Balhoff and Dr. Gary A. Pope. Their mentorship has allowed me to grow, learn, and complete this work. Dr. Balhoff's guidance has been instrumental in my graduate studies and has always made me improve. Dr. Pope's insight has been invaluable, he has encouraged me to learn and experiment, to be creative and produce quality results.

The laboratory staff has made this work possible. Their expertise and advice always helped when I encountered roadblocks in the lab. Special thanks to Nadeeka Upamali and Pathma Liyange. Jose Parra started the work that this thesis is built upon. Gathering so much data was possible with the input of Nathan Hsu, an excellent lab partner.

My friends at the department have always made work more fun. Jenny Ryu, Pengpeng Qi, Jose Parra and Denning Wang were always great company with good advice. My brother Lucas Mejia was always available for discussion and provided valuable advice.

Thanks to the Chemical EOR project sponsors in the Center for Petroleum and Geosystems Engineering for funding this research.

Abstract

Experimental Investigation of Surfactant Flooding in Fractured Limestones

Miguel Mejia, M.S.E

The University of Texas at Austin, 2018

Supervisor: Matthew T. Balhoff, Gary A. Pope

Carbonates are important candidates for enhanced oil recovery, but recovering oil from oil-wet fractured carbonate reservoirs is challenging. Waterflooding bypasses the rock matrix and recovers little oil. Chemical enhanced oil recovery using surfactants increases oil recovery by lowering the interfacial tension, changing the wettability, and generating viscous microemulsions that improve mobility control.

Seven Texas Cream Limestone cores with a permeability of 15-30 md were fractured and saturated with 100% oil. The cores were aged for one week at 78 C to make them oil-wet. The fracture permeability was adjusted so that it was 10,000 times higher than the rock matrix by changing the confining stress. Waterflooding recovered an average of 6.5% of the original oil in place with an oil cut of less than 2% at the end of the waterfloods. Aqueous surfactant-alkali solution was injected after each waterflood.

All of the surfactant floods produced oil cuts of more than 25% soon after injection started. Surfactant slugs of 3 PV, 1 PV and 0.3 PV followed by brine drives recovered 45, 44, and 30% of the remaining oil after the waterfloods. The 1 PV and 0.3

PV slug sizes were more efficient in terms of oil recovered for a given mass of injected surfactant. In both cases, a high salinity surfactant solution was injected to produce a viscous microemulsion in-situ. The viscous microemulsion increased oil recovery by promoting crossflow and improving mobility control. Low surfactant retention is vital for the economics of surfactant floods. The experiments show that using sodium hydroxide caused surfactant retention to be very low in fractured limestone cores. The average surfactant retention was 0.17 mg/g-rock. Decreasing the flow rate increased the oil recovery at a given injected pore volume. Thus changing practical design variables (salinity, surfactant slug size, flow rate) has a significant effect on oil recovery.

Table of Contents

List of Tables

List of Figures

Chapter 1 Introduction

This chapter describes the objective of this thesis and gives a short description of the content of each chapter.

1.1 Objective

Fossil fuels make a significant contribution to the global energy mix in the present and for the foreseeable future. As new discoveries of oil and gas reservoirs become scarce, novel technologies that increase hydrocarbon production from mature reservoirs become more significant.

Carbonate reservoirs make up a large portion of the world's petroleum production and reserves. Recovering oil with waterflooding in carbonate reservoirs is challenging because they tend to be fractured and oil wet. When a waterflood is carried out in such a reservoir, the water flows through the fractures and leaves the rock matrix unswept. The unfractured rock is left with a high remaining oil saturation. The poor sweep is due to both the fractures and the wettability of the rock. Water injected into the formation flows through the paths of least resistance, the fractures. Since the rock is oil wet, the capillary forces prevent the water from imbibing the rock. Enhanced oil recovery (EOR) technologies address these challenges.

Specifically, chemical EOR is a suitable strategy that addresses several of the difficulties simultaneously. Surfactants used in chemical EOR lower the interfacial tension and change the wettability of the rock, and alkali makes the process more robust and economical. The surfactants, oil, and water form a microemulsion that improves the sweep efficiency. EOR technologies must be designed with specific reservoirs in mind. Giant reservoirs are good targets because small improvements generate large payoffs.

This thesis investigates some design factors in chemical EOR that can be taken into account to improve and maximize oil recovery in fractured oil-wet carbonates. Several large reservoirs in the middle east and Mexico fit this description and are the motivation to carry out this work.

1.2 Description of chapters

There are five chapters in this thesis. Chapter 2 provides background information about the motivation for chemical EOR and gives a literature review on chemical EOR, fractured carbonates, and enhanced imbibition. Chapter 3 details the materials and experimental procedures used in the experiments. Chapter 4 shows the experimental results of seven fractured Texas Cream Limestone corefloods using a new surfactant formulation using NaOH and varying the slug size and injection rate. Chapter 5 describes the conclusions from the experiments and details the future work.

Chapter 2 Background and Literature Review

2.1 Background

The global population of 7.6 billion increased at a rate of 1.1% in 2017 and is projected to continue to increase to 9.8 billion in 2050 (UN World Population Prospects, 2017). A larger global population will require an increase in global energy production. The global energy consumption rate is projected to grow 28% during the same period (through 2050) from the current 372 quads (IEA World Statistics Global Energy Supply, 2017).

Fossil fuels are instrumental in meeting those energy needs. Oil in particular will continue to be fundamental in providing the energy necessary for transportation. Both road vehicles and aircraft dependent on hydrocarbon fuels will be used beyond 2040 (BP Energy Outlook, 2018). Oil currently provides about 36% of the global energy consumed and its use is projected to increase from the current 97 million barrels per day to 109 million barrels per day by 2040 (BP Energy Outlook, 2018).

With the discovery of new oil reservoirs decreasing, novel technical solutions are needed to supply the world with the oil it needs. Enhanced oil recovery (EOR) is part of the answer to such a challenge. EOR consists of injecting substances not originally present in the reservoir to increase oil production (Lake et al., 2014; Green and Willhite, 2018). It is usually performed after waterflooding and is sometimes referred to as tertiary recovery. An advantage of EOR over new discoveries is that the existing oilfield infrastructure can be used. For example, some of the wells used for water injection can be used for chemical or gas injection (Lake et al., 2014). This work will focus on chemical EOR because this technique tackles both mobility control and capillary desaturation simultaneously.

Every petroleum reservoir is unique, and every EOR application must be designed according to the specific characteristics of its target reservoir. Yet, some reservoirs share broad characteristics that can be addressed when developing new engineering solutions. Carbonate reservoirs, which can contain 60% of the world's oil (Roehl and Choquette, 1985)., are such a group. Recovering oil from these reservoirs is challenging because over 80% of them are oil wet or mixed wet, and they are often naturally fractured (Roehl and Choquette, 1985). Waterflooding is inefficient because the water flows through the highly conductive fractures and bypasses the oil in the matrix. Very little oil from the reservoir is displaced by the water as the fracture volume is very small (typically less than 2%) (Nelson, 2001) compared to the rock matrix pore volume. Because the rock is oil wet, the water does not imbibe into the rock matrix and very little oil is recovered by waterflooding.

Using surfactants is a viable solution for EOR in naturally fractured, oil-wet carbonate reservoirs. Surfactants show promise because they alter the wettability of the rock, they decrease the interfacial tension, and they form a viscous microemulsion with the water and oil in the rock that can be used for mobility control (Parra et al., 2016; Parra, 2016). The current study shows that surfactants can be used to recover significant amounts of oil from oil-wet fractured carbonates by decreasing the IFT and creating viscous microemulsions, which results in transverse pressure gradients a net driving force for flow into the matrix. Surfactant retention is extremely important in the economics of an EOR project. Minimizing surfactant retention decreases the amount of surfactant needed to recover the oil (Lake et al., 2014; Green and Willhite, 2018). This work also shows that NaOH alkali can be used to reduce the surfactant retention in fractured limestone cores to very low values.

2.2 Enhanced Oil Recovery Overview

The two EOR mechanisms relevant to this study are increasing the capillary number and/or the Bond number (i.e. the trapping number defined below) and reducing the mobility ratio.

2.2.1 Capillary Number

The capillary number is the ratio of viscous to interfacial forces. (Brownell and Katz, 1947; Stegemeier, 1977; Lake et al., 2014). Equation 2.1 is one common definition of the capillary number (Stegemeier, 1977).

$$N_{cl} = \frac{|\bar{\bar{\mathbf{k}}} \bullet \bar{\nabla}\Phi_{l'}|}{\sigma_{ll'}} \tag{2.1}$$

Where k is the permeability tensor, $\bar{\nabla}\Phi_{l'}$ is the flow potential gradient, $\sigma_{ll'}$ is the interfacial tension between the two fluids, l' is the displacing fluid and l is the displaced fluid.

The trapping number is a generalization of the capillary number. It includes the vector sum of the buoyancy and viscous forces (Jin, 1995; Delshad et al., 1996; Pope et al., 2000).

$$N_{T_l} = \frac{|\bar{\bar{\mathbf{k}}} \bullet (\bar{\nabla}\Phi_{l'} + g(\rho_{l'} - \rho_l)\bar{\nabla}\,D)|}{\sigma_{ll'}} \tag{2.2}$$

where g is the gravitational acceleration, $\rho_{l'}$ is the density of the displacing fluid, ρ_l is the density of the displaced fluids, and $\bar{\nabla}\,D$ is the change in depth.

EOR research often involves discovering new ways to increase the trapping number and, therefore decrease the residual oil saturation. Figure 2.1 is an example of experimental data for the residual oil saturation in Berea sandstone at different capillary

numbers (Chatzis and Morrow, 1984). This type of curve is known as a capillary desaturation curve (CDC). Increasing the capillary number above a critical number reduces the residual oil saturation. Increasing the pressure gradient beyond the formation fracture pressure gradient is not desired. In practice, the capillary number is increased by decreasing the interfacial tension (IFT).

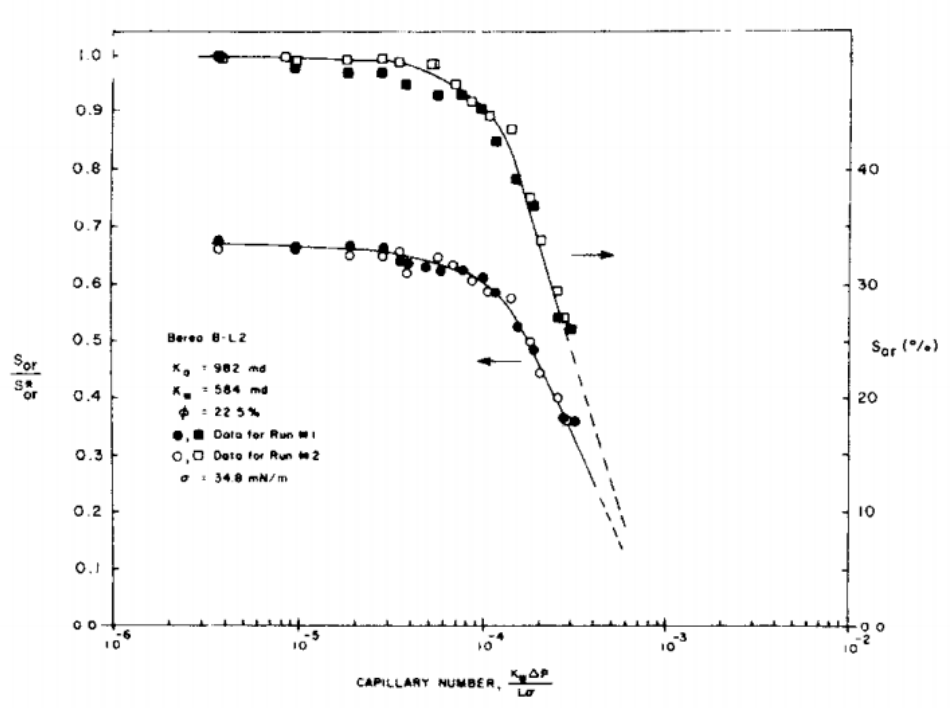

Figure 2.1 Capillary desaturation curve for Berea sandstone. Source: Chatzis and Morrow, 1984

Capillary desaturation curves are not the same in carbonates as in sandstones, as seen in Figure 2.2 (Kamath et al., 2001). Carbonate rocks are usually more heterogeneous and oil wet or mixed wet. There is generally no plateau or critical capillary number after which the residual oil saturation begins to decrease. The decrease is more gradual than for typical sandstones. Nevertheless, general engineering considerations continue to

apply. The pressure gradient applied should not be larger than the fracture pressure gradient, and the capillary number must be increased by reducing the IFT to significantly reduce the residual oil saturation under practical reservoir conditions. Some techniques used to decrease the interfacial tension are miscible flooding and surfactant flooding. This work focuses on surfactant flooding, as it also has the potential to include mechanisms that help with the mobility control, areal sweep, and wettability alteration.

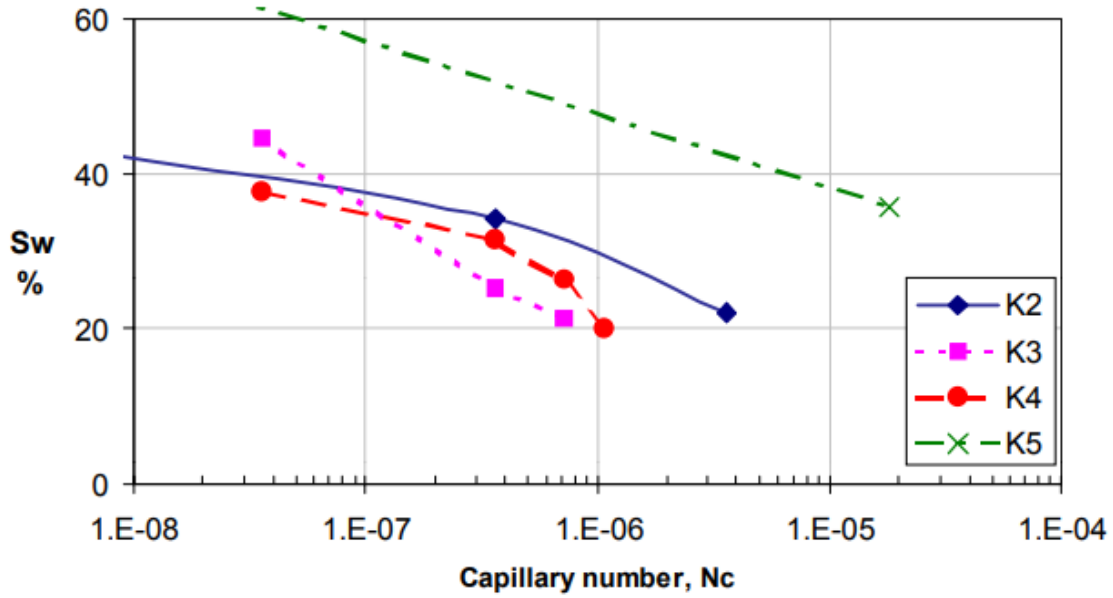

Figure 2.2 Capillary desaturation curve for four carbonate cores. Source: Kamath et al., 2001

2.2.2 Mobility Ratio

The mobility ratio defined by Equation 2.3 is the ratio of the mobility of the displacing phase divided by the displaced phase (Lake et al., 2014, Green and Willhite, 2018).

$$M = \frac{\lambda_{displacing}}{\lambda_{displaced}} = \frac{\left(\frac{k_{r_{displacing}}}{\mu_{displacing}} \right)}{\left(\frac{k_{r_{displaced}}}{\mu_{displaced}} \right)} \tag{2.3}$$

where λ is the fluid mobility, k_r is the relative permeability, and μ is the viscosity. The displacement is stable when M is less than one. The mobility ratio can be decreased by increasing the viscosity of the displacing fluid.

2.3 Chemicals used in EOR

Surfactants are used in EOR to decrease the interfacial tension with the oil. The use of alkali in a chemical solution has several beneficial effects such as soap formation when it reacts with the crude oil, and reduction of surfactant retention. Polymers and co-solvents are also common ingredients of chemical floods. Polymers increase the viscosity of the water to reduce the mobility ratio. Co-solvents can be used to decrease the viscosity of microemulsions or minimize their non-Newtonian behavior, and to increase the solubility of surfactants in aqueous solution (Fortenberry et al., 2015; Tagavifar et al. 2016). However, neither polymers nor co-solvents were used in this study.

2.3.1 Surfactants

Surfactants are surface active agents. They alter the properties of a fluid-fluid interface. Surfactants can lower the interfacial tension between crude oil and water from about 20 dynes/cm to ultra-low values on the order of 0.001 dynes/cm (Bourrel and Schechter, 1988; Lake et al., 2014; Green and Willhite, 2018). The residual oil saturation

can be reduced to nearly zero at the high capillary numbers that are possible at such ultra-low IFT (see Figure 2.1).

Structurally, surfactants typically have polar or charged parts that are attracted to water, i.e. are hydrophilic, and non-polar parts that are attracted to oil, i.e. are hydrophobic. Surfactants are amphiphilic molecules and come in four types. The surfactant can be anionic with a negative charge in the head group; cationic with a positive charge in its head group; nonionic which have polar groups but do not ionize; and zwitterionic which have two groups of opposite charge (Bourrel and Schechter, 1988). One way to characterize these molecules is with the hydrophilic-lipophilic balance (HLB), which indicates the relative tendency of a surfactant to dissolve in oil or water. High HLB surfactants are more soluble in water, with 20 being an extreme on the high end. Surfactants form micelles above a concentration known as the critical micelle concentration (CMC). The surfactant concentration must be significantly higher than the CMC for an ultra-low IFT with the oil to be propagated in the reservoir because of factors such as dilution and adsorption.

Surfactant formulations for chemical EOR are designed for a specific oil and brine and need to be effective over a range of brine compositions at reservoir temperature and for the mineralogy of the reservoir rock. In general, many experiments are needed to optimize a formulation for a specific reservoir. Structure-property models can be used to reduce the number of experiments needed to find the best formulations for a specific oil (Chang, 2018; Chang et al., 2018; Chang et al., 2019).

The surfactants used in this work are Guerbet carboxylate anionic surfactants. They have large, branched hydrophobes synthesized by the Guerbet reaction (Adkins et al., 2012). Branching in the surfactant tails is beneficial. Branching works against the formation of orderly structures that might organize to form gels or liquid crystals

(Bourrel and Schechter, 1988). Disorderly arrangements between long molecules promotes fluidity of the phase. Carboxylate surfactants have been shown to have high performance under harsh reservoir conditions (high temperature, hardness, and salinity) (Adkins et al., 2012; Lu et al., 2012; Jang et al., 2016; Upamali et al., 2018). The number of propylene oxide (PO) and ethylene oxide (EO) groups included in the surfactant tail may be tailored for best performance. Increasing the number of EOs increases hydrophilicity and calcium tolerance whereas increasing the number of POs slightly increases the hydrophobicity and can be optimized to lower IFT.

Internal olefin sulfonate (IOS) surfactants are also used in this study. IOS surfactants are synthesized from olefins with a wide range of carbon numbers and have a twin tailed structure due to roughly midpoint sulfonation, which causes branching and is beneficial in promoting disorder and adverse to the formation of gels and liquid crystals. A mixture of dissimilar surfactants is more effective in achieving ideal microemulsion phase behavior for oil recovery applications (Levitt et al., 2009). Jackson (2006), Levitt et al., (2009), Flaaten et al., (2009), Barnes (2010) and others have demonstrated the effective use of IOS surfactants for this purpose.

2.3.2 Alkali and Surfactant Retention

Alkalis are common ingredients in chemical EOR formulations (Nelson et al., 1984). Introducing alkali in the chemical formulation increases the pH. A potential benefit of high pH is the formation of in-situ soaps (Jenning, 1975; Nelson et al., 1984). If the crude oil is active, naphthenic acids present in the crude oil react with the alkali through the saponification reaction to generate soap. The soaps generated by the alkali and crude oil are generally anionic and will contribute to a further reduction in the IFT.

The presence of the in-situ generated surfactants increases the variety of surfactant molecules and structures. An increase in the variety of surfactants further promotes disorder and works against the formation of orderly structures like gels and liquid crystals. Some soaps may have a negative impact in the IFT of the formulation. Phase behavior tests must be done with the crude oil, alkali, and surfactant to investigate such a possibility.

Increasing the pH of the chemical formulation with alkali is also beneficial because it decreases surfactant retention (Nelson et al., 1984). The higher pH increases the negative surface charge on the rock, resulting in lower adsorption of anionic surfactants on the rock surface. Additionally, the alkali decreases phase equilibration time.

Adsorption of anionic surfactants can be decreased by increasing the pH of the injected solution. The electric charge on the rock surface is determined by the number of sites with a positive or a negative charge. If the number of negatively charged sites is equal to the number of positively charged sites, the net charge on the surface is zero (Sondi et al., 2009). The point of zero charge is also known as the isoelectric point.

The zeta potential is the electric potential between the rock surface and the aqueous phase. A negative zeta potential indicates a negative surface charge on the rock surface. The zeta potential is zero and the pH is fixed (pHiep) at the isoelectric point. Increasing the pH decreases the zeta potential (Tagavifar et al., 2018). A lower zeta potential means the number of negative surface charges on the rock is greater, and anionic surfactant adsorption will be lower. This is one of the reasons why increasing the pH of the injected fluids decreases surfactant retention.

Sodium carbonate is a commonly used alkali in chemical flooding. It is widely used in chemical EOR in sandstones because it has a very low reactivity with silica at a

pH of about 10.5 (Krumrine et al. 1985). However, sodium carbonate may not be appropriate for use in carbonate reservoirs because such reservoirs typically contain gypsum or anhydrite, which reacts with sodium carbonate to precipitate calcium carbonate. Ammonia can be used for the alkali in carbonates with anhydrite and has other advantages as well (Sharma et al., 2014; Wang, 2018; Abalkhail 2018). Sodium hydroxide is not viable in sandstones as it reacts with silica to produce sodium silicate in water. This problem is avoided in limestone where the rock is composed of calcium carbonate.

Sodium hydroxide is another option for alkali in carbonate reservoirs. Recent studies (Maubert et al., 2018; Wang et al., 2018; Abalkhail, 2018) have shown that using sodium hydroxide as an alkali for chemical flooding in Indiana limestone cores resulted in very low values of surfactant retention. The work in this thesis shows sodium hydroxide is also an effective alkali in fractured Texas Cream limestone coreflood experiments.

Sodium hydroxide is a viable alkali for chemical flooding in limestones because it has a low reactivity with calcite (Ehrlich and Wygal, 1977) and in solution has a higher pH than sodium carbonate. The high pH changes the surface charges on the rock surface from positive to negative (Alroudhan et al. 2016), which reduces the adsorption of anionic surfactants. Bunn et al. (2002) showed that the pH of the aqueous phase must be increased by two units above the pHiep for minimum interactions with negatively charged surfactants. Carbonate formations have positive surface charges at neutral pH and sometimes contain minerals such as ankerite and geothite with pHiep of up to 9.7 (Kasha et al. 2015; Alshakhs and Kovscek 2016; Zeltner and Anderson, 1988).

A dilute solution of only 0.2 wt% NaOH increases the pH to about 12.6 (measured at 25 C). Furthermore, the lower molecular weight of sodium hydroxide

compared to sodium carbonate means less is needed to increase the pH. A possible issue with the use of sodium hydroxide is precipitation of calcium hydroxide. Sanaei et al. (2018) used a chemical flooding simulator to show this problem can be mitigated with a soft brine preflood. Karazincir et al. (2011) showed metal complexing agents and scale inhibitors can be added to the chemical flood to prevent scaling in hard brine. However, all pertinent geochemical reactions must be taken into account before selecting the appropriate alkali for a specific reservoir.

2.4 Surfactant Retention

Surfactant retention is caused by both adsorption of surfactants on the rock surface and phase trapping of microemulsions or macroemulsions in the porous medium (Zhang and Somasundaran, 2006; Nelson and Pope, 1978; Walker et al., 2012; Jang et al., 2016). Retention is the difference between the surfactant injected and surfactant produced during the chemical flood. Surfactant retention is the main economic consideration in the application of commercial surfactant flooding applications (Lake et al., 2014). A low surfactant retention requires less mass of surfactant to be injected and therefore reduces the cost of the chemical flood.

Phase trapping of viscous phases such as microemulsions and macroemulsions can be reduced by the use of co-solvents and the implementation of a salinity gradient, which will be discussed in more detail further in this chapter (Pope et al., 1979; Hirasaki et al., 1983; Upamali et al., 2016; Jang et al., 2016).

Coreflood experiments have been successful in reducing surfactant retention to very low levels. Jang et al. (2016) carried out alkaline-surfactant-polymer corefloods in sandstones that had average retention values of 0.061 mg/g-rock, and went as low as

0.007 mg/g-rock for cores with up to 12 wt% clay content. Surfactant retention in carbonate cores reported in the literature have been typically higher than for sandstones. Solairaj et al. (2012) reported a retention value of 0.34 mg/g-rock in Estillades Limestone. Levitt and Bourrel (2016) reported an average retention value of 0.58 mg/g-rock in 40 corefloods in Estillades Limestone. Chevallier et al. (2013) reported surfactant retention values ranging from 0.38 to 1.9 mg/g-rock. Recent advances have significantly lowered the surfactant retention values in carbonates; Maubert et al. (2018) showed an average retention value of 0.15 mg/g-rock in three coreflood experiments and 0.25 mg/g-rock with very hard brine. Wang et al. (2018) and Abalkhail (2018) also used sodium hydroxide as well as ammonia as an alkali in carbonate cores and obtained retention values of 0.14 and 0.02 mg/g-rock, respectively. Such low values of surfactant retention make sodium hydroxide an attractive option to use in the current experimental study of surfactant floods in fractured limestone cores.

2.5 Salinity Gradient

Imposing a salinity gradient is an extremely important practice in chemical flooding. It increases the robustness of the process by including the uncertainty of several key reservoir variables such as variable oil composition in the chemical flood design (Pope et al., 1979; Hirasaki et al., 1983; Lake et al., 2014; Green and Willhite, 2018).

A surfactant slug is typically injected at or near optimum salinity since this is required to yield the lowest IFT possible. However, the surfactant retention will be relatively high unless the slug is followed by a polymer or brine drive with a lower salinity (Type I phase behavior). The lower critical salinity (LCS) where the transition occurs between type III and type I phase behavior is always uncertain in a reservoir

because of variations in oil composition, temperature, pressure, etc. that are unknown and difficult to quantify. In addition, mixing higher salinity or hardness brines in front of the slug or due to crossflow with adjacent layers must be taken into account in some cases. Thus for a robust flood the drive salinity should be lower than the LCS. If the initial salinity/hardness is lower than the slug salinity, then that causes a reverse salinity gradient and must be addressed using a different strategy, e.g. by injecting the surfactant slug above optimum salinity, or by conducting a preflood.

2.6 Microemulsion Phase Behavior

Microemulsions are thermodynamically stable liquids made up of surfactants, oil, and brine (Bourrel and Schechter, 1988). Windsor (1954) classified microemulsions as Type I, Type II, or Type III. A Type I microemulsion consists of a microemulsion phase of oil in water and an excess oil phase. A Type II microemulsion consists of a microemulsion phase of water in oil and an excess aqueous phase. A Type III microemulsion consists of a three-phase system of excess oil phase, excess aqueous phase, and microemulsion phase. The Type III microemulsion phase is a bicontinuous phase of brine and oil and has ultra-low interfacial tension between the excess aqueous and oil phases.

In the laboratory, the phase behavior samples are made by combining the brine, surfactants, and oil in a pipette or test tube. The samples are mixed and allowed to equilibrate. Traditionally, a fast-forming microemulsion with low viscosity at Type III is the objective. The surfactant formulation is optimized by trial and error. The number of propylene oxide (PO) groups, ethylene oxide (EO) groups, surfactant ratios, and cosolvent combinations are varied methodically to achieve the best possible formulation.

Such a formulation will produce a microemulsion-brine-oil system with ultra-low IFT and low, Newtonian viscosity under a wide range of conditions (Levitt et al., 2009; Pinnawala et al., 2018; Flaaten et al., 2009).

A surfactant formulation is tested by performing a salinity scan. The phase behavior should transition from Type I to Type III to Type II with increasing salinity. An oil concentration scan should also be performed to ensure that the formulation produces ultra-low IFT and favorable rheology at low and high oil concentrations.

An aqueous stability test must also be done to ensure the surfactant solution is a clear, stable aqueous phase (no phase separation or precipitation) under reservoir conditions. The aqueous salinity test is of critical importance. The chemicals must be in an aqueous form with no precipitates or multiple phases in order for the formulation to transport properly through the porous medium without chromatographic separation, high retention, loss of mobility control, and other adverse effects.

Once the phase behavior samples are prepared, they are mixed frequently to promote faster equilibration. A qualitative assessment of the IFT and rheology (the emulsion test) can be completed before the samples fully equilibrate. In the emulsion test, the pipette is shaken and the color, droplet size, and fluidity are visually examined. The desired characteristics indicating low IFT and low viscosity are a creamy color with no visible drops and a high fluidity when shaken. Fast separation of the phases indicating a fast approach to equilibrium phase behavior after the shaking stops is also desirable.

A quantitative measure of the IFT of the samples is recorded with the solubilization ratios. The amounts of brine solubilized, σ_w, and oil solubilized, $\sigma_{o,}$ are recorded until the samples reach equilibrium. The IFT is then determined from the Huh (1979) equation which gives the interfacial tension as a function of the solubilization ratios.

$$\gamma = \frac{C}{\sigma^2} \tag{2.4}$$

Where σ is in dimensionless units and γ is in dynes/cm when C is 0.3. The constant C is typically assumed to be 0.3. A good formulation has a solubilization ratio of 10 or higher, leading to an IFT of 0.003 dynes/cm or less. This is a significant reduction from the IFT between oil and water without surfactant, normally 20-30 dynes/cm. The optimal salinity is defined as that when the oil and water solubilization ratios are equal. The optimum salinity obtained with the solubilization ratios is usually close to the optimal salinity determined by the emulsion test.

2.6.1 Microemulsion Viscosity

Type III microemulsions often have a viscosity 3 to 10 times higher than the oil and are sometimes shear thinning as well. For most applications, a low Newtonian microemulsion viscosity is desired for better mobility control and lower surfactant retention (Walker et al., 2012). However, Lu et al. (2017) showed that the density and viscosity of the microemulsion can be taken into account in chemical flooding design to perform gravity stable surfactant floods in sandstones. In those corefloods, there was no need for polymer to have favorable mobility control. The viscosity of the microemulsion and the flooding velocity were adjusted to ensure the displacement front was stable. More recently, Parra et al., (2016) showed that higher microemulsion viscosities led to higher oil recoveries in fractured carbonate cores with high permeability ratios between the fracture and the rock matrix. This contradicts the common assumption (Lu et al. 2012) that a high microemulsion viscosity is always detrimental to the prospects of the chemical flood.

The high Type III microemulsion viscosity (compared to oil) is used in this study to improve the areal sweep efficiency of a chemical flood without polymer. The microemulsion viscosity is a function of multiple variables. Once the oil and surfactant formulation have been selected, the microemulsion viscosity will vary depending on the brine salinity as well as the fraction of oil in the microemulsion can be seen in Figure 2.3 (Tagavifar et al., 2016).

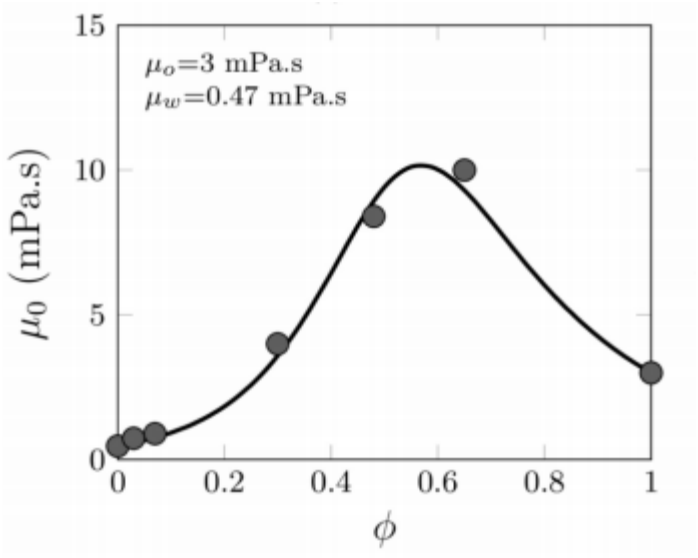

Figure 2.3 Microemulsion viscosity as a function of the fraction of oil in the microemulsion. Source: Tagavifar et al., 2016

2.7 Naturally Fractured Carbonates

Carbonate rocks are formed either through a chemical precipitation process, or by the biologic precipitation and accumulation of organic material (Peters, 2012). Carbonate reservoirs are important sources of global oil production. They hold 50-60% of the world's oil reserves (Van Golf-Racht, 1982; Roehl and Choquette, 1985; Nelson, 2001). Well known examples include the Yates field in West Texas, the Cantarell in offshore

Mexico, and Ghawar in Saudi Arabia. Most carbonate oil reservoirs are naturally fractured and are oil wet or intermediate wet (Chilingar and Yen, 1983). Oil and gas operators involved in primary recovery caused by oil and rock expansion (Lake and Walsh, 2008) often ignore the heterogeneities inherent in these types of reservoirs. However, these conditions make secondary recovery challenging. Brine injected during waterflooding flows through the highly permeable fractures, leaving the rock matrix unswept.

The fractures can be several orders of magnitude more permeable than the rock matrix, while holding less than 2% of the reservoir pore volume. Barrenblat (1960) described reservoirs with high fracture connectivity and high permeability contrasts between the fracture and the matrix as double porosity systems as seen in Figure 2.4. Nelson (2001) described them as Type II reservoirs where most of the reservoir permeability is in the fractures and the total porosity in the rock matrix as seen in Figure 2.5.

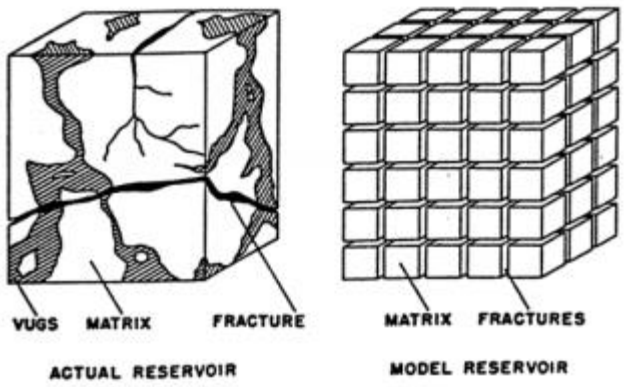

Figure 2.4 Double porosity system where fractures have most permeability but least porosity. Source: Barenblatt (1960)

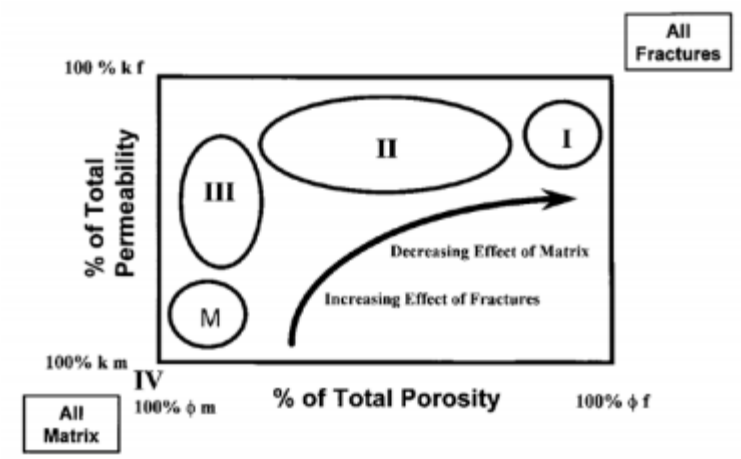

Figure 2.5 Type II fractured reservoir system described by Nelson. Source: Nelson (2001)

2.7.1 Flow in Fractures

Most of the fluid flow in naturally fractured carbonate reservoir occurs in the fractures. Flow in fractures is approximated here starting with the fluid equation of motion derived by Cauchy (1827).

$$\frac{\partial}{\partial t}\rho\mathbf{u} = -[\nabla\bullet\rho\mathbf{uu}] - \nabla p - \nabla\bullet\boldsymbol{\tau} + \rho\mathbf{g} \tag{2.5}$$

Where ρ is the fluid density, $\boldsymbol{u}$ is the fluid velocity, p is the pressure, $\boldsymbol{\tau}$ is the stress tensor, and $\boldsymbol{g}$ is the gravitational acceleration. In this equation, the right hand side is the rate of increase of momentum. The first term on the right hand side is the rate of momentum addition by convection. The second term on the right hand side is the rate of momentum addition by molecular transport. The third term on the right hand side is the external force on the fluid. All the terms are per unit volume.

For very slow flow of an incompressible, Newtonian fluid at steady state, the equation simplifies as follows.

$$\nabla p + \nabla \bullet \boldsymbol{\tau} - \rho \mathbf{g} = 0 \tag{2.6}$$

The analytical solution for Newtonian fluid velocity in equation 2.6 for a slit is:

$$u(z) = \frac{1}{2\mu}\left(\frac{P_i - P_o}{L}\right) z(b - z) \tag{2.7}$$

Where P_i is the pressure at the inlet, P_o is the pressure at the outlet, μ is the viscosity of the fluid, L is the length of the core, and z is the distance from one wall of the fracture to the other wall. Integrating the velocity across the fracture from $z = 0$ to $z = b$ and multiplying by the diameter of the core, D, gives the flow rate inside the fracture.

$$q = -\frac{Db^3}{12\mu}\left(\frac{P_i - P_o}{L}\right) \tag{2.8}$$

Darcy's Law is:

$$q = -\frac{kA}{\mu}\left(\frac{P_i - P_o}{L}\right) \tag{2.9}$$

The fracture aperture (b) can be estimated using the slit analog of the Hagen-Poiseuille equation and Darcy's law. Setting both equations equal, one obtains the following where b is the fracture aperture, D is the diameter of the core, k is the effective permeability, and A is the cross-sectional area of the core.

$$k = \frac{b^3 D}{12A} \tag{2.10}$$

Solving for b, and considering only the fracture area and permeability, we get the following equation.

$$k = \frac{b^2}{12} \tag{2.11}$$

If one considers the effective permeability of the entire core for this fracture aperture, the following result can be obtained:

$$k_{eff} = \frac{b^3}{3D\pi} \tag{2.12}$$

2.7.2 Flow in Rock Matrix

When fluid flow in porous media is slow, it can be described by Darcy's law. For multiphase flow, each phase is assumed to have its own pressure gradient. The total flow is the sum of the oil and water flowing if the phases are incompressible, as shown next:

$$q_w = \frac{kk_{rw}A}{\mu_w}\frac{\Delta p}{\Delta l} \tag{2.13}$$

$$q_o = \frac{kk_{ro}A}{\mu_o}\frac{\Delta p}{\Delta l} \tag{2.14}$$

$$q_o + q_w = q_{total} \tag{2.15}$$

The subscripts '*o*' and '*w*' correspond to oil and water. The relative permeability is k_r, and is a function of the saturations in the rock. The relative permeability functions are themselves dependent on many factors including the geochemistry, type of fluid, electrolyte and chemical composition, wettability and IFT, among others.

2.8 Imbibition of Naturally Fractured Carbonates

Imbibition in carbonate rocks has been widely studied, especially under static conditions (Austad et al., 1998; Standnes and Austad, 2000; Xie et al., 2005; Seethepalli et al., 2004; Sagi et al., 2013; Li et al., 2016). Some of the factors affecting such experiments are the wettability of the rock and the capillary pressure. Using surfactants in oil-wet carbonate rocks is promising because they reduce the capillary pressure to negligible values, increase the oil relative permeability by reducing the IFT, and change the wettability of the rock to more water-wet. These effects result in substantially higher oil recovery than with water alone. Buoyancy forces and small viscous forces become important at low IFT.

2.8.1 Capillary Pressure

Capillary pressure is the pressure difference between two immiscible fluids. The capillary pressure depends on the curvature of the interface separating the fluids (Peters, 2012). A simplified case for the Young-Laplace equation for capillary pressure in a tube is:

$$P_c = \frac{2\sigma\cos(\theta)}{r} \tag{1.16}$$

Where P_c is the capillary pressure, σ is the interfacial tension, θ the contact angle, and r is the radius of the tube. In an oil-wet rock, the contact angle will be greater than 90 degrees. Under this condition, the capillary pressure is negative. For water to displace the oil in the rock, it must overcome this capillary pressure.

Surfactants are a solution to this challenge. As explained previously, surfactants reduce the interfacial tension to negligible values. The capillary pressure in turn becomes

negligible as well. Surfactants also change the wettability of the rock, as explained in the next section.

2.8.2 Wettability

Wettability is the tendency of a fluid to adhere and spread on a solid surface in the presence of another immiscible fluid (Peters, 2012). Most carbonate reservoir rocks are oil-wet or intermediate wet. Chilingar and Yen (1983) looked at 161 carbonate core samples from around the world and examined their wettability. They determined that 8 percent were water-wet, 12 percent were intermediate-wet, 65 percent were oil-wet, and 15 percent were strongly oil-wet. Imbibition of water into the rock matrix is severely limited when the rock matrix is oil-wet.

Surfactants can change the wettability of rocks from oil-wet to water-wet. Once surfactant molecules come in contact with the solid rock surface, they might adsorb and change the surface properties. All surfactants alter the wettability of the rock but to widely different degrees. Standnes et al. (2002) used dilute cationic surfactant solutions to change the wettability of oil-wet rocks. Seethpalli et al. (2004) also changed the wettability of oil-wet rocks using dilute solutions of anionic surfactants. Zhang et al. (2006) showed that alkali-surfactant mixtures modified the wettability of a marble plate. Gupta and Mohanty (2008) showed that surfactants change the wettability of carbonates at high temperatures.

2.8.3 Enhanced Imbibition Studies at ultra-low IFT

Reducing the IFT to ultra-low values allows the buoyancy forces to overcome the capillary forces and produce the oil in the rock matrix. The oil relative permeability increases significantly when the IFT is reduced to ultra-low values. Li et al. (2016) derived an analytical model that describes this process and how it scales with the reservoir dimensions. In the model, oil is produced almost linearly when plotted against the square root of non-dimensional time. The model compares favorably to experimental data using cores of different dimensions as well as synthetic porous micromodels (Mejia, 2018). Li et al. (2016) concluded that low IFT is more beneficial than wettability alteration because it has a greater impact on the oil relative permeability and also at sufficiently low IFT (high Bond numbers) the residual oil saturation is reduced.

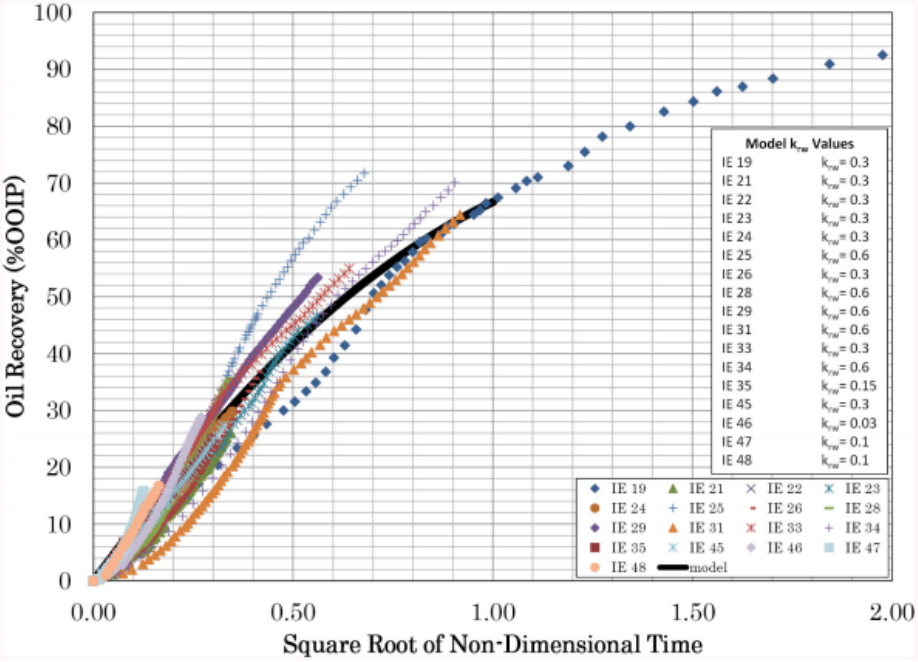

Figure 2.6 Oil recovery in static imbibition experiments of different dimensions. Source: Li et al., 2016

During surfactant imbibition into the matrix, viscous and buoyancy forces are both present. Abbasi et al. (2009) carried out simulations using the UTCHEM simulator suggesting that small transverse viscous pressure gradients between the fractures and the rock matrix contribute to a higher oil recovery. Because there is pressure connectivity between the fractures and the matrix, there must be net flow from the fractures to the rock matrix. That is the only way to equalize the pressures and preserve mass balance. Zapata and Lake (1981) explain this process as vertical equilibrium. Applying a pressure drop across the fracture promotes crossflow, and increases the speed of replacement of the oil in the rock matrix by the aqueous solution flowing through the fractures.

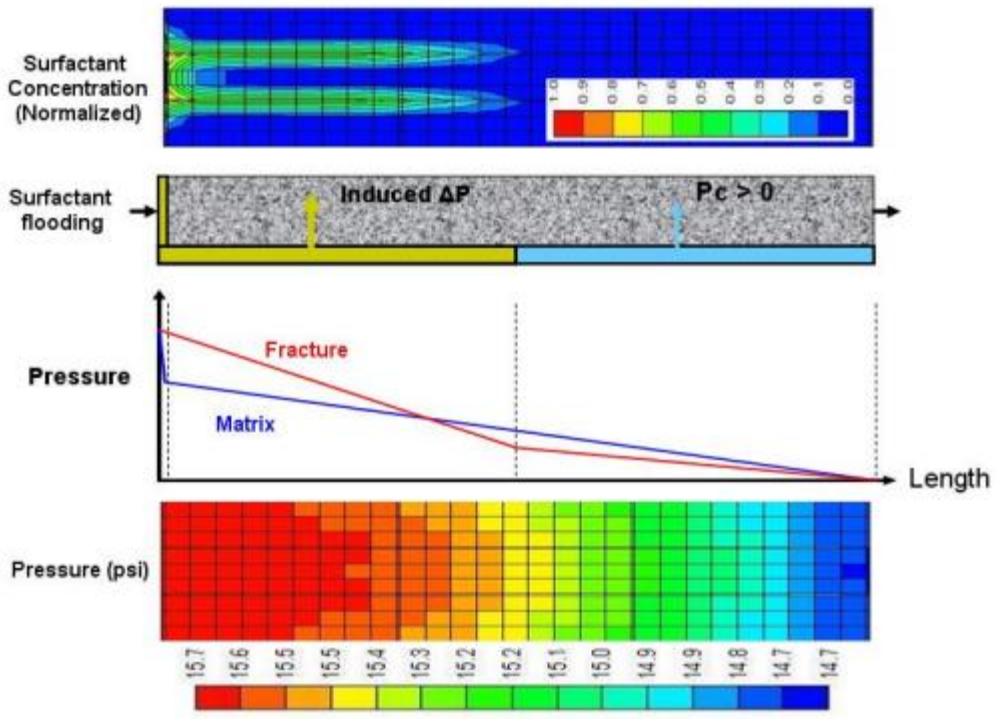

Figure 2.7 Simulation of chemical flood with crossflow between fractures and matrix. Source: Abbasi et al. (2009)

Building on the concept of viscous crossflow, Parra (2016) performed alkali-surfactant corefloods where he varied the salinity of the injected surfactant solution. Parra (2016) obtained higher oil recoveries for experiments where the salinities were higher as shown in Figure 2.7. The higher viscosities labeled on the legend correspond to higher injection salinities. The results can be explained by the in-situ formation of viscous microemulsions when the oil, surfactant and brine mix.

The viscosity of the microemulsion is a complex function of many variables. One of those variables is the salinity of the brine. As presented in Tagavifar et al. (2016), the microemulsion viscosity reaches a maximum at some point in the salinity phase behavior scan. The viscous microemulsion increases the viscous crossflow as and improves the mobility control, thus increasing the oil recovery. Parra (2016) designed the chemical floods to show that the viscosity of the microemulsion formed in-situ can be taken into account to obtain the best results in the chemical flood.

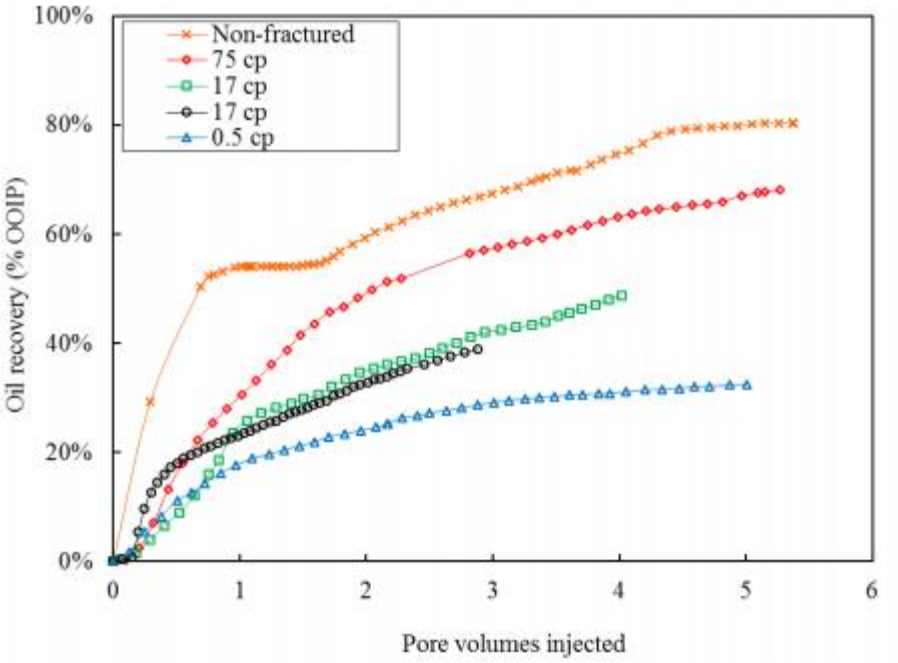

Figure 2.8 Oil recovery comparisons for chemical floods with different salinities. The higher viscosities in the legend correspond to higher salinities. Source: Parra (2016)

Parra (2016) did eight corefloods in both fractured and non fractured cores showing the effects of transverse viscous pressure gradients caused by viscous microeumulsions formed in-situ. The results of Parra (2016) are shown in Table 2.1.

Table 2.1 Summary of results of Parra (2016). Source: Parra (2016)

Table 4.3 Performance data for the Silurian Dolomite coreflood experiments

Coreflood number	non-FRAC 1	FRAC 1	FRAC 2
Initial			
S_{oi}	0.62	1	1
Waterflood (100,000 ppm TDS)			
Trapping/bond number*	$5x10^{-6}$	$5x10^{-9}$	$9x10^{-9}$
S_{orw}	0.37	0.57	0.43
Surfactant flood (80,000 ppm TDS)			
Viscosity, cp		0.5	0.5
Bond number		$6x10^{-5}$	$1x10^{-4}$
S_{orc}		0.29	0.21
Surfactant-polymer flood (80,000 ppm TDS)			
Viscosity, cp	23	30	30
Trapping/bond number*	$3x10^{-3}$	$6x10^{-5}$	$1x10^{-4}$
S_{orc}	0.07	0.24	0.17

Table 4.4 Performance data for the Texas Cream Limestone coreflood experiments

Coreflood number	non-FRAC 2	FRAC 3	FRAC 4	FRAC 5	FRAC 6
Waterflood					
Salinity, ppm TDS	80,000	100,000	80,000	95,000	65,000
Trapping/Bond number	$3x10^{-7}$		$4x10^{-10}$		
S_{orw}	0.47	0.97	0.96	0.97	0.98
Surfactant flood					
Salinity, ppm TDS	80,000	80,000	80,000	95,000	65,000
IFT, mN/m	0.002	0.002	0.002	0.0006	0.006
Microemulsion viscosity, cp	17	17	17	75	0.5
Pressure drop, psi/ft	8.0	0.8	0.9	1.1	0.4
Trapping/Bond number*	$1x10^{-7}$		$5x10^{-6}$		
S_{orc}	0.20	0.61^{+}	0.47	0.30	0.66

Previous coreflood experiments by Jose Parra showed the oil recovery from fractured TCL cores increased when the microemulsion viscosity increased. Several pore volumes of a 1% surfactant solution were injected in each of his corefloods. Such large amounts of surfactant are unlikely to be used in the field. The fracture setup in Parra (2016) was challenging to control because it was done by manually roughing the fracture.

The formulation used by Parra contained EDTA. The EDTA dissolves limestone and therefore has a high consumption, so it may not be practical to use it in the field.

This work is the next step in the study of enhanced imbibition and transverse viscous pressure gradients in fractured Texas Cream Limestone Cores. A new fracture set-up where Teflon strips are used as spacers is presented. A new formulation with no EDTA was developed and is shown. Sodium hydroxide is used as an alkali in the chemical flood to minimize surfactant retention in fractured Texas Cream Limestone cores, and the effects of slug size and flow rate on oil recovery are investigated.

Chapter 3 Materials and Procedures

3.1 Materials

3.1.1 Crude oil

The crude oil used in this research is a light crude oil with an API gravity of 29 produced from a carbonate reservoir with a temperature of 78 Celsius. The oil was filtered with a 0.45 micron cellulose filter at 80 degrees Celsius before being used in all experiments. The oil used in all experiments was undiluted dead oil with a viscosity of about 11cp at 78 degrees Celsius.

3.1.2 Surfactants

The chemical formulation for all the experiments is a 1% solution by weight made up of 0.5% C28-25PO-45EO-carboxylate, 0.2% C15-18 IOS and 0.3% C19-28 IOS. The main surfactant was synthesized by adding EO and PO to a C28 Guerbet alcohol then carboxylated at The University of Texas at Austin. The Internal olefin suflonates (IOS) with a range of carbon numbers were provided by Shell Chemical Company.

3.1.3 Alkali and brines

All the brines were prepared with laboratory grade salts. Sodium chloride, sodium bicarbonate, sodium sulfate, and sodium hydroxide all had a purity of at least 99.5% and were purchased from Fisher Scientific. The brines prepared were all filtered with 0.45 micron cellulose filters before being injected in the cores.

3.1.4 Cores

Texas Cream Limestone cores were used in all experiments. Porosity ranged from 27 to 30% and permeability ranged from 15 to 33 md. The cores are cylindrical with a

diameter of 1.5 inches and a length of about 12 inches. The cores all looked uniform and homogeneous. No macroscopic impurities could be observed by visual inspection. Figure 3.1 shows the block from where the cores were cut. Fine laminae can be seen horizontally in the block. The cores were cut so that the layers would align along the length of the core. Table 3.1 shows the powder X-ray diffraction (XRD) on Texas Cream Limestone. The rock mineralogy is almost pure limestone and virtually no clays are present.

Figure 3.1 Texas Cream Limestone block from which cores were extracted

Table 3.1 Mineralogy of Texas Cream Limestone

Mineral	(Weight Percent)	Density (g/cm3)
Quartz	0.7	2.65
K-Feldspar	0	
Plagioclase	0	
Calcite	98.8	2.72
Dolomite	0	
Siderite	0	
Pyrite	0	
Hematite	0	
Phyllosilicates	0.5	2.64
Total	100	2.71

3.2 Procedures

3.2.1 Brines and surfactant solutions

Brines were prepared with deionized (DI) water with a resistivity of 18 ohm-m. The salts were dissolved in the DI and the solutions were mixed with a magnetic stir bar. Before injecting the brines in any core, they were filtered with a 0.45 micron cellulose filter.

The surfactants were diluted in brine from concentrated solutions already prepared. The surfactant solutions injected into the cores were mixed at 78 Celsius because of their cloudiness at room temperature. After mixing, they were filtered with the same filter pore size as the brines before being loaded into a column and injected. The solutions were degassed with argon before being loaded in the columns as well as vacuumed while inside the columns to minimize oxygen exposure.

3.2.2 Phase behavior and aqueous stability samples

Phase behavior samples were prepared in 4 ml pipettes. The aqueous volumes were added first with varying salt concentrations. Aqueous volumes were recorded to

measure solubilization ratios later. Oil was added last. The pipettes were then argon blanketed and sealed with a flame torch. Immediately after sealing, the pipettes were shaken every couple of hours to promote equilibration. For the formulation used in this thesis, the phase behavior samples equilibrated after 5 weeks.

Aqueous stability samples were prepared in 15 ml glass vials. Only the aqueous components in the phase behavior samples at volumes of 10 ml were included. The samples were shaken after preparation and placed in an oven at 78 Celsius. The objective was to create a clear solution with no precipitates or phase separation at the salinity of the injected surfactant solution.

3.2.3 Experimental Procedure

The following procedure is a template for what was done in all the experiments presented in this thesis:

1) The core mass and dimensions are measured.
2) The core is shrink wrapped and put into a core holder.
3) Matrix permeability is measured using a gas permeameter.
4) The core is then removed from the core holder and sawed into two halves.
5) The fractured core is placed in a 100 Celsius oven for 24 hours to dry after it is sawed. The dimensions and mass are measured again once the core is dry.
6) The core is arranged with spacers to support the fracture and placed back into the core holder.
7) The core is vacuumed for six hours.
8) The core is 100% oil saturated. The pore volume is measured from the volume of oil imbibed taking into account the dead volume of 4 mL. The dead volume consists of 4 three-way valves in the core holder and nylon tubing from the oil

bomb to the core holder. The porosity is calculated from the pore volume divided by the bulk volume.

9) The core is aged for one week at 78 Celsius.
10) The fractured core is oil flooded to measure the single-phase oil permeability. The confining stress is adjusted to achieve the desired permeability.
11) The core is water flooded with 85,000 ppm NaCl solution at a specified flow rate until the oil cut is consistently less than 3%.
12) The core is flooded with a specified amount of surfactant solution at a specified flow rate.
13) The core is flooded with 1 PV of 60,000 ppm NaCl brine, or until the oil cut is consistently less than 3%.
14) The surfactant concentration in the effluent samples is measured with the hyamine titration method. The pH of each sample is also measured.

3.2.4 Fracture preparation

The fractured core was prepared in the following way:

1. The whole core was measured and weighed. The length was measured with a ruler along the core's length three times, and the average was reported. The diameter was measured with a caliper three times, and the average was reported. The mass was measured with a Sartorius electronic scale.
2. The core was cut along its length into two halves with an electric saw.
3. The two halves were dried at 90 degrees Celsius for 24 hours to dry the water used by the saw to cut the core.
4. The core was measured and weighed again after being cut following the same procedure as in step 1.

5. Two strips of Teflon with a width of 1 mm and a length of 1 foot were cut to be used as spacers to maintain the fracture open. The Teflon used is the same one used to shrink wrap the cores. Teflon was used because it was easy to cut with precision and it is very unreactive. Another option, steel, was not used because it is prone to rusting, and damaging the surfactant. The Teflon was first heated in an oven to allow it to shrink, and then cut with a box cutter blade using a straight edge on top of a table to maintain the 1 mm wide dimension constant. The spacers' width was measured with a caliper after they were cut.
6. The two 1 mm wide Teflon spacers were put on the edges of the core to keep the fracture open.
7. The two halves were carefully put together to keep the Teflon spacers in place.
8. The two halves were shrink wrapped and put in the core holder.

		 	
3.2a) Core's dimensions and mass are measured.	3.2b) Core is sawed in half with an electric saw.	3.2c) Teflon spacers 1 mm wide are cut and placed at the edges of the fracture.	3.2d) Top and bottom halves are assembled together and fractured core is shrink wrapped

Figure 3.2 Steps of core and fracture preparation

3.2.5 Coreflood setup

The heat-shrunk cores were placed inside a Viton rubber sleeve of the stainless steel core holder to carry out the experiments. Confining pressure was applied to the core by pumping mineral oil into the annulus of the core. The core holder has a working pressure and temperature of 2,000 psi and 300 F respectively. Confining pressure was applied to the core by pumping mineral oil into the annulus of the core holder. The Viton

sleeve is a barrier between the core and mineral oil in the annulus. O-rings ensure that the core is sealed from the annulus where mineral oil lies as well as the outside of the core holder. The heat shrink wrap also acts as a final protection in case of a mineral oil leak. The core-holder has three pressure taps along its length that allow for sectional pressure measurements. It has valves attached to these as well as inlet and outlet valves. Figure 3.2 shows a schematic of a coreflood set-up. In all the experiments, the core-holder was set up vertically and the flow direction was from the bottom of the core to the top of the core. The experiments were carried out at constant flow rates. Chemicals were injected from glass or polycarbonate columns. The injected fluids were displaced in the columns by mineral oil using Teledyne ISCO pumps model 500 D.

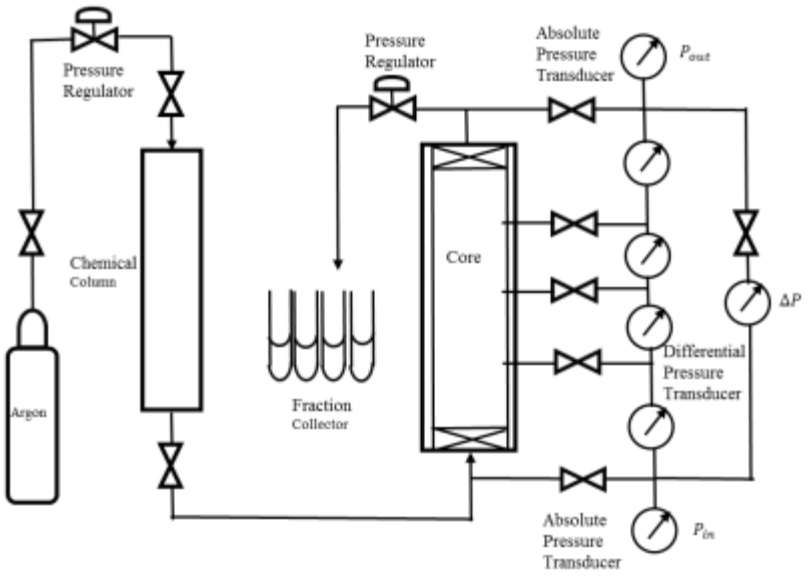

Figure 3.3 Simplified schematic of core flood set up. Source: Qi (2018)

3.2.6 Hyamine titration

The surfactant concentration in the effluent tubes was measured with a two-phase hyamine titration method. The cationic surfactant Hyamine complexes with anionic surfactants in the effluent, resulting in a heavy complex that is extracted into the chloroform layer. The chloroform is the heavier phase relative to aqueous phase and the end point is determined by color shift of an indicator Bromocresol green (BG). A high pH buffer was prepared by combining 300ml of 17.28g/l $Na_4P_2O_7$.10 H_2O in DI, 100ml of 23.91 g/l $Na_5P_3O_{10}$ in DI and 80ml of n-Propanol. The pH was 10-10.5. Bromocresol green solution was prepared by mixing 0.1 g of indicator in 1 L of deionized water. A small amount of propanol was added to facilitate complete dissolution of BG in water. 0.002 molar hyamine 1622 was used as titrant. The hyamine concentration is kept low in order to improve accuracy. 0.5 ml of effluent samples were transferred to 40 mL glass vial with 6 ml of high pH buffer, 1 ml of BG indicator, and 5 ml of chloroform. Then a 0.002 M hyamine solution was added in small increments (typically 10-50 microliters) and the resulting sample was mixed and shaken vigorously. After 2 minutes, the vial was observed to determine if the blue color of the indicator had transferred to the bottom chloroform phase in the vial. This step is repeated until the end point is reached. Small increments and shaking were needed to determine the exact point at which this occurred. The amount of hyamine added was then converted to a surfactant concentration using a calibration curve made with the injected surfactant solution.

3.2.7 Rheometer

The viscosity of the brines, oil, and microemulsion were measured in an ARES LS-1 rheometer by TA Instruments. The double wall geometry was used as this minimizes evaporation at 78 Celsius to produce more accurate measurements.

3.2.8 Salinity and pH measurements

Salinity measurements were done with a refractometer by Fisher Scientific. pH measurements were done with a pH probe. Both types of measurements were carried out at room temperature.

3.2.9 Sample collection

Each effluent test tube took approximately one day to fill. If no seal was used, some water evaporated from the samples which results in oil cuts that are higher than the true values. Rubber stoppers were used to minimize evaporation in the effluent tubes. The test tubes collecting the effluent samples were switched manually to properly position the stopper in the next tube after the collection of one sample was completed.

Chapter 4 Results

This chapter describes the experimental results for a series of corefloods in fractured Texas Cream Limestone cores. The purpose of the experiments was to observe the effect of several variables including chemical slug size and flow rate on the oil recovery and surfactant retention. The surfactant formulation was developed by Nadeeka Upamali and specifically tuned to increase the viscosity of the microemulsion.

4.1 Phase Behavior, Microemulsion Viscosity, and Rock Properties

The chemical formulation used for the coreflood experiments is 0.5% C28-25PO-45EO-carboxylate, 0.2% C15-18 IOS, 0.3% C19-28 IOS, 20,000 ppm Na_2CO_3, 20,000 ppm Na_2SO_4, and 5,000 ppm NaOH and variable concentrations of NaCl. Na_2SO_4 was included in the formulation because the sulfate ion reduces the calcium ion concentration when gypsum is present in the rock (Maubert et al., 2018), and the calcium concentration must be low to prevent precipitation of calcium hydroxide. Gypsum was not known to be present in the TCL cores, but most carbonates do have gypsum or anhydrite in them. The reason for using sodium hydroxide is that it has a higher pH than sodium carbonate, but using both alkalis results in both a high pH and a more robust design.

The phase behavior was observed by conducting NaCl scans with 30% SAMA 247-T oil at 78 Celsius. The phase behavior formulation was named NFR-01. Figure 4.1 shows the phase behavior after 3 months of equilibration. Optimum salinity is 80,000 ppm TDS based on equal solubilization ratios, and 82,500 ppm TDS based on the emulsion test. The formulation is aqueous stable at 85,000 ppm TDS. The type III

window starts at 75,000 ppm and goes up to 85,000 ppm. The samples took one month to equilibrate.

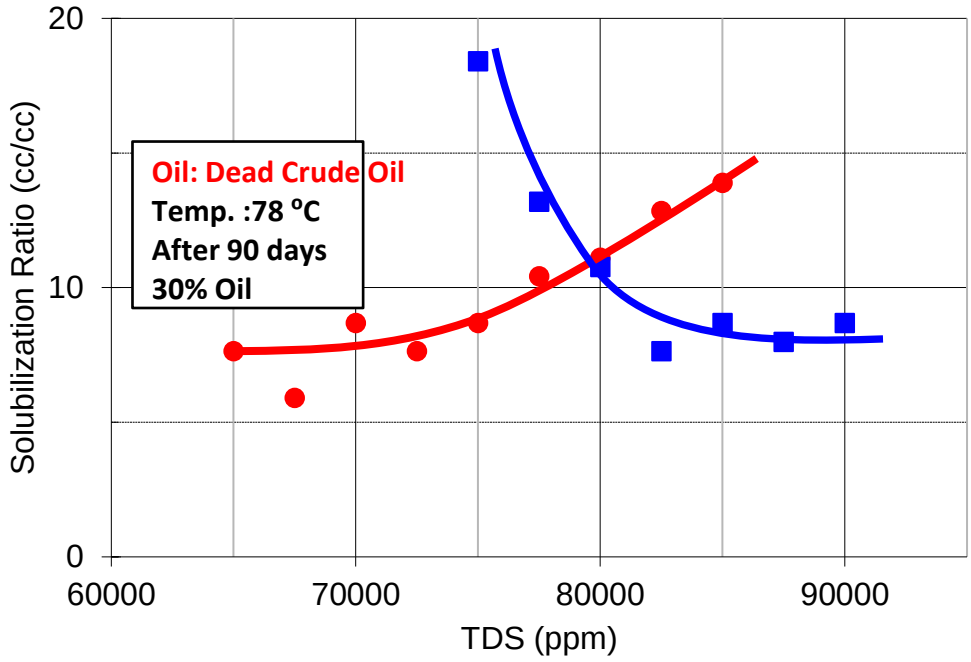

Figure 4.1 Solubilization ratio vs salinity for salinity scan with 30% oil volume for formulation NFR-01

Several large samples with a volume of 80 milliliters were prepared to measure the viscosity of the middle phase microemulsions at different salinities. Samples were prepared at 70,000 ppm, 75,000 ppm, 77,500 ppm, 82,500 ppm, and 85,000 ppm. The 75,000 ppm sample was accidentally shaken and the middle phase mixed brine when trying to extract the middle phase. This mixture was not in equilibrium and therefore the viscosity measurement was not accurate. The viscosity of the 77,500 ppm TDS sample was measured, but the microemulsion sample was probably extracted incorrectly since the viscosity was close to the viscosity of water. Extracting the samples is challenging because after spending 45 days in the 78 degrees Celsius oven and being shaken several

times, the walls of the glass tubes become less clear as the sodium hydroxide reacts with the glass. This, and the fact that the middle phase must be extracted fast to prevent cooling, makes it a challenge to carry out the measurements. To minimize the chances of error, the samples should be extracted and placed in the couette within 30 seconds, and the measurements should be made using the double wall geometry in the rheometer to minimize the surface area where evaporation can occur. As shown in Figure 4.2, the microemulsions are slightly shear thinning. The 77,500 ppm and 70,000 ppm measurements at shear rates less than 4.6 s^{-1} were not reproducible so those data are not shown. Figure 4.3 shows the viscosities at 1 and 10 s^{-1} as a function of salinity and Figure 4.4 shows the same data as a function of the oil concentration in the microemulsion.

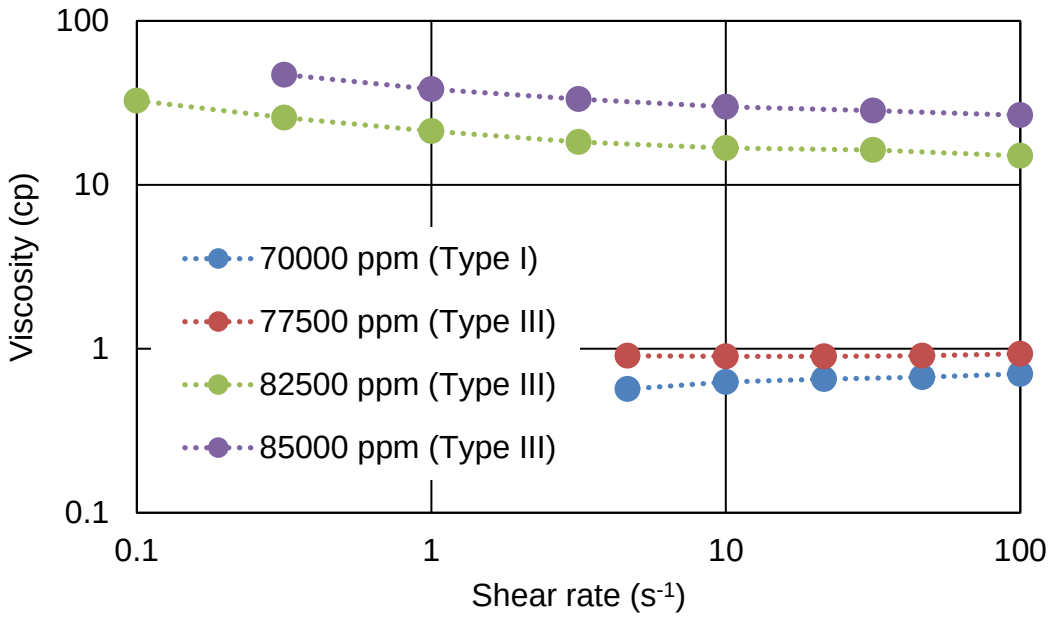

Figure 4.2 Microemulsion viscosity vs shear rate for microemulsion samples at different salinities

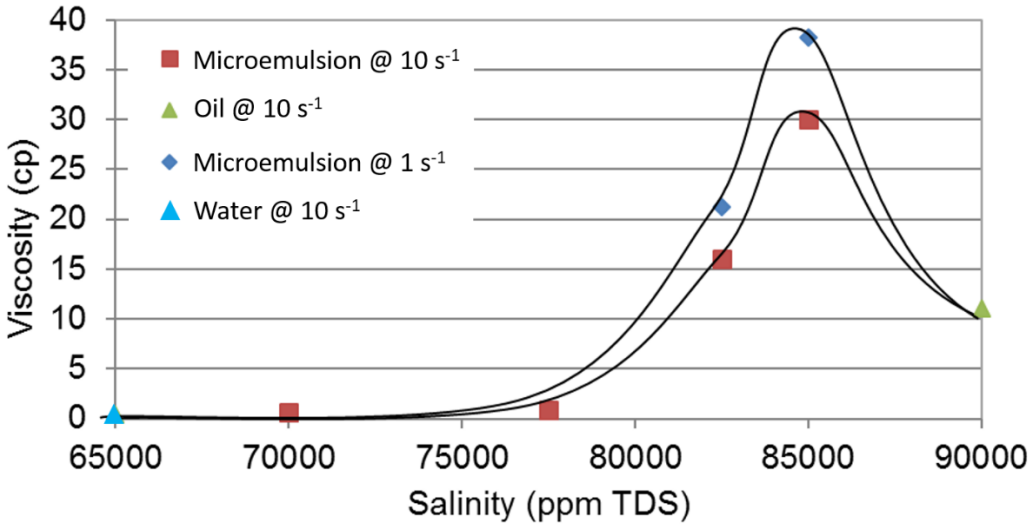

Figure 4.3 Microemulsion viscosity vs salinity measured at 1 and 10 s^{-1}

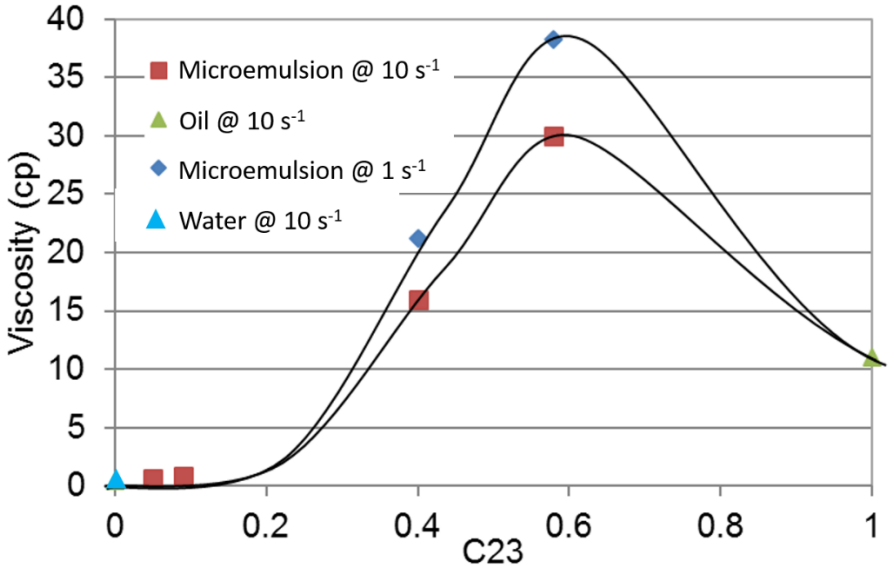

Figure 4.4 Microemulsion viscosity vs oil concentration in the microemulsion (C23) measured at 1 and 10 s^{-1}

Table 4.1 shows a summary of the Texas Cream Limestone cores used in this thesis. Seven experiments were carried out. They are named FRAC 9-16. The first 8 FRAC experiments and their results can be found in Parra (2016).

Table 4.1 Summary of Texas Cream Limestone cores used in FRAC 09-16

Property	Unit	FRAC-09	FRAC-10	FRAC-11	FRAC-13	FRAC-14	FRAC-15	FRAC-16
Mass before cutting	g	649.6	621.74	629.2	631.09	632	624.3	636
Mass after cutting	g	628.4	603.52	618.4	574	601.8	596.92	603.1
Length	cm	29.8	29.5	29.51	28.57	28.8	28.8	27.8
Diameter	cm	3.76	3.7	3.72	3.75	3.7	3.76	3.76
Cross-sectional Area	cm2	11.14	10.75	10.75	11.04	10.75	11.1	11.1
Bulk Volume	mL	332.4	317.2	317.2	315.6	309.66	319.23	308.7
Porosity based on 2.72 g/cm^3 calcite density		0.28	0.28	0.27	0.329	0.283	0.311	0.279
Pore volume based on density	mL	93.6	88.6	85.6	97.76	87.53	99.24	86.07
Porosity from saturation	%	0.28	0.27	0.28	0.299	0.28	0.309	0.287
Pore Volume	mL	92.5	87.5	86.9	94.4	89.16	98.72	88.6
Matrix air permeability	md	32	30	28	19	18	18	17.5

4.2 Chemical Flood with a Rough Fracture Experiment FRAC-09

The objective of the FRAC-09 experiment was to test the performance of a new surfactant formulation in a fractured Texas Cream Limestone core. Previous coreflood experiments by Parra (2016) showed higher oil recovery from fractured TCL cores at higher values of the microemulsion viscosity. The previous FRAC-01-08 experiments can be found in Parra (2018). Several pore volumes of a 1% surfactant solution were injected in each of Parra's corefloods. Such large amounts of surfactant are unlikely to be used in the field. The amount of surfactant required to produce oil depends in part on the mass needed to satisfy surfactant retention in the rock. Recent experiments using limestone cores has shown that NaOH alkali reduces surfactant retention in non-fractured limestone cores (Maubert et al., 2018, Wang et al., 2018, Wang 2018). This experiment was the first test of the use of NaOH in a fractured core. The formulation used by Parra contained EDTA. The EDTA dissolves limestone and therefore has a high consumption, so it may not be practical for use in chemical floods of carbonate reservoirs. Parra (2016) had the same three main surfactants as in NFR-01 at the same concentrations. The salt concentrations in Parra (2016) were 10,000 ppm Na_4EDTA, 30,000 ppm Na_2CO_3 and different concentrations of NaCl. The first step in this new development was to test the performance of the new formulation and optimize it as needed. The new formulation (NFR-01) contains NaOH and Na_2SO_4, and contains no Na_4EDTA. NaOH was added to increase the pH of the solution and reduce surfactant retention.

The procedure described in Chapter 3 for using spacers to keep the fracture open had not been developed yet at the time of this first coreflood experiment. Instead of using

spacers, the fracture was roughed manually with a sharp tool. The confining pressure was then adjusted to achieve the target permeability. The core's dimensions are shown in Table 4.1.

4.2.1 Air permeability

The permeability of the dry rock matrix was measured using an air permeameter. Figure 4.2 shows the air permeability measurements for the core used in the FRAC-09 experiments.

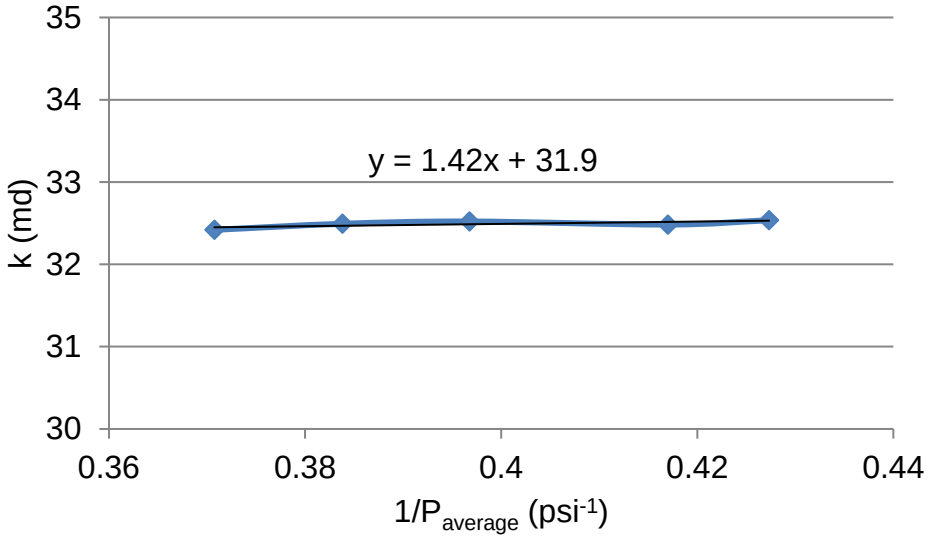

Figure 4.5 Air permeability measurement for FRAC-09 core

4.2.2 Oil saturation

The core was saturated with crude oil after being vacuumed for 6 hours. The pore volume of the rock is 92.5 mL and porosity is 28%. The core was placed in a 78 Celsius oven and aged for seven days. The core was then flooded with dead crude oil with a

viscosity of 12 cp. The confining pressure was 300 psia. Figure 4.6 shows the pressure drop during the single-phase oil flood at a constant flow rate of 0.7 ml/min. The whole pressure drop decreases from about 5 psi because the injection pump was turned on before the outlet valve was opened. A steady state pressure drop of 0.35 psi is reached after about 0.25 pore volumes injected. The sectional pressure drops do not add up to the whole pressure drop, most likely because the sectional pressure taps were not perfectly aligned with the fracture. The effective oil permeability of the fractured core calculated from Equation 3.1 is 14 Darcy. The fracture aperture 'b' calculated from Equation 3.2 fracture aperture is 0.017 cm. The permeability of the fracture calculated from Equation 3.3 is 2,400 Darcy.

$$k = \frac{Q\mu L}{A(P_i - P_o)} = 245 * \frac{(0.7\frac{ml}{\min} * 11\text{cp} * 29.8cm)}{(11.2cm^2 * 0.36psi)} = 14,070md \qquad (3.1)$$

$$b = \left(3\pi D k_{eff}\right)^{\frac{1}{3}} = \left(3 * \pi * 0.0376m * 14Darcy * \frac{9.87E^{-13}m^2}{1Darcy}\right)^{\frac{1}{3}} = 0.00017m \qquad (3.2)$$

$$k_{fracure} = \frac{A_{total}k_{effective} - 2A_{matrix}k_{matrix}}{A_{fracture}} = \qquad (3.3)$$

$$\frac{(11.1cm^2 * 14Darcy - (11.1cm^2 - 3.76cm * 0.017cm) * 0.032\,\text{Darcy}}{3.76cm * 0.017cm} = 2,429Darcy$$

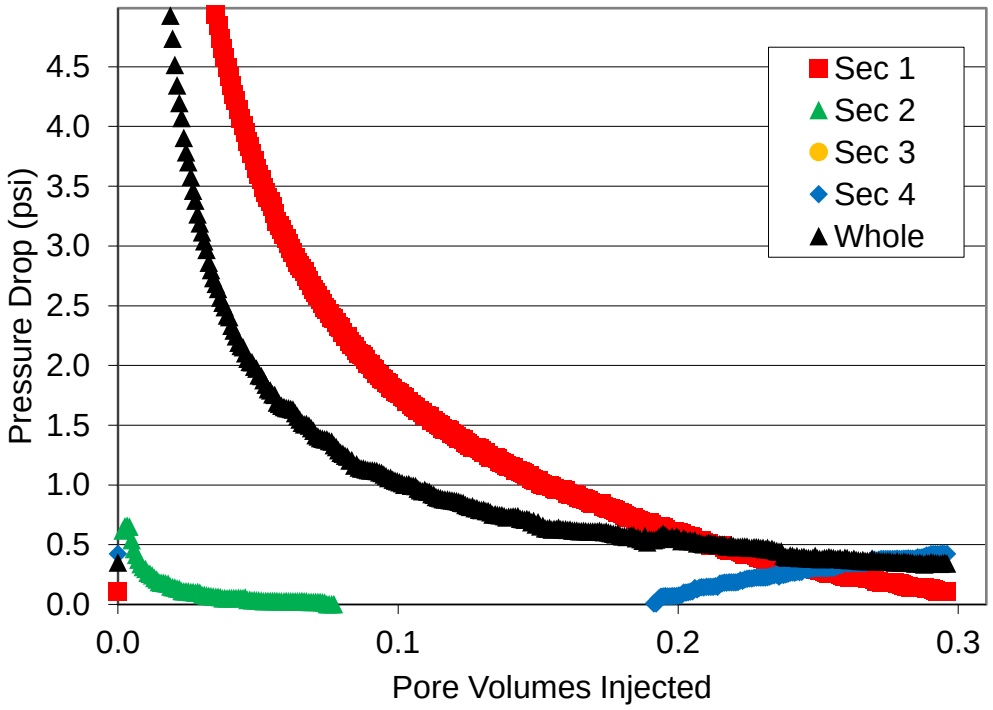

Figure 4.6 Pressure drop during single-phase oil flood of FRAC-09 experiment

4.2.3 Waterflood

The core was waterflooded with 92,000 ppm NaCl brine at a flow rate of 0.3 mL/min, equivalent to an interstitial velocity of 5 ft/day based on the whole core, with a confining pressure of 300 psia. Water broke through after displacing 2 mL of oil. The confining pressure was increased to 500 psi after 0.5 PVS of brine injection to reduce the permeability of the fracture to a value similar to what Parra measured in his corefloods, and the core was waterflooded with 70,000 ppm NaCl brine at a flow rate of 0.3 mL/min. Under similar conditions, Parra measured the fracture aperture during the single-phase oil flood to be 0.09 cm.

The oil saturation after the waterflood was 0.91. Figure 4.7 shows the oil saturation, oil cut and oil recovery from the waterflood. There is an increase in the oil cut from 0% to 25% as soon as the confining pressure is increased at 0.5 PVI. The waterflood pressure drop is shown in Figure 4.8. The whole pressure drop increased from 0.1 psi to 0.4 psi after the confining stress was increased from 300 psia to 500 psia at 0.5 PVI. This increase in pressure drop indicates a decrease in the permeability of the fracture. The water permeability using the cross-sectional area of the whole core is 200 md.

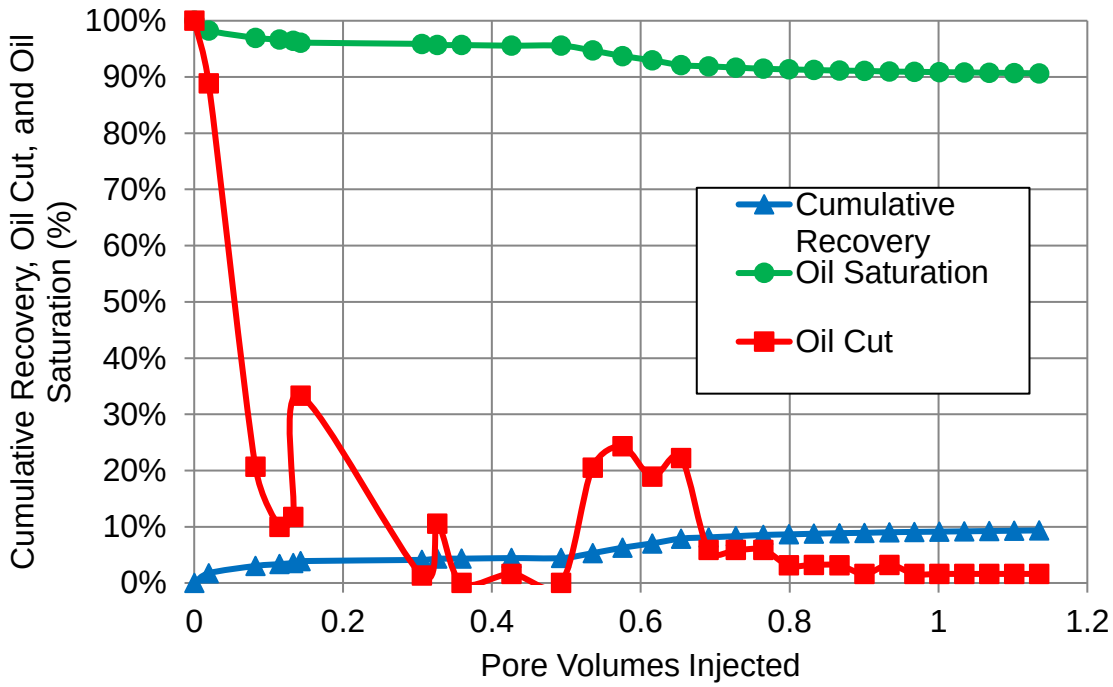

Figure 4.7 Waterflood oil recovery, oil saturation, and oil cut for FRAC-09 experiment

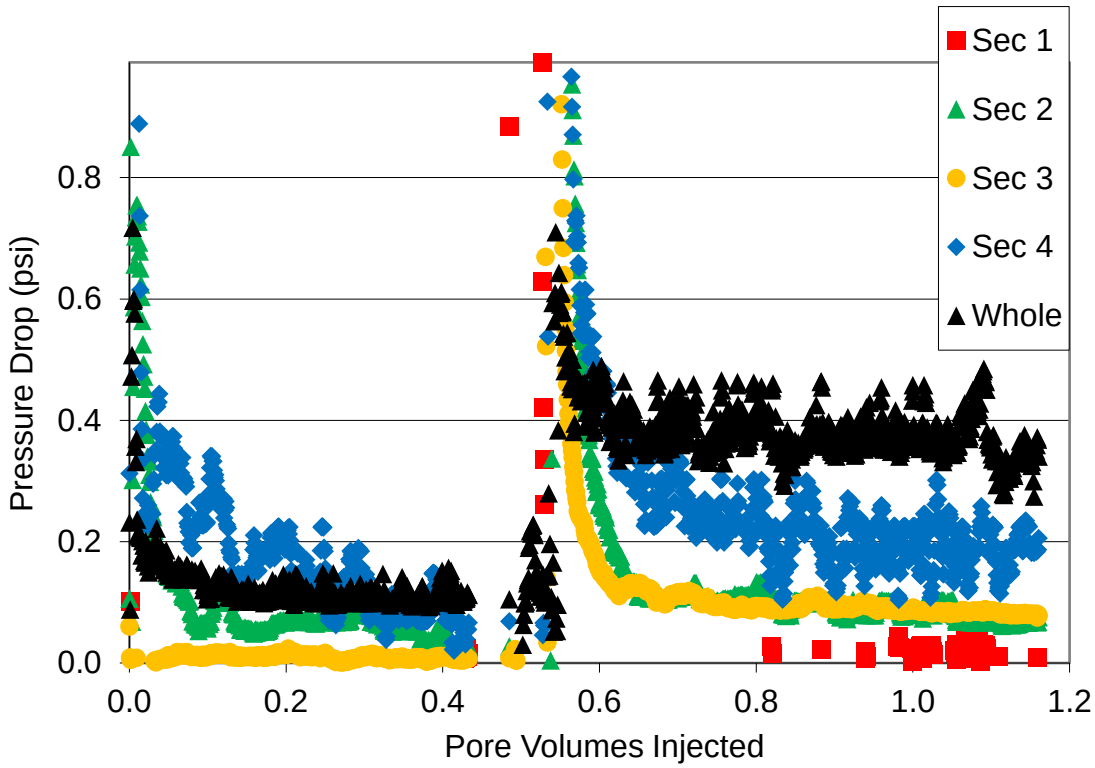

Figure 4.8 Pressure drop during waterflood for FRAC-09 experiment

4.2.4 Chemical Flood

The core was flooded with a surfactant solution with a salinity of 70,000 ppm TDS, at a rate of 0.01 mL/min. With a porosity of 28% and cross-sectional area of 11.10 cm^2 the interstitial velocity was 0.15 ft/day based on the whole core. Assuming all of the flow is in the fracture and the fracture to be a rectangular parallelogram with an aperture of 0.09 cm and a porosity of 1, the velocity in the fracture would be 14 ft/day. The oil saturation after 4.3 PV was 0.58 and the maximum pressure drop was 0.5 psi, as shown in Figure 4.10. At around 1 PV of surfactant injection, mechanical problems with the pressure setup occurred causing the pressure drop to decrease to negative values. Because

of this, the pressure setup was bled at around 1.5 PV. The section pressure drops do not add up to the whole pressure drop. The pressure drop across the whole core was about 0.4 psi at 3 PV.

The pressure drop of 0.4 psi during the surfactant injection was about 30 times higher than the pressure drop of the waterflood scaled to the same flow rate of 0.01 ml/min even though the viscosity of the water and surfactant solution were nearly the same. This behavior can be explained by the formation of a viscous microemulsion inside the core when the injected surfactant solution mixes with the oil. The viscous microemulsion results in a lower fluid mobility and higher oil recovery.

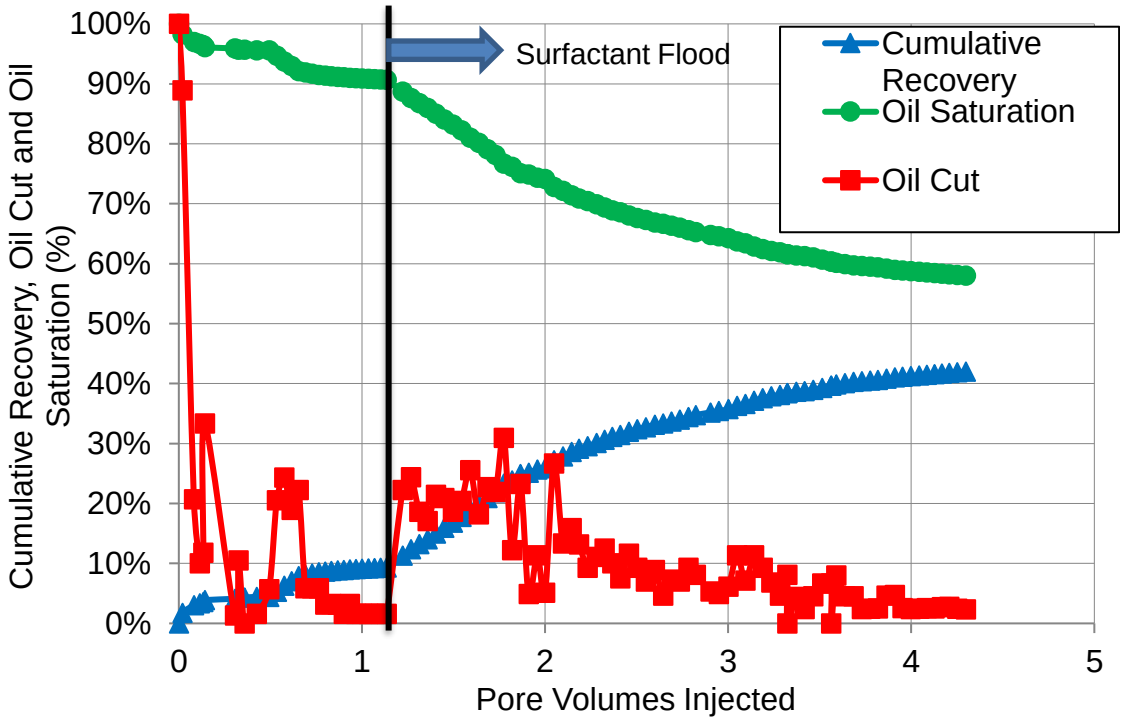

Figure 4.9 Oil recovery, oil saturation, and oil cut for entire FRAC-09 experiment

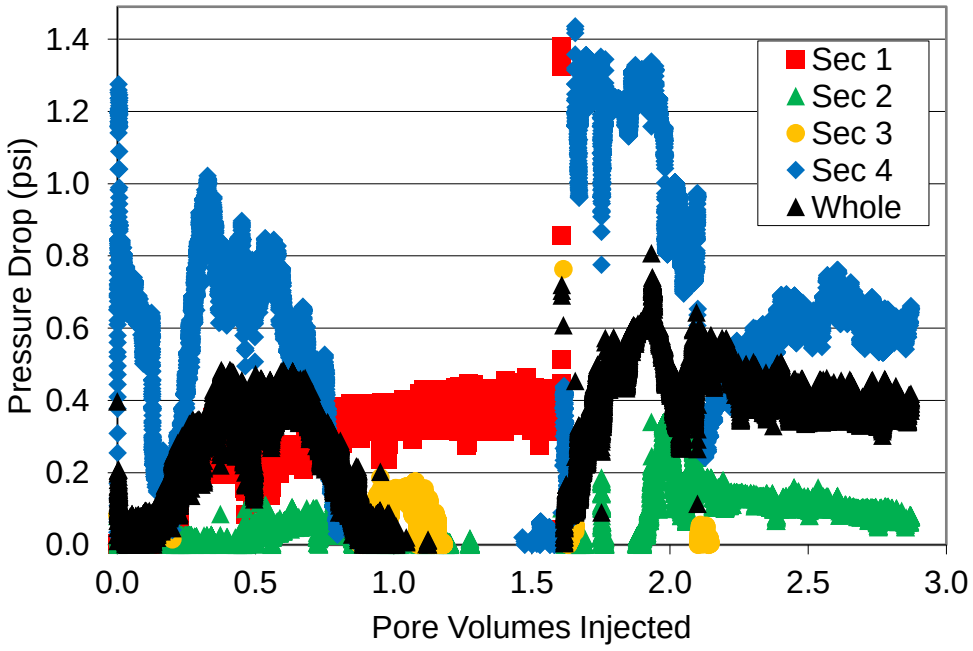

Figure 4.10 Pressure drop during chemical flood for FRAC-09 experiment

4.2.5 Surfactant retention

The surfactant concentration in the effluent samples was measured with the hyamine titration method. By visual inspection, it is notable that the effluent samples all showed a relatively dark color in the aqueous phase. The surfactant concentration in the effluent samples is shown in Figure 4.11 and the calibration curve used to determine effluent surfactant concentrations is shown in Figure 4.12. The concentration of surfactant in effluent samples peaked at about 9800 ppm at 0.55 PV. The surfactant retained was calculated by subtracting the mass of surfactant in the effluent samples from the mass of the surfactant injected. At 0.55 PV the injected surfactant was 0.85 mg/g-rock, and the produced surfactant was 0.64 mg/g-rock, so the retention was 0.21 mg/g-

rock. The total amount of surfactant injected was 4.50 mg/g-rock, and the amount recovered at the end of the injection was 4.13 mg/g-rock, and the surfactant retention was 0.37 mg/g-rock.. The minimum increase in hyamine volume for the titration was 20 µl. Using the calibration curve, 20 µl translates to 223 ppm of surfactant. If the analyte is missing exactly 20 µl to reach the end point, then adding titrant contributes very little error. If the analyte is very close to the end point, an addition of 20 µl adds the maximum error of 20 µl of 223 ppm. The indicator will only change color if one reaches or exceeds the amount of titrant required to reach the end point. The surfactant concentration measurements with the hyamine titration method using repeaters are therefore overestimates of the true surfactant effluent concentration. One can consider the maximum amount of error corresponding to the minimum volume of hyamine added for each step determining the surfactant concentration.

The maximum effluent concentration does not reach the injected concentration due to experimental error. The effluent samples had to be diluted 4X due to the presence of crude oil, which prevents accurate interpretation of the end point when present. If one considers the maximum effluent concentration as the injected concentration instead of the one obtained by the calibration curve, the retention value is 0.19 mg/g-rock. Considering an uncertainty surfactant concentration of 223 ppm in each effluent sample, and 0.21 mg/g-rock to be an overestimate, the surfactant retention for FRAC-09 lies between 0.19 mg/g-rock and 0.21 mg/g-rock.

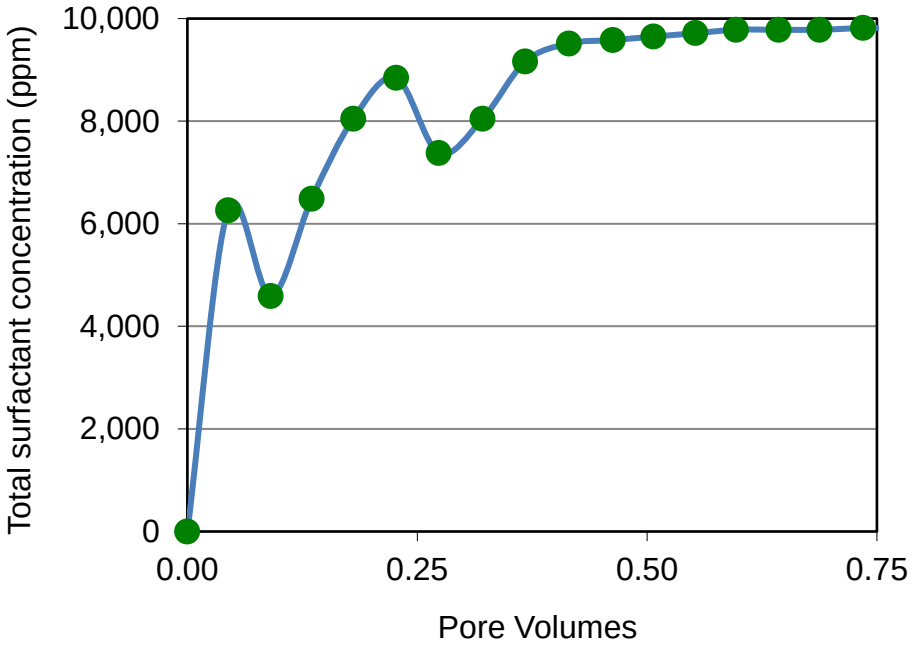

Figure 4.11 Effluent surfactant concentration for FRAC-09 experiment

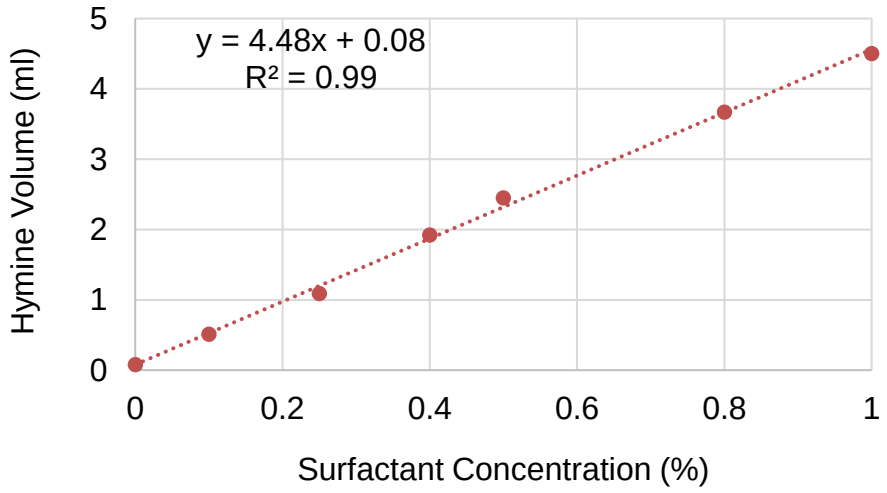

Figure 4.12 Calibration curve used to determine surfactant concentration in effluent samples for FRAC-09

4.3 Chemical Flood with Spacers in the Fracture Experiment FRAC-10

The objective of the FRAC-10 experiment was to test the performance of the new surfactant formulation in a fractured Texas Cream Limestone core using the Teflon spacers described in Chapter 3 to maintain a constant fracture aperture. Surfactant retention was measured upon completing the experiment. The properties of the core used in this experiment are shown in Table 4.1.

4.3.1 Air permeability

The air permeability was measured at 1000 psi confining pressure before the core was cut. Figure 4.13 shows the pressure drop at different flow rates. The air permeability was determined from the intercept of permeability versus reciprocal pressure data plotted in Figure 4.14 to account for the Klinkenberg effect.

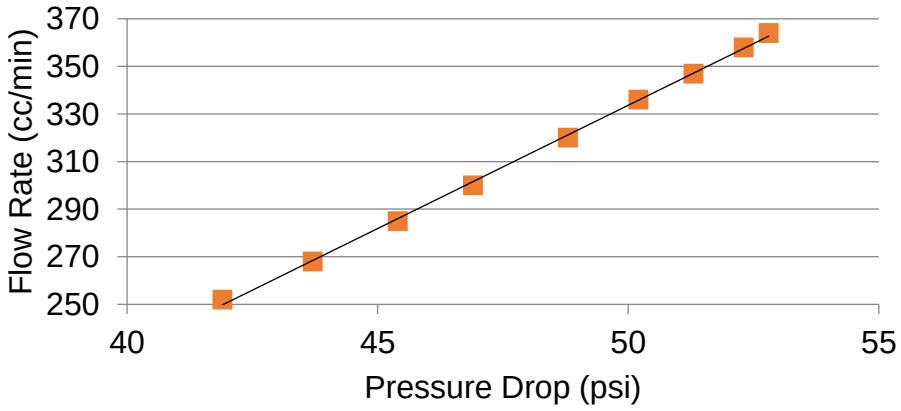

Figure 4.13 Air Flow rate vs Pressure drop for FRAC-10 experiment

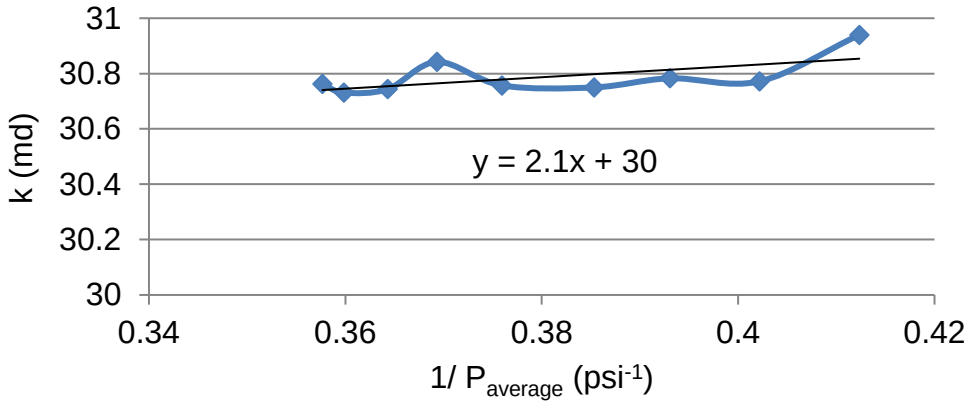

Figure 4.14 Permeability vs Reciprocal pressure for permeability measurement for FRAC-10 core

4.3.2 Oil Saturation

The core was saturated with dead crude oil after being vacuumed for 6 hours. The pore volume of the rock was 87.5 mL and porosity was 27%. The core was placed in the 78 Celsius oven and was aged for seven days. The core was flooded with dead crude oil with a viscosity of 11 cp at constant flow rate. The confining stress was maintained at 500 psi using a hydraulic pump. The permeability of the fracture is a function of its aperture. The fracture aperture is a function of the confining stress applied. The confining stress during the oil flood for each experiment is selected in order to achieve a specific desired permeability, of 300 md in this case. The air permeability is not the same as the oil permeability, as different fluids give different values. Air permeability was measured at 1,000 psi to maintain consistency with Parra (2016) in measuring the permeability of Texas Cream Limestone. The oil was filtered using a 0.45 microns cellulose acetate filter. Two oil floods were carried out to measure the single-phase permeability to oil. Table 4.2 shows the oil permeability measurements at different flow rates for the FRAC-10 experiment. Figure 4.15 shows the pressure drop across the core for the first two flow

rates in Table 4.2. Figure 4.16 shows the pressure drop across the core for the last three flow rates in Table 4.2. The oil permeability was around 600 md for the whole core. The measured oil permeability at the lowest flow rate of 0.01 was lower, 290 md, than the other measurements. All the other measurements are in good agreement. At such a low flow rate the data is less accurate and takes a very long time, over one day, to equilibrate.

It is also important to note that the pressure drops across the sections of the core did not add up to the total pressure drop, which was also the case in the previous fractured core floods in Texas Cream Limestone.

Table 4.2 Oil Permeability measurements at several flow rates in FRAC-10 experiment

Flow rate (ml/min)	Pressure drop (psi)	Permeability (md)
0.1	1.22	590
0.04	0.57	632
1	12.37	582
0.3	3.47	623
0.01	0.25	288

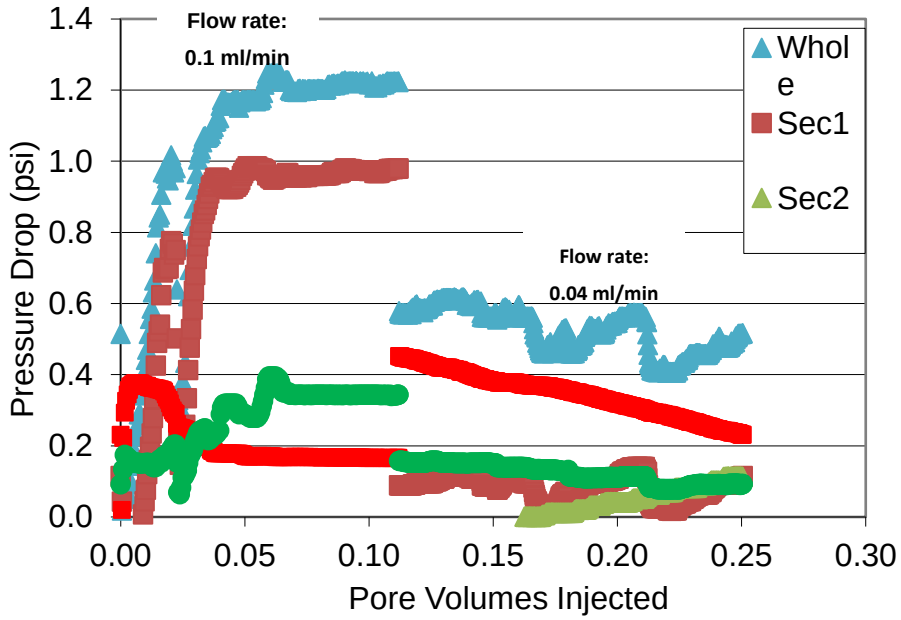

Figure 4.15 Oil flood pressure drop data measured at first two flow rates shown in Table 4.2

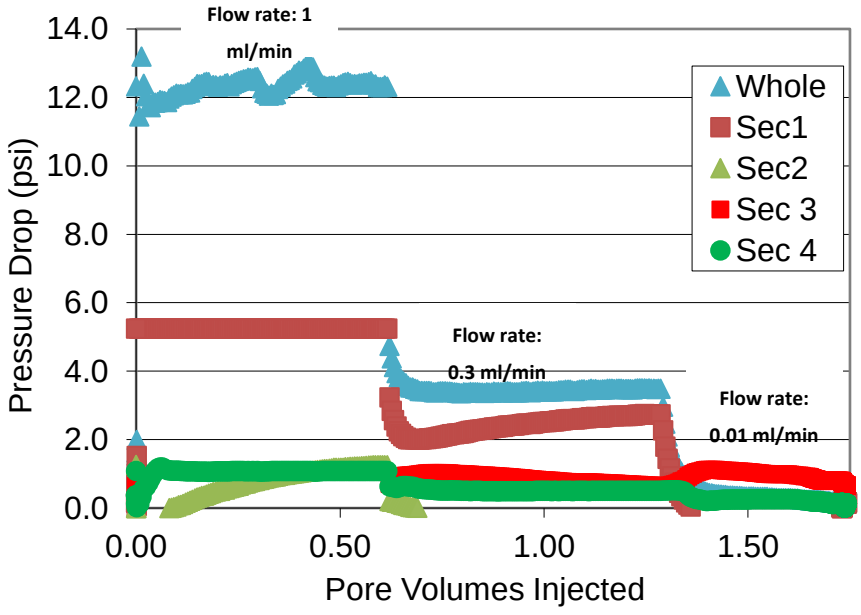

Figure 4.16 Oil flood pressure drop data measured at last three flow rates shown in Table 4.2

The fracture aperture was estimated to be 0.006 cm and the fracture permeability 280 Darcy using the equations shown in Chapter 2.

As shown below, the effective oil permeability of the fractured core was 600 md, the fracture aperture was 0.006 cm and the permeability of the fracture was 278 Darcy.

$$Q = -\frac{kA}{\mu}\left(\frac{P_i - P_o}{L}\right) k = \frac{Q\mu L}{A(P_i - P_o)} = 245 * \frac{(0.1\frac{ml}{\min} * 11\text{cp} * 29.5cm)}{(10.75cm^2 * 1.22\,psi)} = 590md \qquad (3.4)$$

$$b = \left(3\pi D k_{eff}\right)^{\frac{1}{3}} = \left(3 * \pi * 0.037m * 0.6Darcy * \frac{9.87E^{-13}m^2}{1Darcy}\right)^{\frac{1}{3}} = 0.000059m \qquad (3.5)$$

$$k_{fracure} = \frac{A_{total}k_{effective} - 2A_{matrix}k_{matrix}}{A_{fracture}} = \qquad (3.6)$$

$$\frac{(11.1cm^2 * 0.6Darcy - (10.75cm^2 - 3.7cm * 0.006cm) * 0.032\,\text{Darcy}}{3.7cm * 0.006cm} = 278Darcy$$

4.3.3 Waterflood

The core was waterflooded with 10,000 ppm NaCl brine at a flow rate of 0.3 mL/min, equivalent to an interstitial velocity of 4.7 ft/day based on the whole core area and porosity of 27%. A back pressure regulator was used for an initial water flood. It was difficult to tell when water broke through because when the initial oil entered the back pressure regulator, the oil remained inside and water came out first. The oil saturation after the water flood was 96%. Total oil production after the waterflood was 4mL. 2 mL out of the total 4 mL produced were part of the dead volume of the system.

Figure 4.17 shows the oil saturation, oil cut, and oil recovery from the water flood. The water flood pressure drop data are shown in Figures 4.18 and 4.19. The water permeability was 60 md using a pressure drop of 1.5 psi and a water viscosity of 0.4 cp based on the second water flood without a back pressure regulator.

A second water flood was carried out with the purpose of conducting a tracer test. The second waterflood had a higher salinity of 70,000 ppm and was also injected at 0.3 mL/min. Samples of 3.1 mL were collected in test tubes. The salinity of each sample was measured with a refractometer. The refraction indices were normalized between the initial and final values. Figure 4.20 shows a plot of normalized salinity versus volume injected. The pore volume was calculated by measuring the area over the curve and subtracting a dead volume of 2 ml as described in Qi (2018). The effluent salinity was higher than the initial value after the second test tube. The fracture was clearly open and very permeable. The long tail towards the end of the tracer test indicates a high heterogeneity. The swept pore volume calculated from the tracer data was 3.5 mL. The second water flood did not use a back pressure regulator. This was with the purpose of maintaining consistency with the set-up used during the oil flood and to reduce the noise in the pressure drop measurements.

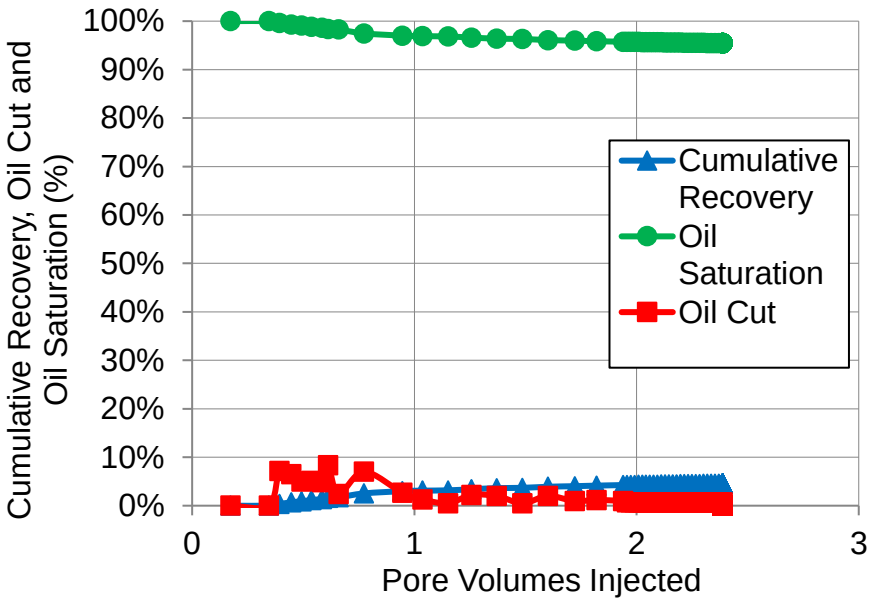

Figure 4.17 Oil cut, recovery, and saturation during waterflood for FRAC-10 experiment

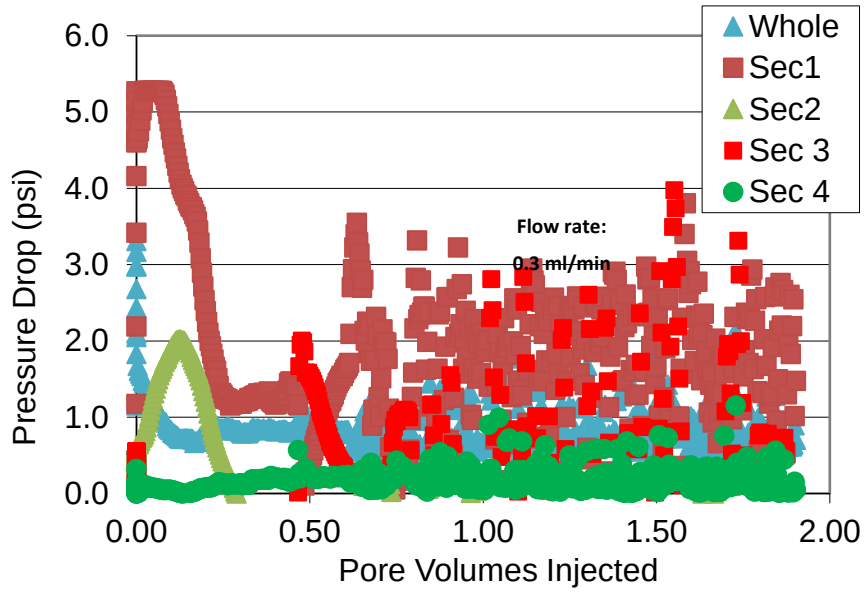

Figure 4.18 Pressure drop with back pressure regulator during waterflood for FRAC-10 experiment

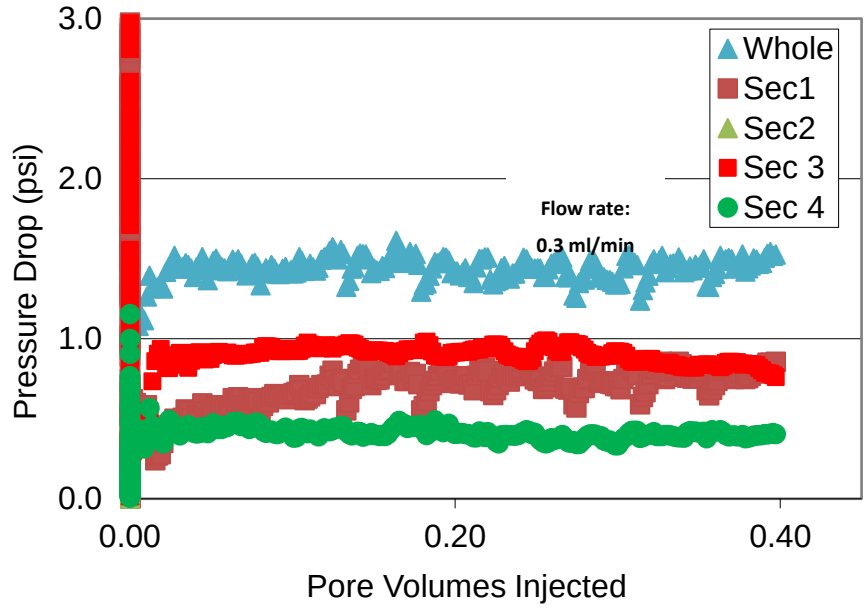

Figure 4.19 Pressure drop without back pressure regulator during waterflood for FRAC-10 experiment

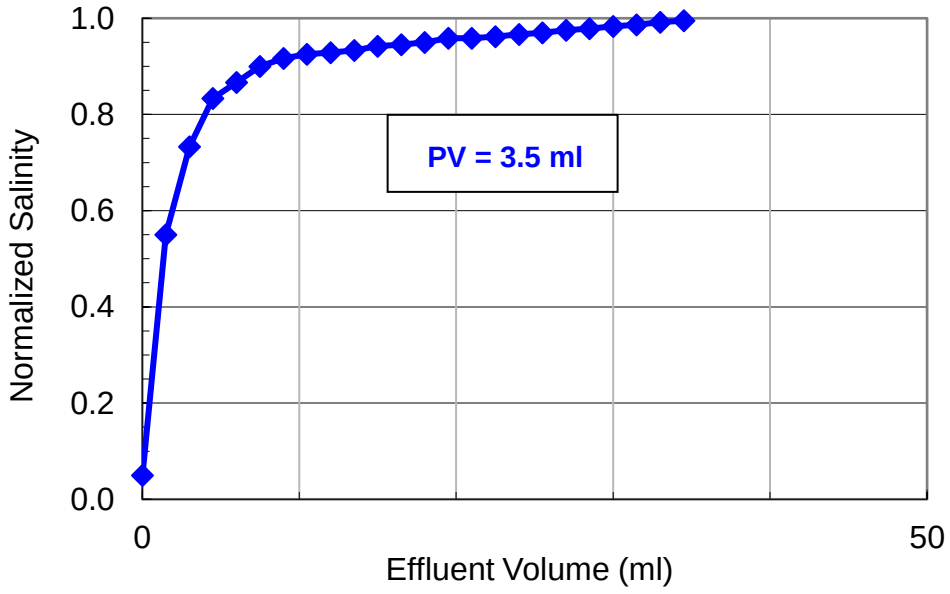

Figure 4.20 Tracer test during waterflood in FRAC-10 experiment

4.3.4 Chemical flood

The oil recovery from the chemical flood can be seen in Figure 4.21. 43% of the oil remaining after the waterflood was recovered. The oil saturation at the end of the chemical flood was 53%. The core was flooded at a flow rate of 0.01 ml/min with a surfactant solution with a salinity of 70,000 ppm TDS. This salinity was selected to compare the results of this experiment with the FRAC-09 experiment, which was also carried out at 70,000 ppm TDS and did not have Teflon spacers.

The injection rate was equivalent to an interstitial velocity of 0.16 ft/day based on the 10.75 cm^2 cross sectional area of the whole core with 27% porosity, and 21 ft/day based on the estimated fracture area with no porosity. The oil solubilization ratio at 70,000 ppm was estimated to be 7.1 and the IFT between oil and the microemulsion calculated from the Huh equation is 0.006 dynes/cm.

Figure 4.22 shows the pressure drop data during the chemical flood. As in previous experiments, the sectional pressure drops do not add up to the whole pressure drop. By visual inspection, the core looked ‘cleaner’ at the bottom as shown in Figure 4.23. The fracture aperture looked open, and the Teflon used for the spacers had the same thickness before and after the experiment.

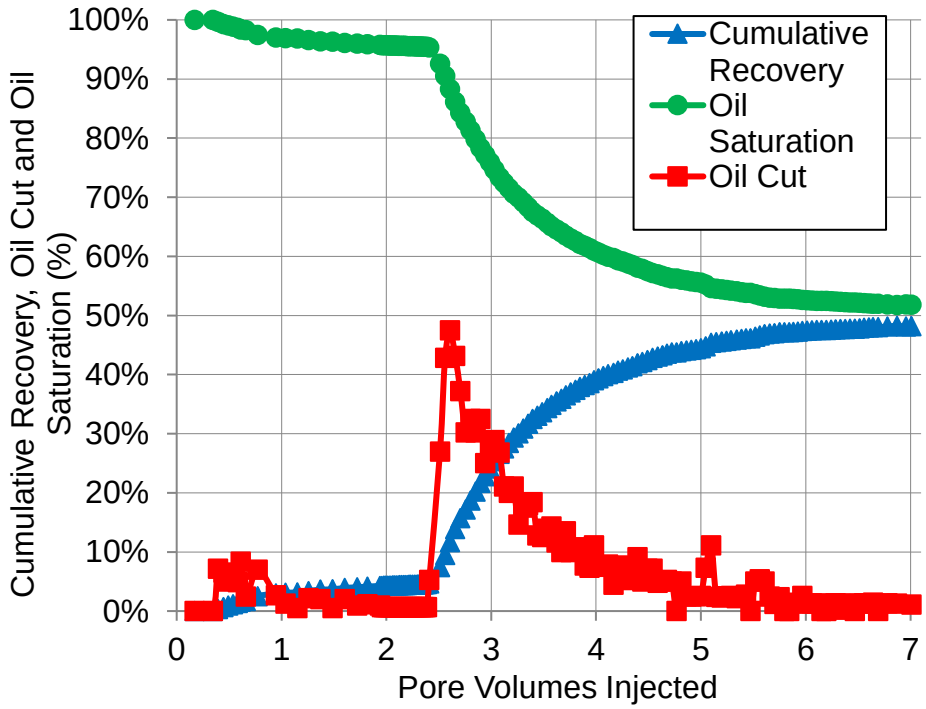

Figure 4.21 Oil cut, saturation, and recovery during entire FRAC-10 experiment

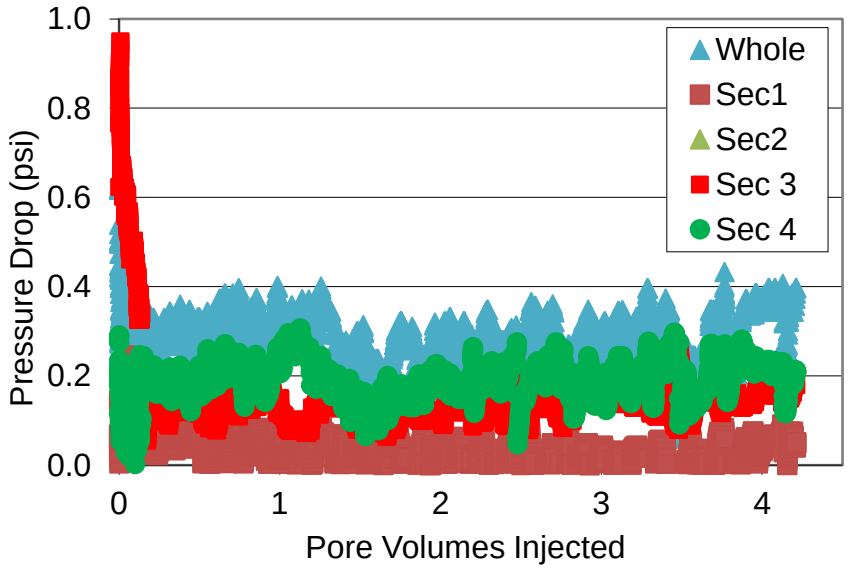

Figure 4.22 Chemical flood pressure drop for FRAC-10 experiment

Figure 4.23 Image of core used in FRAC-10 after the surfactant flood

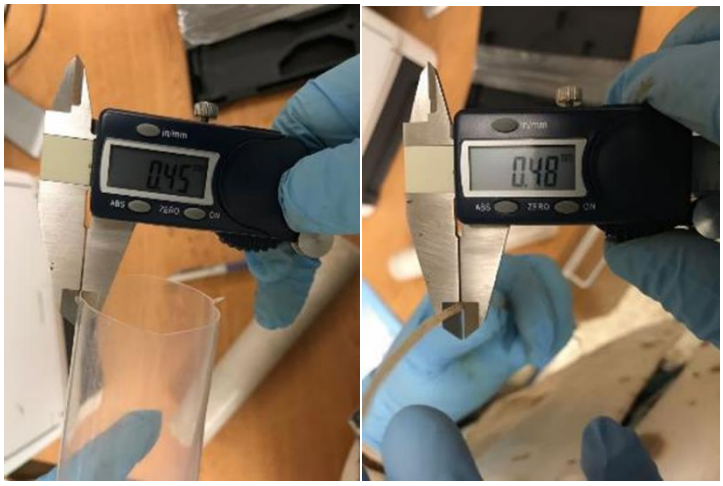

Figure 4.24 Teflon thickness before and after the surfactant flood

4.3.5 Surfactant retention

The concentration of surfactant in the effluent was measured using the hyamine titration method. The effluent surfactant concentration can be seen in Figure 4.25, which was determined using the calibration curve seen in Figure 4.26. The surfactant retention was determined using a mass balance assuming the surfactant concentration in the core at the end of the surfactant flood was the same as the injected concentration of 1%. We know the mass injected because the flow rate and concentration are kept constant. We know the mass out of the core because of the effluent concentration. These two values equal the mass in the pores plus the surfactant retained. The surfactant retained is therefore the mass of surfactant injected minus the mass of surfactant produced minus the mass of surfactant in pores.

The mass of surfactant in the pores in this calculation is taken to be the volume of displaced oil multiplied by the surfactant concentration (1%). With this method, surfactant retention is about 0.25 mg/g-rock as shown in Figure 4.27. The effluent surfactant concentration did not reach the injected value of 1 wt%. The maximum effluent concentration is 0.974 wt%. This is probably due to measurement error. The minimum volume of hyamine added in the titration was 20 µL. That corresponds to 230 ppm. The dilution of the samples 4X amplifies the error. Following the same method but multiplying by the measured effluent concentration (0.974%) in the pores, the surfactant retention is measured to be 0.23 mg/g-rock. Subtracting 230 ppm to the effluent measurements, we get a minimum titration value of 0.21 mg/g-rock. The surfactant retention lies between 0.21 and 0.25 mg/g-rock.

The surfactant retention is low considering the core is a fractured limestone with a low matrix permeability. This result supports the claim that including NaOH in the

formulation reduces surfactant retention by increasing the pH to 12.6. The effluent pH measured at 2 PV was 12.57.

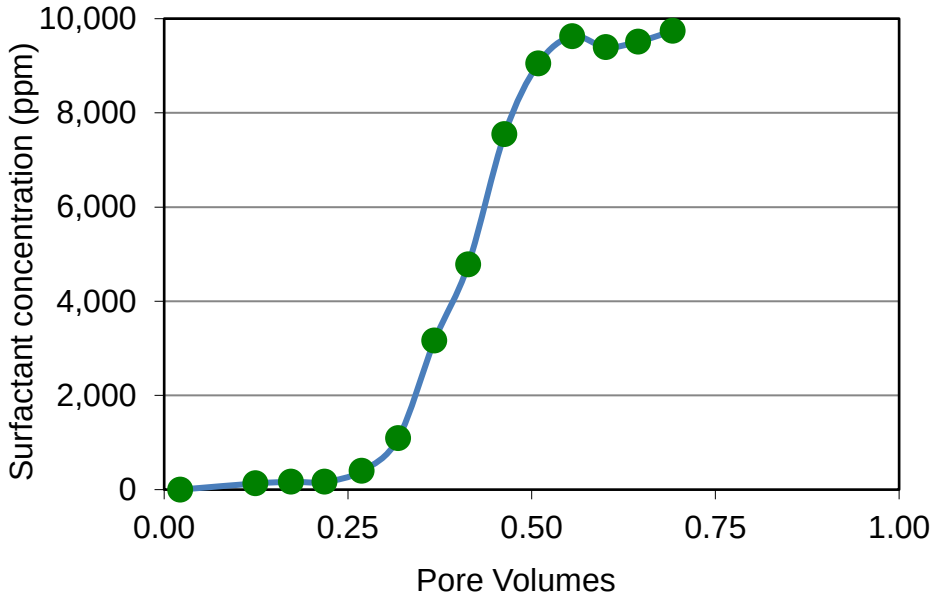

Figure 4.25 Effluent surfactant concentration for FRAC-10 experiment

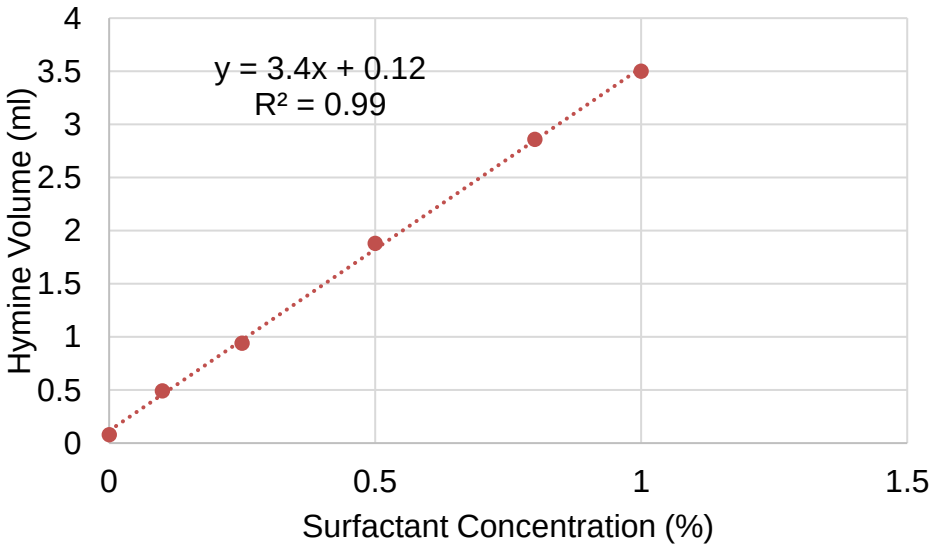

Figure 4.26 Calibration curve to determine surfactant concentration for FRAC-10 experiment

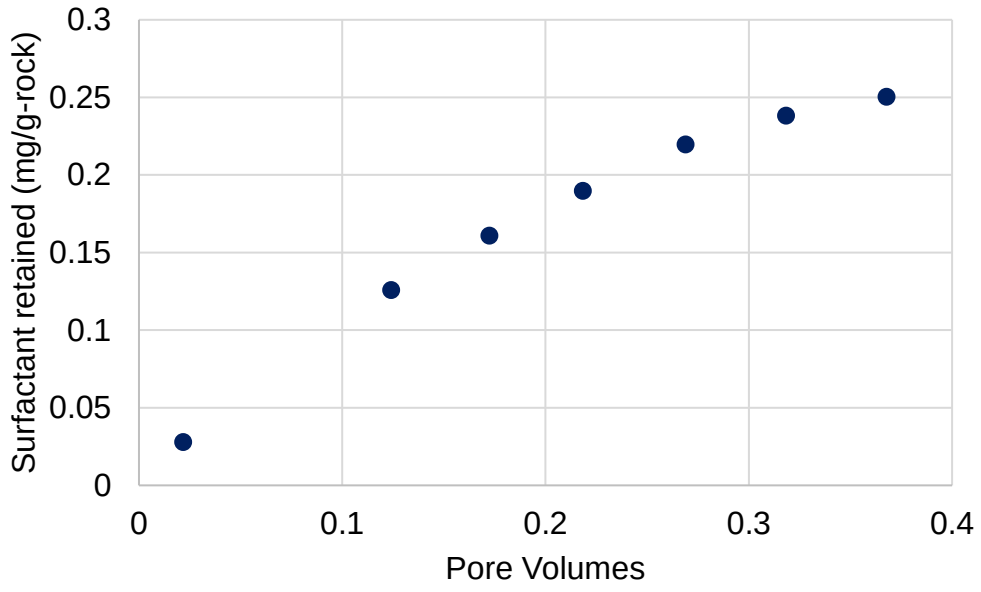

Figure 4.27 Surfactant retention for FRAC-10 experiment

4.4 Chemical Flood with Spacers and Salinity Gradient FRAC-11

The objective of the FRAC-11 experiment was to test the performance of an alkali-surfactant salinity gradient in a fractured Texas Cream Limestone core. The salinity gradient was imposed to minimize surfactant retention. The salinity of the waterflood and the surfactant slug was 85,000 ppm TDS. The optimum salinity was 80,000 ppm and the upper limit of type III was 85,000 ppm TDS. The microemulsion had a viscosity of 38 cp at 1 s^{-1} at 85,000 ppm TDS. The drive salinity was 65,000 ppm TDS. The lower limit for type III was 75,000 ppm TDS. Only the concentration of sodium chloride was changed to modify the concentrations of the surfactant and chase fluids.

As in the FRAC-10 experiment, two Teflon spacers were placed between the two halves of the core to keep the width of the fracture constant throughout the experiment. The properties of the core used in this experiment are shown in Table 4.1.

4.4.1 Air permeability

The air permeability was measured at 1000 psi of confining pressure before the core was cut. Figure 4.27 shows the pressure drop at different flow rates. The air permeability was determined to be 28 md from the intercept of permeability versus reciprocal pressure data plotted in Figure 4.14 to account for the Klinkenberg effect.

The air permeability of the fractured core at 500 psi of confining pressure was also measured to be 1.7 Darcy following the same procedure. Figures 7 and 8 show the same information as Figures 5 and 6, but for the fractured core at 500 psi of confining pressure.

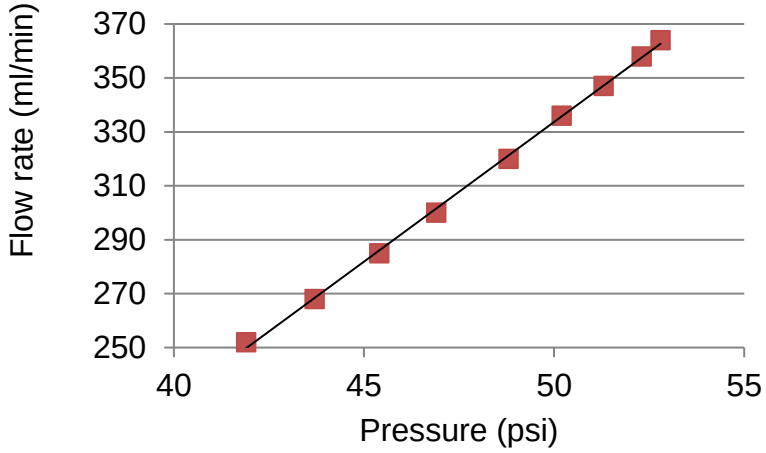

Figure 4.28 Air flow rate vs pressure drop for unfractured rock in FRAC-11 experiment

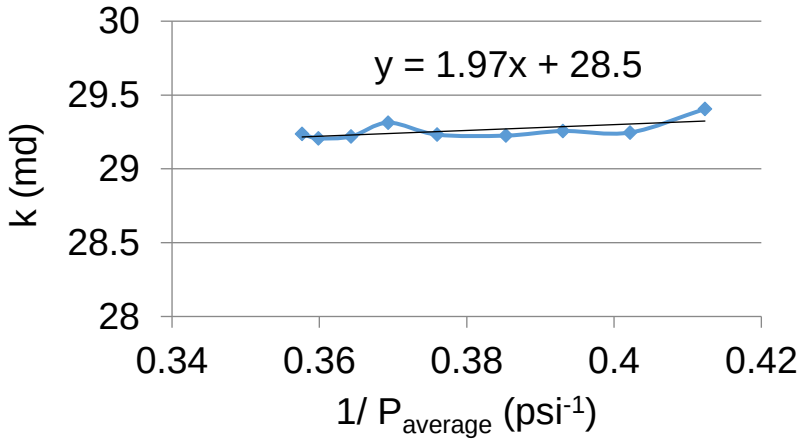

Figure 4.29 Permeability vs reciprocal pressure for unfractured permeability measurement for FRAC-11 experiment

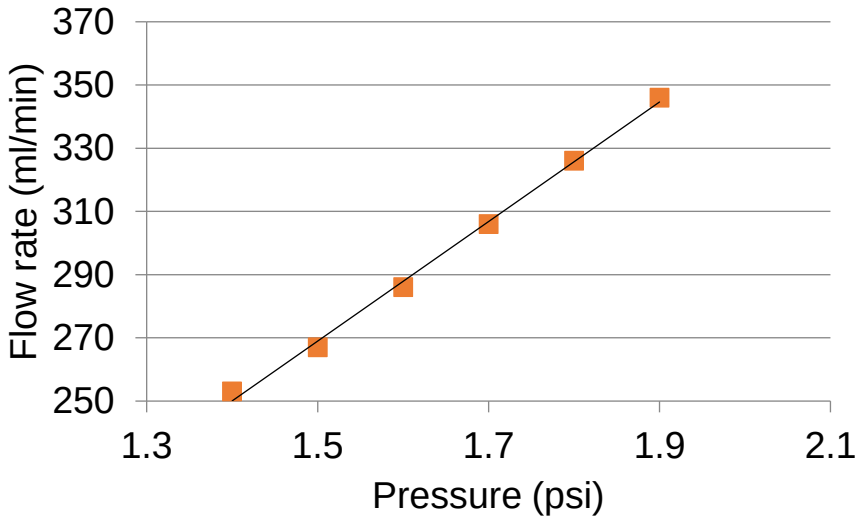

Figure 4.30 Air flow rate vs pressure drop for fractured rock in FRAC-11 experiment

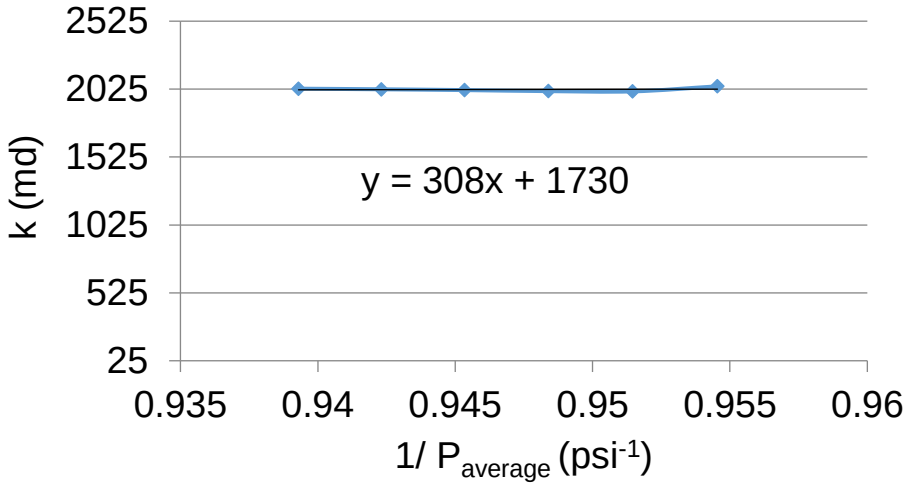

Figure 4.31 Permeability vs reciprocal pressure for fractured permeability measurement for FRAC-11 experiment

4.4.2 Oil saturation

The core was saturated with dead crude oil after being vacuumed for 7 hours. The pore volume of the rock is 86.9 mL and porosity is 28%. The core was placed in the 78 Celsius oven and was aged for ten days. The core was flooded with dead crude oil with a viscosity of 11 cp at four flow rates (0.01 ml/min, 0.03 ml/min, 0.5 ml/min, 1 ml/min). The confining stress was maintained at 500 psi using a hydraulic pump.

The oil permeability was around 500 md for the whole core. The pressure drops measured between the pressure taps did not add up to the whole pressure drop. The raw data can be seen in Figure 4.31. Figure 4.32 shows only the whole pressure drop for the different rates. The single phase oil permeability calculated for the different rates are given in Table 4.3. As shown below, the fracture aperture is 0.0057 cm and its permeability is 230 Darcy.

$$Q = -\frac{kA}{\mu}\left(\frac{P_i - P_o}{L}\right) k = \frac{Q\mu L}{A(P_i - P_o)} = 245 * \frac{(0.5\frac{ml}{\min} * 11cp * 29.51cm)}{(10.75cm^2 * 6.8\,psi)} = 530md \quad (3.7)$$

$$b = \left(3\pi D k_{eff}\right)^{\frac{1}{3}} = \left(3 * \pi * 0.037m * 0.53Darcy * \frac{9.87E^{-13}m^2}{1Darcy}\right)^{\frac{1}{3}} = 0.000057m \quad (3.8)$$

$$k_{fracure} = \frac{A_{total}k_{effective} - 2A_{matrix}k_{matrix}}{A_{fracture}} = \quad (3.9)$$

$$\frac{(10.75cm^2 * 0.53Darcy - (10.75cm^2 - 3.7cm * 0.0057cm) * 0.028\,\text{Darcy}}{3.7cm * 0.0057cm} = 230Darcy$$

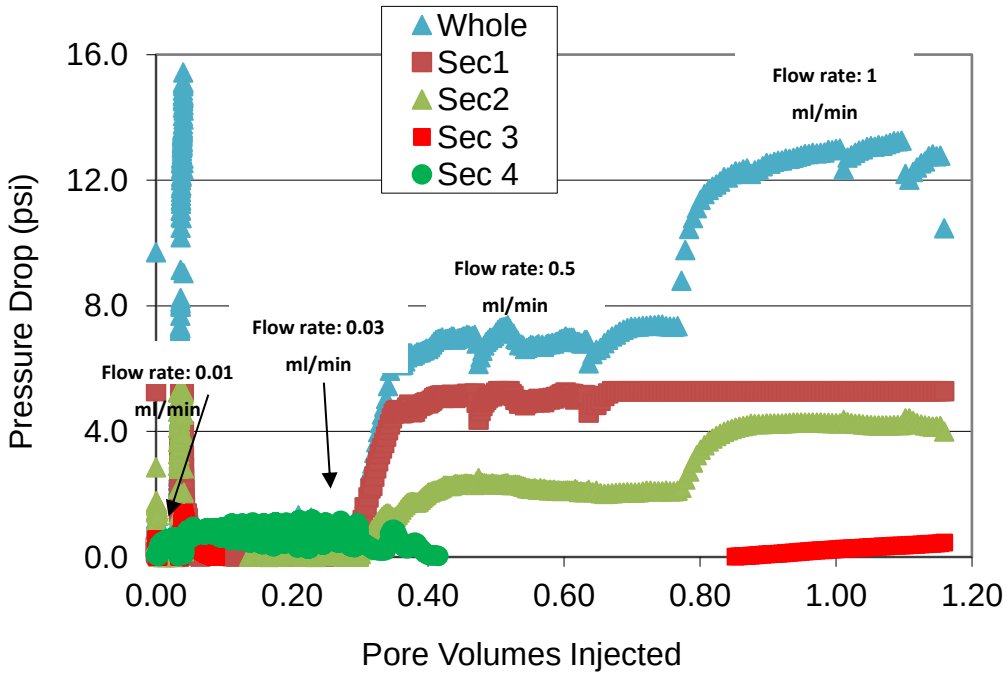

Figure 4.32 Oil flood pressure drop for FRAC-11 experiment, all sections

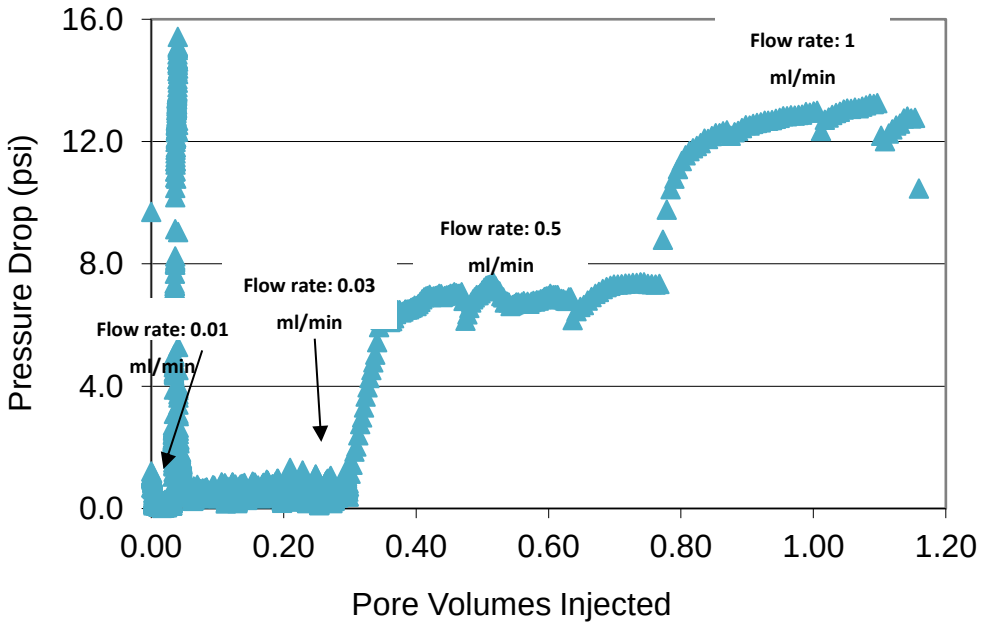

Figure 4.33 Whole oil flood pressure drop for FRAC-11 experiment

Table 4.3 Oil Permeability measurements at several flow rates in FRAC-11 experiment

Flow rate (ml/min)	Pressure drop (psi)	Permeability (md)	Pressure gradient (psi/ft)
0.01	0.13	554	0.13
0.03	0.55	393	0.57
0.5	6.8	530	7.03
1	13	554	13.4

4.4.3 Waterflood

The core was water flooded with 85,000 ppm NaCl brine at a flow rate of 0.3 mL/min, equivalent to an interstitial velocity of 4.78 ft/day based on the whole core area

of 10.75 cm^2 and 27% porosity. The oil saturation after the water flood was 91.4%. Figure 14 shows the oil saturation, oil cut, and oil recovery from the water flood. The water flood pressure drop is shown in Figure 15. The apparent permeability to water was 43 md using a pressure drop of 2 psi and a water viscosity of 0.433 cp. As in the single phase oil flood, the pressure drops from the sections of the core do not add up to the whole pressure drop.

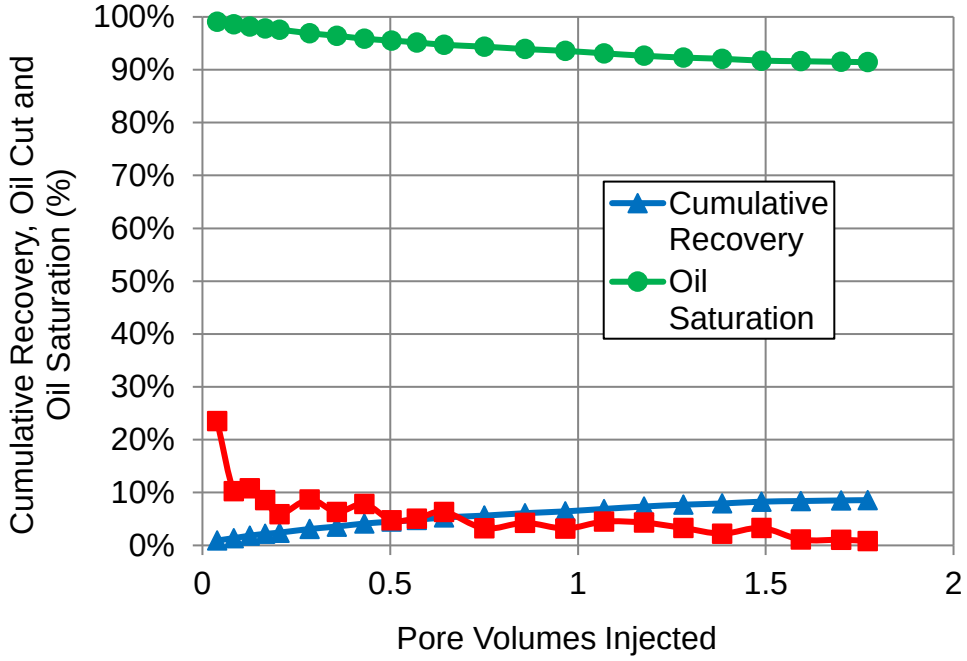

Figure 4.34 Waterflood oil cut, recovery, and saturation for FRAC-11 experiment

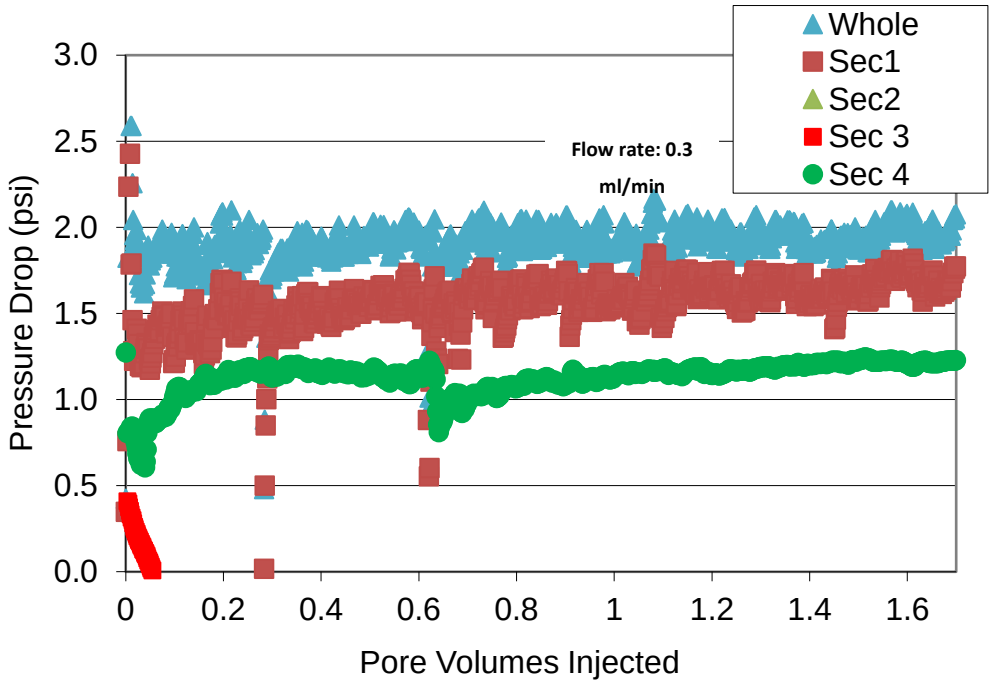

Figure 4.35 Waterflood pressure drop for FRAC-11 experiment

4.4.4 Chemical flood

The oil recovery from the chemical flood can be seen in Figure 4.34. 41% of the oil remaining after the waterflood was recovered. The core was flooded with a surfactant solution with a salinity of 85,000 ppm TDS, at a flow rate of 0.01 ml/min. This is equivalent to an interstitial velocity of 0.16 ft/day based on the cross sectional area of the whole core and 28% porosity, and 22.8 ft/day based on the estimated fracture area alone. A 1 PV surfactant slug was injected followed by a brine drive of 65,000 ppm NaCl. The oil solubilization ratio at 85,000 ppm is estimated to be 8.7 and the IFT between oil and the microemulsion calculated from the Huh equation is 0.004 dynes/cm.

Figure 4.35 shows the pressure drop during the chemical flood. The sectional pressure drops do not add up to the whole pressure drop. The whole pressure drop was around 0.5 psi/ft. This pressure drop of 0.5 psi is significantly higher than the one observed at the same rate during the single phase oil flood (0.13 psi). It is also higher than the waterflood pressure drop scaled down by the 30x difference in flow rate (0.066 psi). This high pressure drop during the chemical flood shows a viscous microemulsion formed in-situ. The viscosity of the microemulsion at 85,000 ppm TDS was 30 cp. The pressure drop continued to increase during the brine drive, reaching a maximum of 0.75 psi/ft after 1 PV of brine before decreasing to 0.5 psi/ft. It is notable that although this surfactant flood used only one fourth the amount of surfactant used in FRAC-10, but the oil recovery was similar because of the higher slug salinity and as shown below the salinity gradient resulted in a very low surfactant retention.

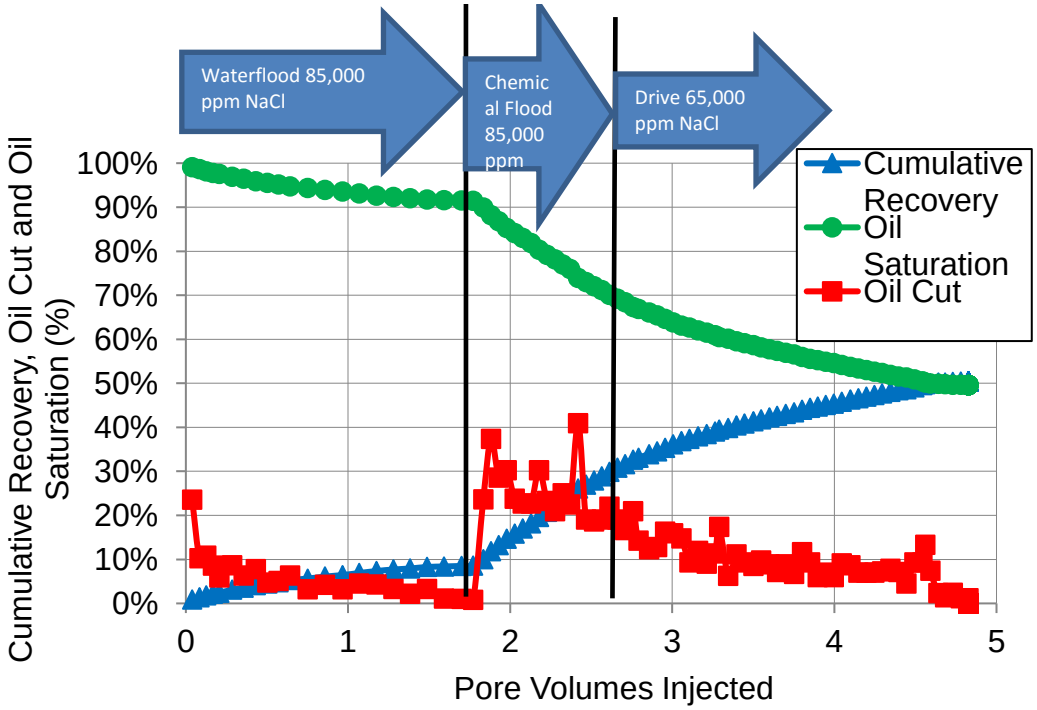

Figure 4.36 Oil cut, recovery, and saturation for entire FRAC-11 experiment

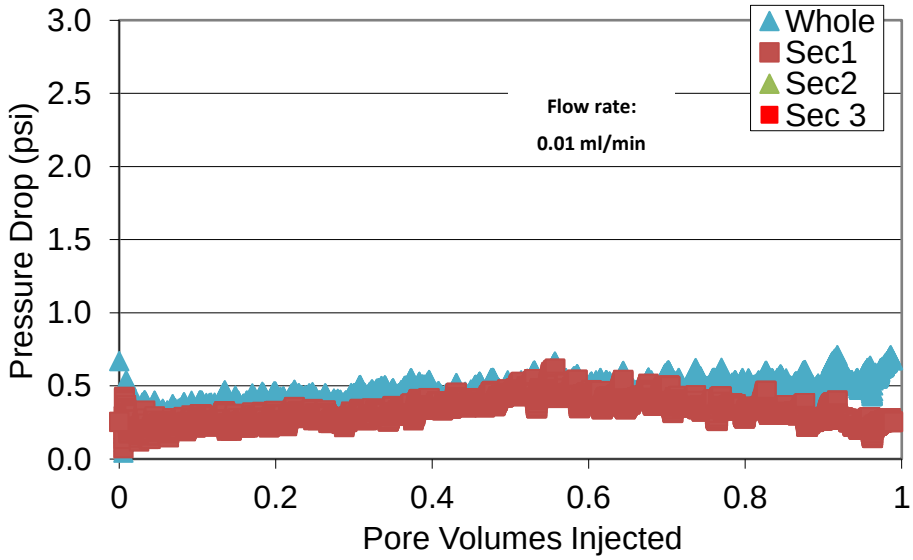

Figure 4.37 Pressure drop for FRAC-11 chemical flood

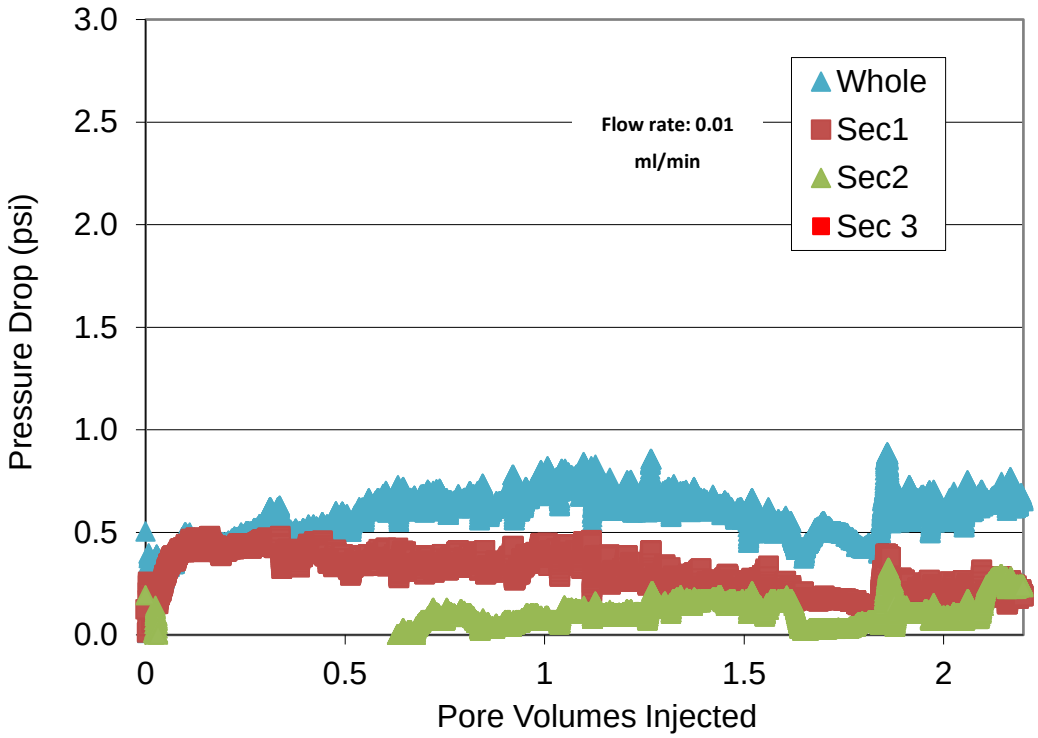

Figure 4.38 Pressure drop for FRAC-11 brine drive

4.4.5 Surfactant retention

The concentration of surfactant in the effluent was measured using the hyamine titration method. The effluent surfactant concentration can be seen in Figure 4.35, which was determined using the calibration curve seen in Figure 4.36. The surfactant retention was determined using a mass balance. Since the concentration of surfactant and volume of each test tube were known, the mass of surfactant out of the core could be determined. The mass of surfactant going into the core was assumed to be 1% throughout the chemical flood. The retention calculated was 0.108 g-surfactant/g-rock. The effluent concentration did not reach 1% concentration due to experimental error. The error is

amplified in the dilution process where each effluent sample is diluted 4x in order help with the end point interpretation when crude oil is present. Carrying out the mass balance assuming the injected concentration is the same as the maximum effluent concentration, the retention is 0.01 mg/g-rock. From this analysis, the retention values ranged between 0 and 0.11 mg/g-rock. The low retention value indicates that the use of NaOH and a salinity gradient were very effective in terms of achieving a very low surfactant retention.

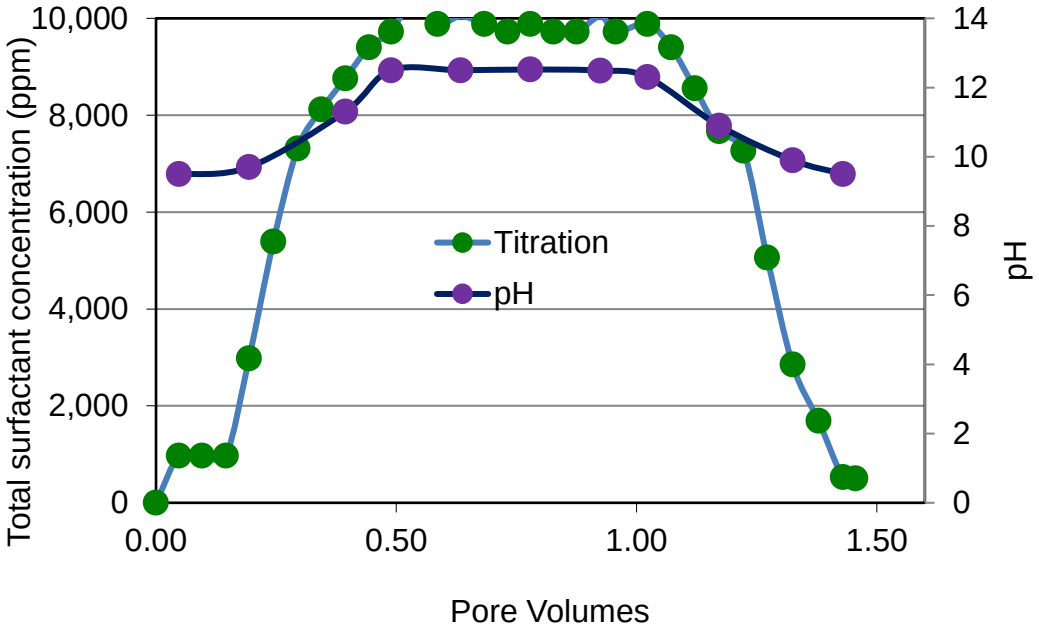

Figure 4.39 Effluent surfactant concentration

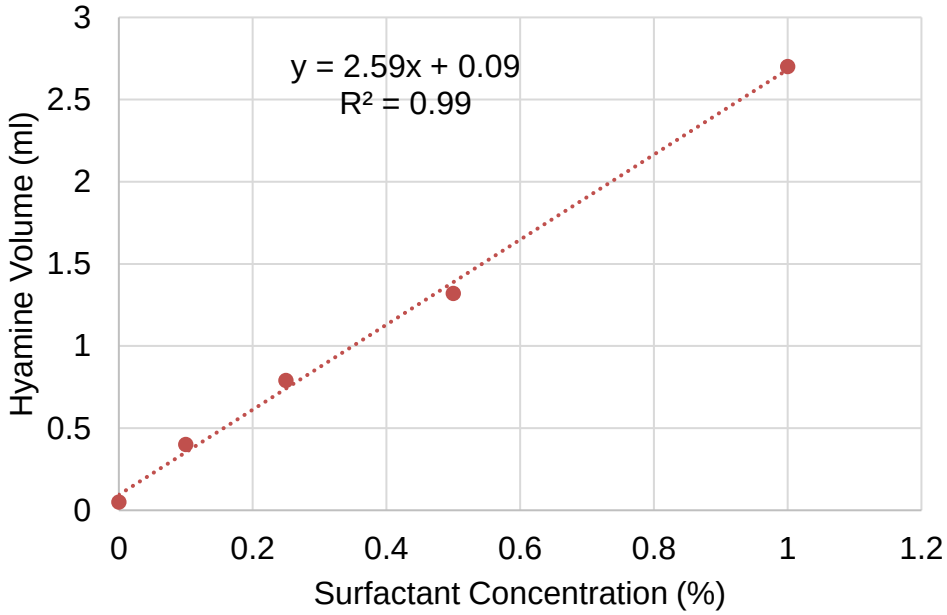

Figure 4.40 Calibration curve to measure for surfactant concentration

4.5 Chemical Flood with Spacers, 0.3 PV chemical slug, and Salinity Gradient FRAC-13

The initial objective of the FRAC-13 experiment was to test the performance of a 0.3 PV surfactant slug in a fractured Texas Cream Limestone core. The rock properties for the Texas Cream Limestone core used in the FRAC-13 experiment can be seen in Table 4.6. The oil recovery following the first 0.3 PV surfactant slug with a salinity of 85,000 ppm followed by 1.4 PV of brine with a salinity of 60,000 ppm was 27%. The optimum salinity is 80,000 ppm and the upper limit of type III is 85,000 ppm TDS. The microemulsion had a viscosity of 38 cp at 1 s^{-1} at 85,000 ppm TDS. The lower limit for

type III is 75,000 ppm TDS. NaOH was not used in the brine drive. The higher pH of the drive may have increased the surfactant retention and reduced the oil recovery.

Two more floods were done in the same core. A 0.3 PV slug followed by brine was injected at the same rate in the second flood and increased the oil recovery to 33%. The NaOH concentration in the second and third brine drives was 0.3%. The brine pH was 11.8. The flow rate of the third flood was 5 times higher (0.05 ml/min) than the first two floods; however, no significant additional oil was recovered (the effluent just looked like impure water, but not too dark). An important conclusion of this experiment was that it is a lot more efficient to inject a 0.9 PV surfactant slug followed by a brine drive than to inject three 0.3 PV surfactant slugs with brine drives in between following each slug. Comparing this experiment to FRAC 11, where surfactant injection was continuous, it can be said that if other variables are kept the same (even the mass of surfactant injected) oil will be recovered faster with a 1 PV slug rather than three 0.3 PV slugs.

While the results of this FRAC-13 experiment are valid, no alkali was used during the first brine drive. The decrease in pH likely caused the surfactant retention to be higher and the oil recovery to be lower than they would have been if alkali had been included in the brine drive. This is because surfactant retention increases as pH decreases. The retention for this experiment was measured to be 0.2 mg/g-rock. While a lot of oil was left behind (66.9%), the amount of oil recovered by the first chemical flood and brine drive (27%) was significant considering only 0.3 PV of surfactant at 1% concentration was used.

4.5.1 Air permeability

The air permeability was measured at 1000 psi confining pressure before the core was cut. Figure 4.38 shows the pressure drop at different flow rates. The air permeability was determined to be 19 md from the intercept of permeability vs reciprocal pressure data plotted in Figure 4.39 to account for the Klinkenberg effect.

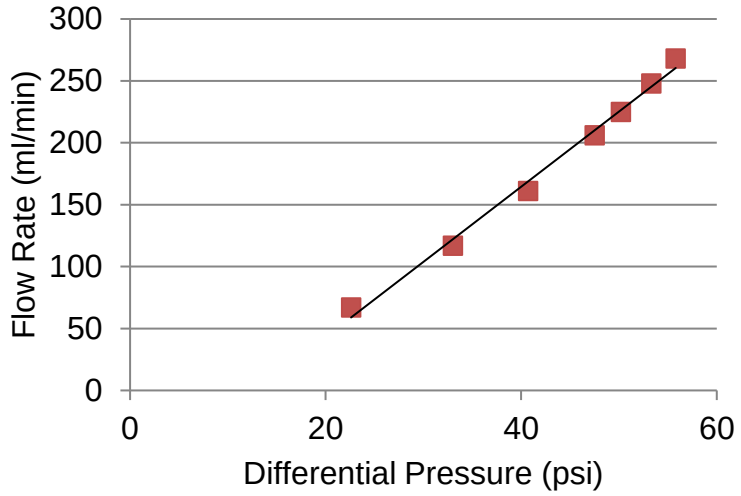

Figure 4.41 Flow rate vs pressure drop to determine rock matrix permeability

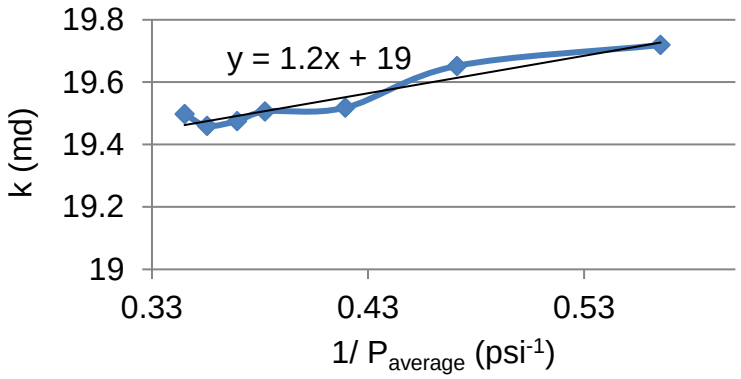

Figure 4.42 Permeability vs average pressure to determine rock matrix permeability

4.5.2 Oil saturation

The core was saturated with dead crude oil. The pore volume of the rock was 94.4 mL and porosity is 30%. The core was placed in the 78 Celsius oven and was aged for four days. The core was flooded with dead crude oil with a viscosity of 11 cp at a rate of 0.5 and 0.2 ml/min while the confining pressure was increased in steps. The flow rate was decreased because the oil column was running out of oil. The goal was to achieve a fracture permeability on the order of 10,000 times that of the rock matrix permeability. An effective permeability to oil of 340 md would achieve this result. Table 4.4 shows the confining pressure increments as well as the calculated effective permeabilities.

A multi-rate permeability test followed the fracture aperture setup. Figure 9 shows the pressure drops during the oil flood at different rates (0.05, 0.02, 0.08, and 0.01 ml/min). The permeability of the fracture was determined the following way using the equations in Chapter 2:

$$Q = -\frac{kA}{\mu}\left(\frac{P_i - P_o}{L}\right) k = \frac{Q\mu L}{A(P_i - P_o)} = 245 * \frac{(0.05\frac{ml}{\min} * 11\text{cp} * 29.9cm)}{(11.04cm^2 * 1psi)} = 350md \quad (3.10)$$

$$b = \left(3\pi D k_{eff}\right)^{\frac{1}{3}} = \left(3 * \pi * 0.0375m * 0.35Darcy * \frac{9.87E^{-13}m^2}{1Darcy}\right)^{\frac{1}{3}} = 0.000049m \quad (3.11)$$

$$k_{fracure} = \frac{A_{total}k_{effective} - 2A_{matrix}k_{matrix}}{A_{fracture}} = \quad (3.12)$$

$$\frac{(11.04cm^2 * 0.34Darcy - (11.04cm^2 - 3.75cm * 0.0049cm) * 0.019\,\text{Darcy}}{3.75cm * 0.0049cm} = 184Darcy$$

Table 4.4 Permeability for different confining pressures in FRAC-13 experiment

Flow rate (ml/min)	Confining stress (psi)	Pressure drop (psi)	Permeability (md)	Pressure gradient (psi/ft)
0.8	100	0.54	10300	0.58
0.5	150	0.52	6700	0.55
0.5	200	0.92	3800	0.98
0.5	250	1.89	1850	2.02
0.5	300	3.1	1130	3.3
0.2	325	1.8	780	1.91
0.2	350	2.16	650	2.3
0.2	400	4.1	340	4.3

Table 4.5 shows the calculated permeabilities at the different imposed flow rates during the multi-rate oil permeability test. The measured permeabilities at 0.05 and 0.08 agree with each other. The measured permeability at 0.02 is higher than expected, but there is more error and the pressure takes a very long time to equilibrate at such low rates. At 0.01 ml/min, the pressure reading for the whole core was 0.01 psi and very slowly creeping up. The value is not reported in the table.

Table 4.5 Oil Permeability measurements at several flow rates in FRAC-13 experiment

Flow rate (ml/min)	Pressure drop (psi)	Permeability (md)
0.05	1	349
0.02	0.3	465
0.08	1.8	310

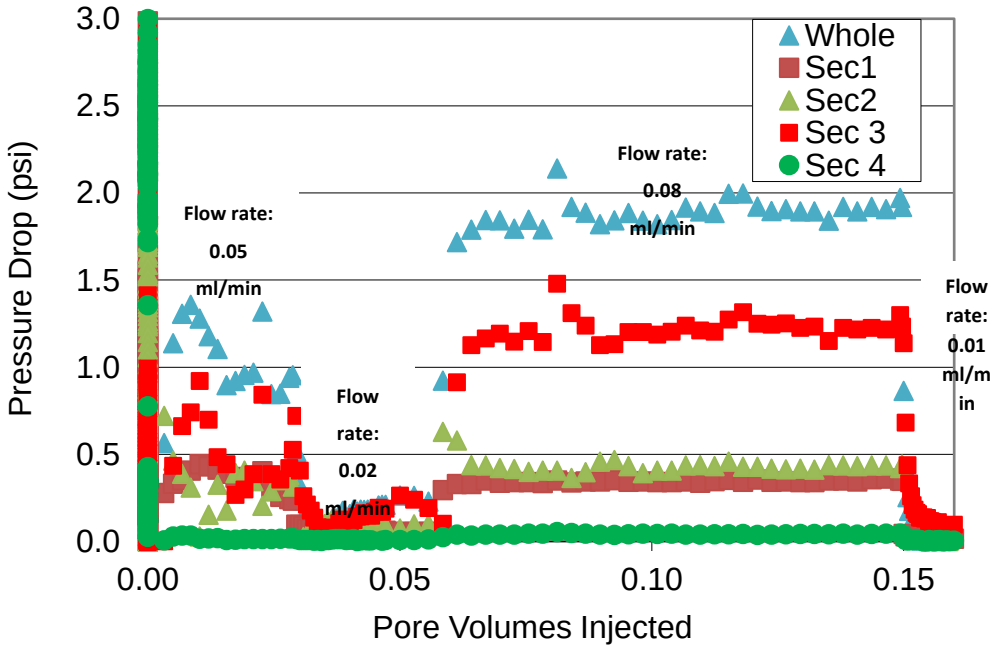

Figure 4.43 Pressure drop during single phase oil flood

4.5.3 Waterflood

The core was water flooded with 85,000 ppm NaCl brine at a flow rate of 0.3 mL/min, equivalent to an interstitial velocity of 4.12 ft/day based on the whole core. The oil saturation after the water flood was 93.6%. Figure 4.41 shows the oil saturation, oil cut, and oil recovery from the water flood. The water flood pressure is shown in Figure 4.42. The apparent permeability to water was 35 md using a pressure drop of 2.5 psi and a water viscosity of 0.433 cp. As in the single phase oil flood, the pressure drops from the sections of the core do not add up to the whole pressure drop. There is a lot of scatter in the data, making it hard to determine the pressure drop precisely.

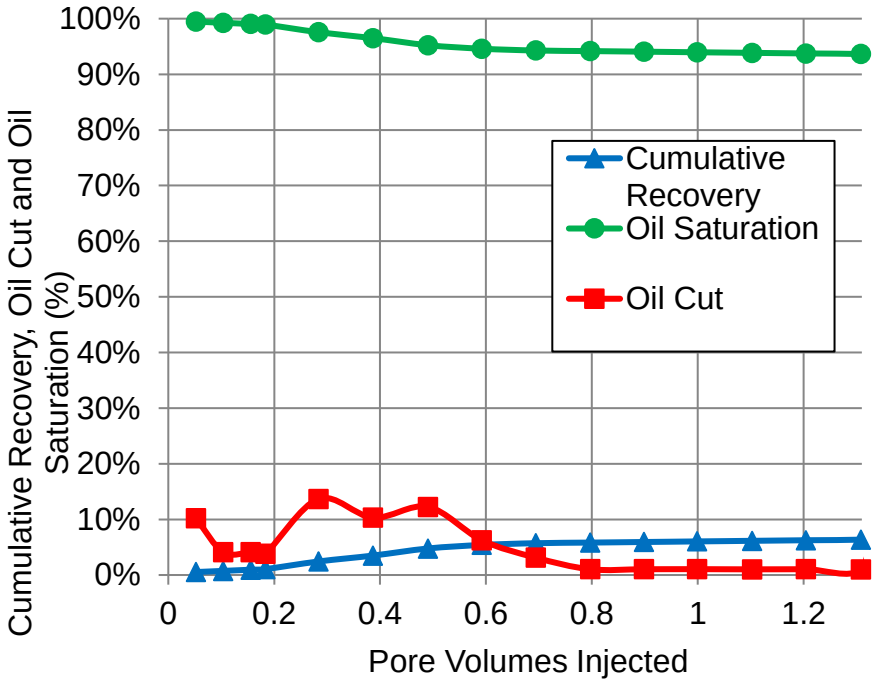

Figure 4.44 Waterflood oil cut, saturation, and recovery for FRAC-13 experiment

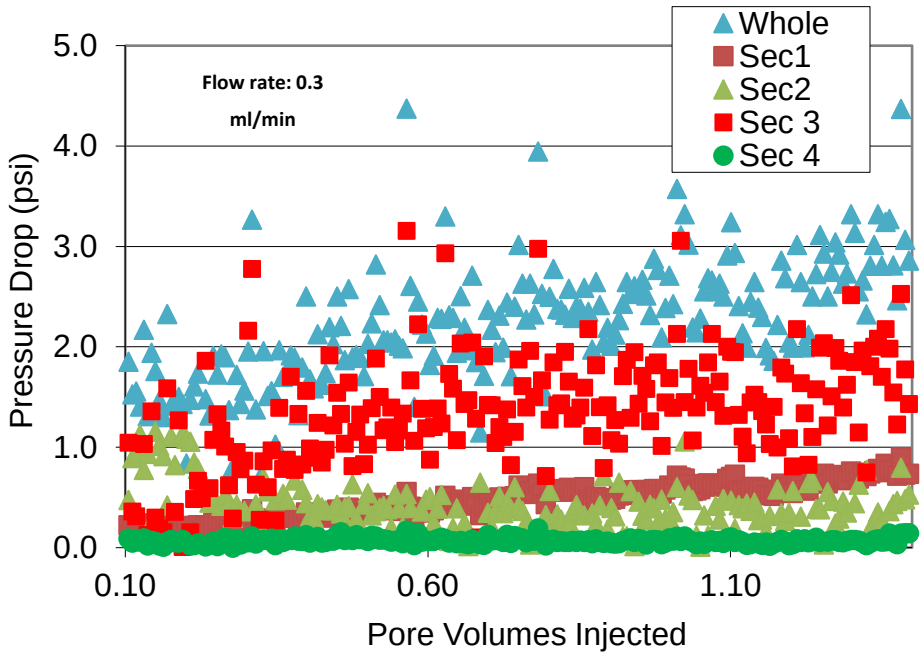

Figure 4.45 Waterflood pressure drop for FRAC-13 experiment

4.5.4 Chemical Flood

The oil recovery from the chemical flood can be seen in figure 4.43. The oil recovery was 33% after 6.5 PV. Three separate chemical floods were carried out on this core, one after the other. For each flood, the core was flooded with a surfactant solution that has 85,000 ppm TDS, at a rate of 0.01 ml/min. This is equivalent to 0.14 ft/day based on the cross sectional area of the whole core and porosity of 30%, and 25.6 ft/day based on the estimated fracture area alone. A slug of 0.3 pore volumes of surfactant was injected into the core during each chemical flood. The slugs were followed by a brine drive of 65,000 ppm NaCl. The oil solubilization ratio at 85,000 ppm is estimated to be 8.7 and the IFT between oil and the microemulsion calculated from the Huh equation is 0.004 dynes/cm. Most of the oil, 27%, was recovered during the first chemical flood and brine drive. The second chemical flood recovered about 4% of the oil, and the last

chemical food recovered nearly no oil despite it being carried out at a flow rate 5X (0.05 ml/min) that of the previous two. The efficiency of the flood appears to depend in part on the initial oil saturation.

Figure 4.44 shows the pressure drop during the chemical floods and subsequent brine drives. There is so much scatter in the data that the pressures are hard to determine precisely. Nevertheless, the pressure is lower than the values expected, with a whole pressure drop of about 0.1 psi/ft on average, which would give a permeability of 2 Darcy for a 30 cp fluid. I was expecting pressure measurements on the order of 0.5 psi/ft. The pressure sections do not add up, and the scatter on all the sections is so high that they are not very useful in determining section permeabilities. Figure 4.45 shows the same pressure data for the whole core without the sectional pressure drops. Still, there are clear pressure increases whenever surfactants are injected, reaching about 0.2-0.3 psi/ft vs 0.05 psi/ft for water only. This is again indication of a viscous microemulsion forming in-situ.

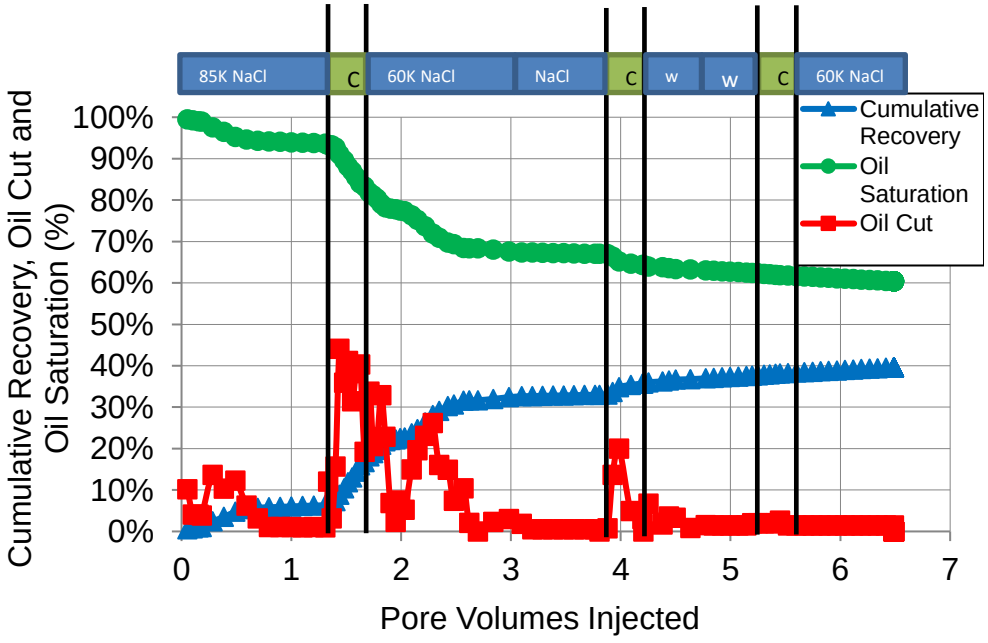

Figure 4.46 Oil cut, saturation, and recovery for FRAC-13 experiment

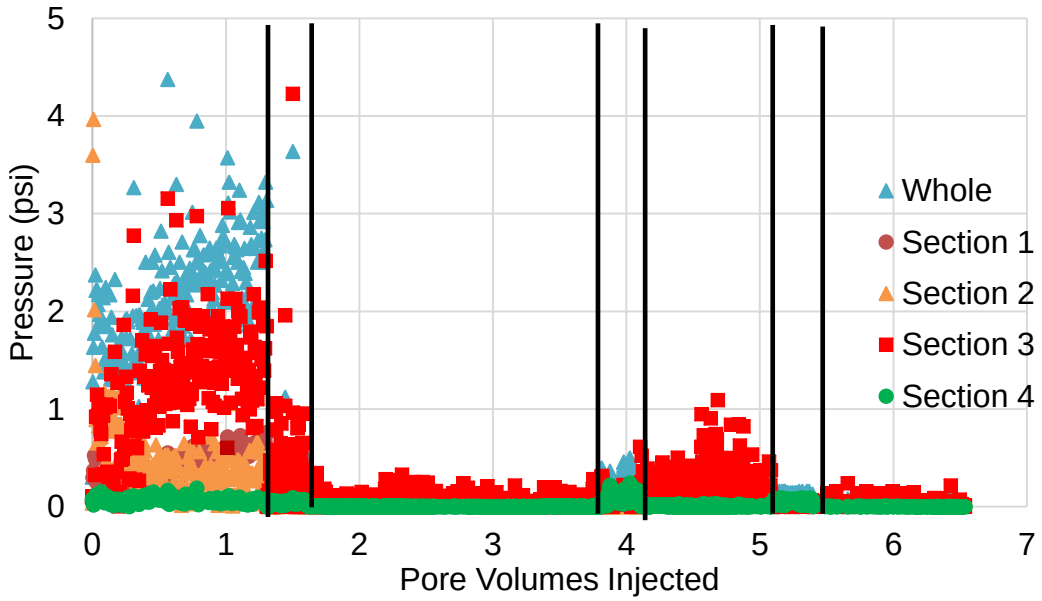

Figure 4.47 Entire experiment pressure drop for FRAC-13

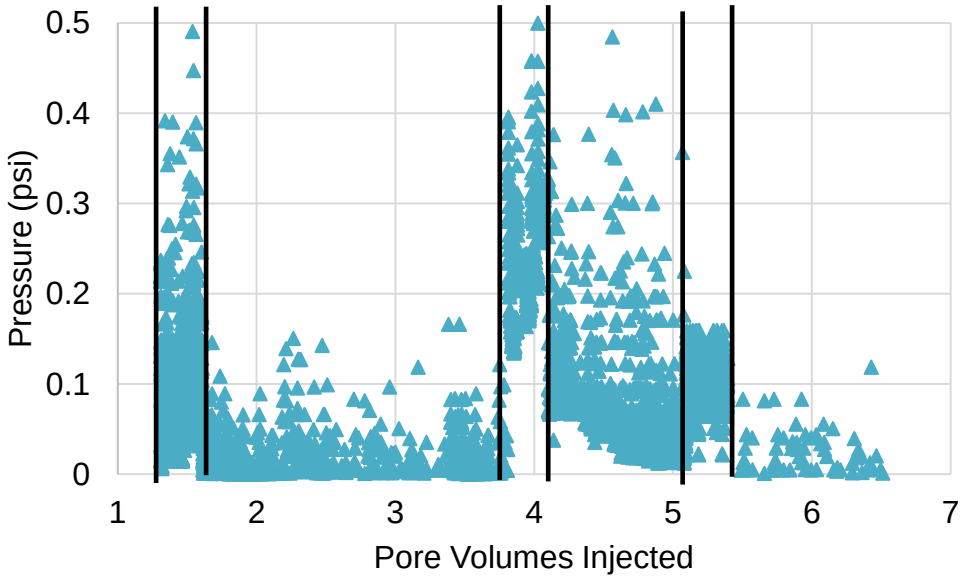

Figure 4.48 Entire experiment pressure drop for FRAC-13 whole pressure drop only

4.5.5 Surfactant retention

The effluent surfactant concentration was measured using the hyamine titration method. The effluent surfactant concentration can be seen in Figure 4.46, which was determined using the calibration curve seen in Figure 4.47. The surfactant retention was determined using a mass balance. Since the concentration of surfactant and volume of each test tube was known, the mass of surfactant out of the core could be determined. The mass of surfactant going into the core was assumed to be 1% throughout the chemical flood. The retention calculated was between 0.14 and 0.2 g-surfactant/g-rock for the first slug, and 0.11 and 0.18 g-surfactant/g-rock for the second slug. The error ranges were determined with the minimum increment of hyamine added during the titration, 20µl, which translates to 256 ppm of surfactant using the calibration curve. The low retention value indicates that the use of NaOH and a salinity gradient are very favorable to achieve surfactant retention with the formulation, oil, and rock used in this experiment. The brine drive during the first chemical flood did not include NaOH. The pH of the flood can be seen decreasing from 12.6 during the maximum to 9 after the chemical slug. The second brine drive did include NaOH at a concentration of 0.3wt%. The pH only decreases to 11.9 after chemical flood.

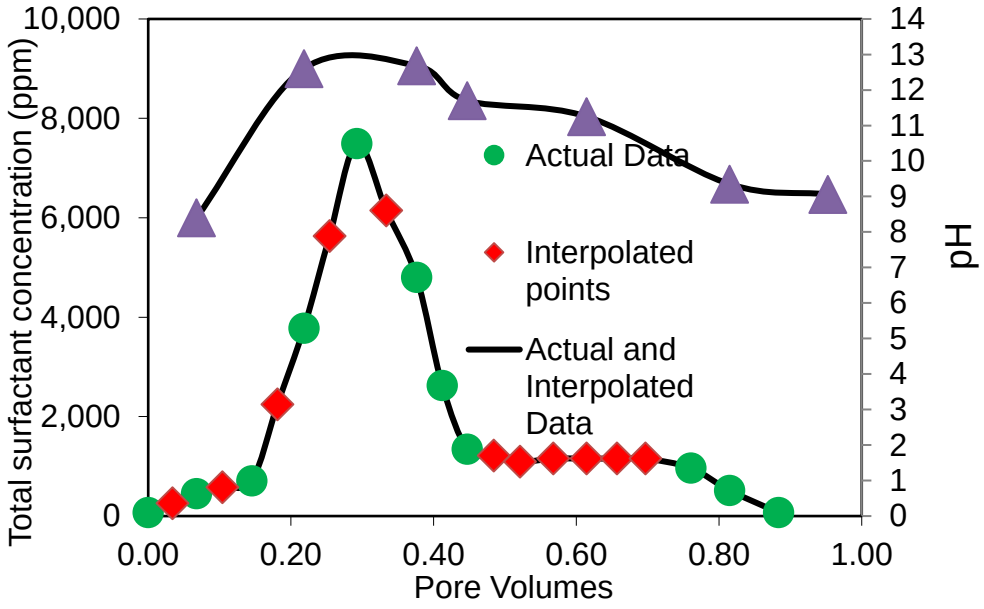

Figure 4.49 Surfactant concentration and pH effluent of effluent tubes for first chemical slug

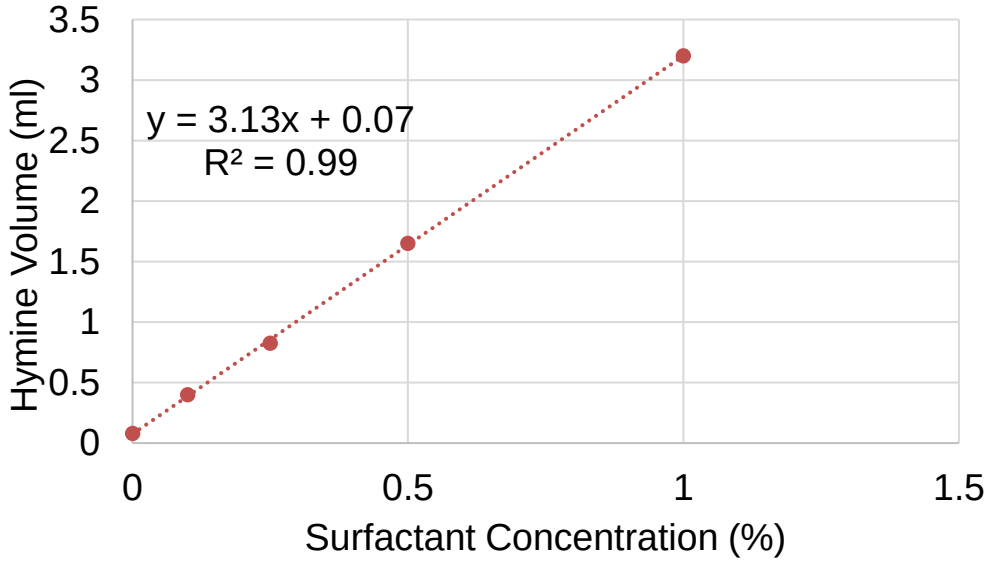

Figure 4.50 Calibration curve to determine surfactant concentration

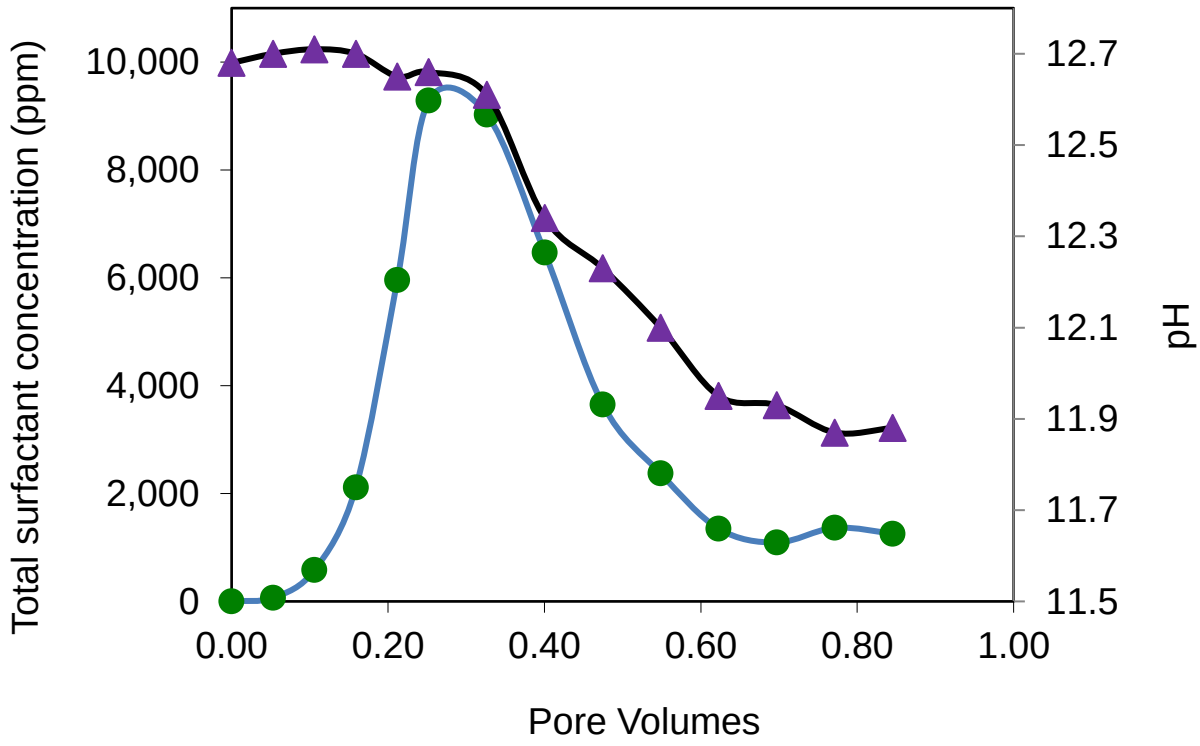

Figure 4.51 Effluent surfactant concentration and pH for second chemical slug

4.6 Chemical Flood with Spacers, varying fracture aperture FRAC-14

The objective of the FRAC-14 experiment was to test the oil recovery from a fractured core with a lower fracture permeability of 100 Darcies and a lower fracture to matrix contrast compared to previous experiments. The FRAC-14 experiment had a contrast of 1,000 compared with 10,000 for FRAC-11. The properties of the core used in this experiment are shown in Table 4.11.

Air permeability

The air permeability was measured at 1000 psi confining pressure before the core was cut. Figure 4.49 shows the pressure drop at different flow rates. The air permeability was determined from the intercept of permeability vs reciprocal pressure data plotted in Figure 4.50 to account for the Klinkenberg effect. The air permeability was 18 md.

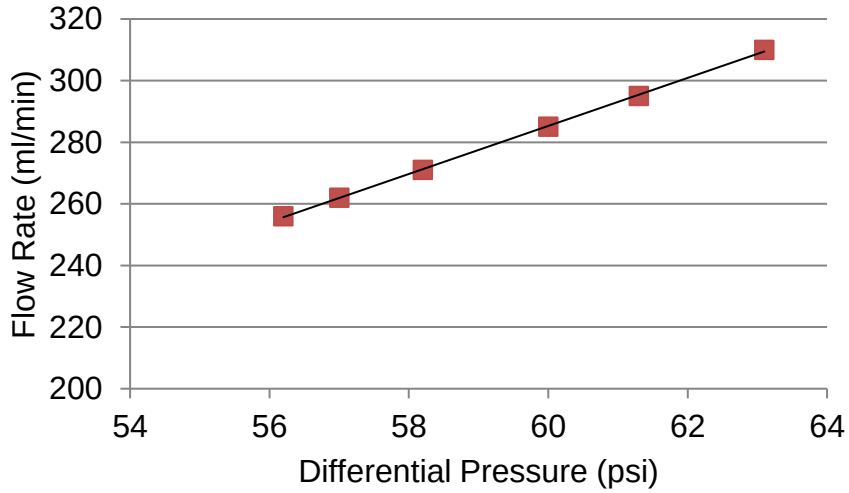

Figure 4.52 Flow rate vs pressure drop to determine rock matrix permeability

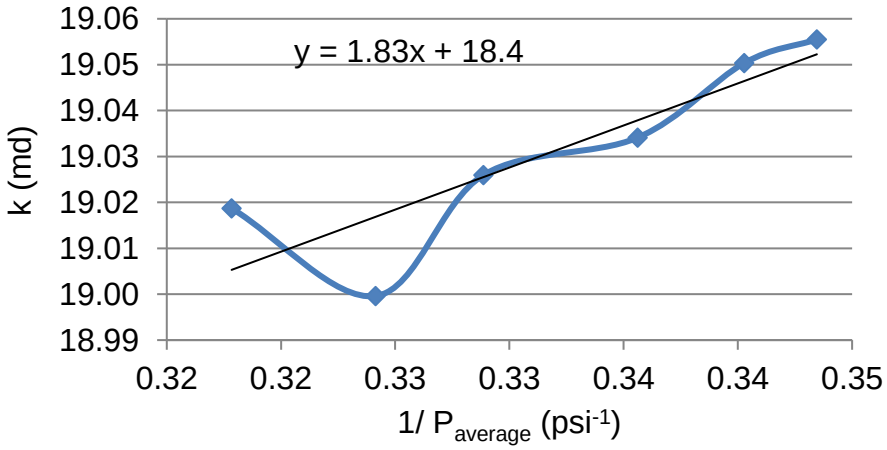

Figure 4.53 Permeability vs average pressure to determine rock matrix permeability

First oil saturation

The core was flooded with dead crude oil with a viscosity of 11 cp at rates of 0.035, 0.01, 0.02, and 0.04 ml/min. The goal was to achieve a fracture permeability of 50 Darcy. An effective oil permeability of 40 md would have achieved this result. After increasing the confining stress in increments of 50 psi, a permeability of 50 md was achieved at 1800 psi. This step took 4 days because it takes a long time for the pressure to equilibrate and it also required more crude oil, which was of limited supply. Table 4.6 shows the calculations for this step, and Figure 4.51 shows this first oil multi-rate test. The pressures between the sections don't make too much sense as they don't add up to the total pressure. The calculations were carried out with the equations in Chapter 2, namely:

$$Q = -\frac{kA}{\mu}\left(\frac{P_i - P_o}{L}\right) k = \frac{Q\mu L}{A(P_i - P_o)} = 245 * \frac{(0.02\frac{ml}{\min} * 11\text{cp} * 29.8cm)}{(10.75cm^2 * 2.6psi)} = 54md \quad (3.13)$$

$$b = \left(3\pi D k_{eff}\right)^{\frac{1}{3}} = \left(3 * \pi * 0.037m * 0.05Darcy * \frac{9.87E^{-13}m^2}{1Darcy}\right)^{\frac{1}{3}} = 0.000026m \quad (3.14)$$

$$k_{fracure} = \frac{A_{total}k_{effective} - 2A_{matrix}k_{matrix}}{A_{fracture}} = \quad (3.15)$$

$$\frac{(10.75cm^2 * 0.6Darcy - (10.75cm^2 - 3.7cm * 0.0026cm) * 0.018\text{Darcy}}{3.7cm * 0.0026cm} = 22Darcy$$

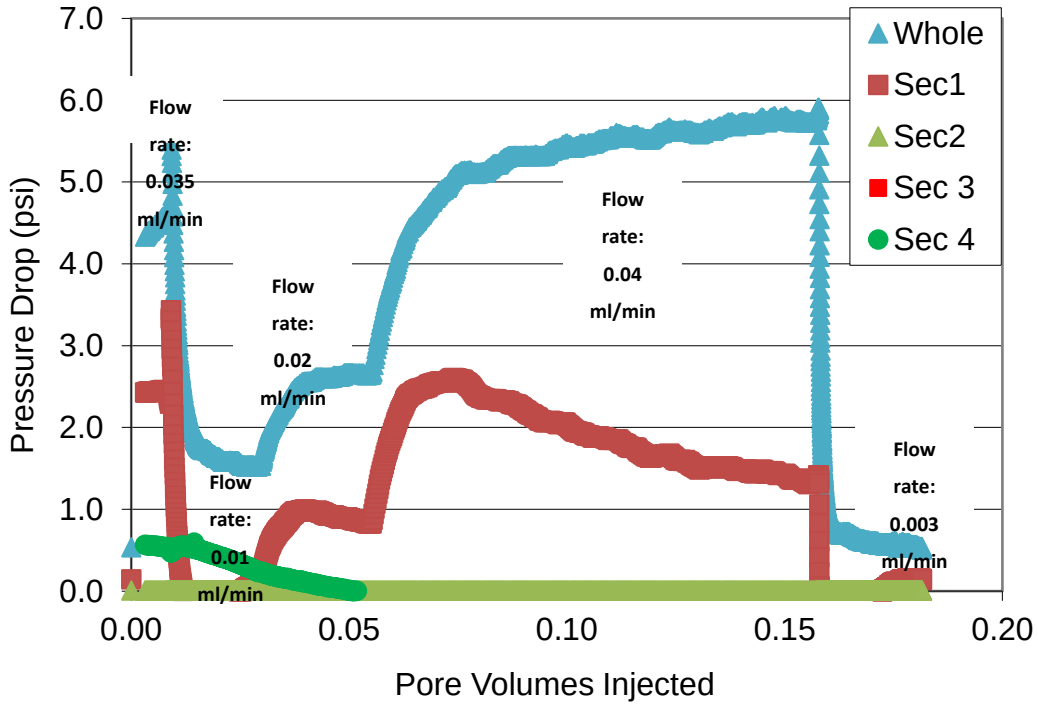

Figure 4.54 Pressure drops during first oil flood to determine rock permeability for FRAC-14 experiment

Table 4.6 First oil permeability measurements at several flow rates in FRAC-14 experiment

Flow rate (ml/min)	Pressure drop (psi)	Permeability (md)
0.035	4.6	55
0.01	1.5	47
0.02	2.6	54
0.04	5.8	50
0.003	0.36	40

First waterflood

The morning after the oilflood, a waterflood of 85,000 ppm NaCl was performed. Unfortunately, the fracture had closed overnight. The pressure drop reached 12 psi at a

flow rate of 0.1 ml/min, which was subsequently lowered to 4 psi at 0.01 ml/min, and then 1 psi at 0.005 ml/min. Figure 4.52 shows the whole pressure drop for this step, the section pressure drops were either negative, or did not add up to the total pressure drop. The biggest evidence that the fracture was indeed closed was the continued oil production. The waterflood was stopped after 0.6 PV to prevent further oil production. At the end of this waterflood, 25 ml of oil were recovered and the oil saturation was 71%. Figure 4.51 shows the oil recovery from this waterflood.

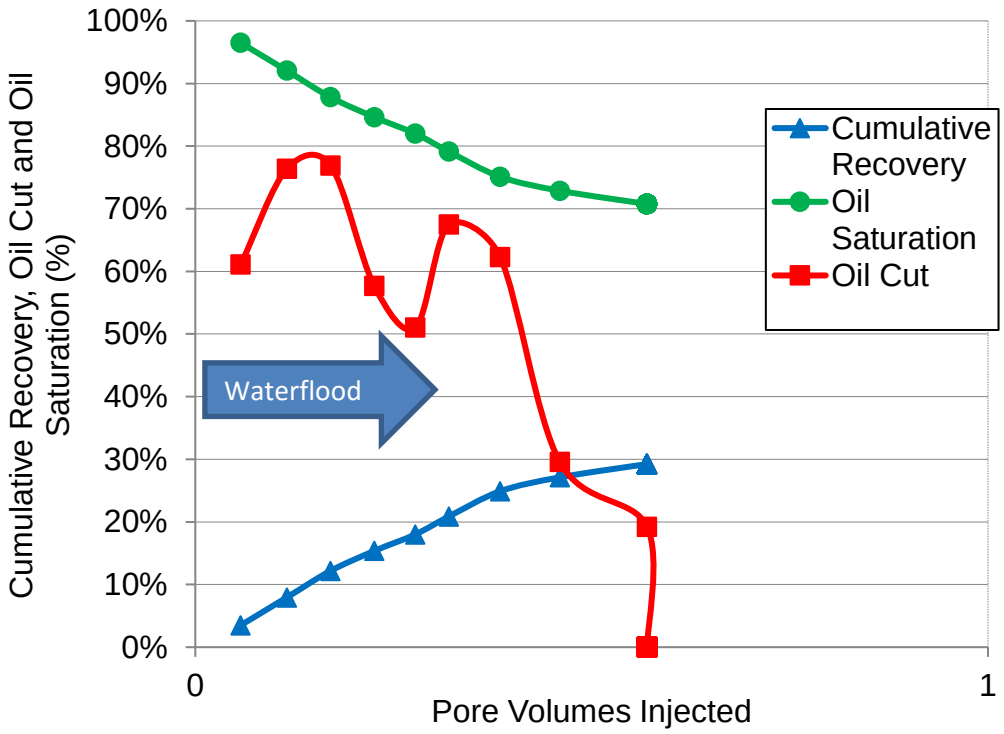

Figure 4.55 First waterflood oil cut, recovery, and saturation for FRAC-14 experiment

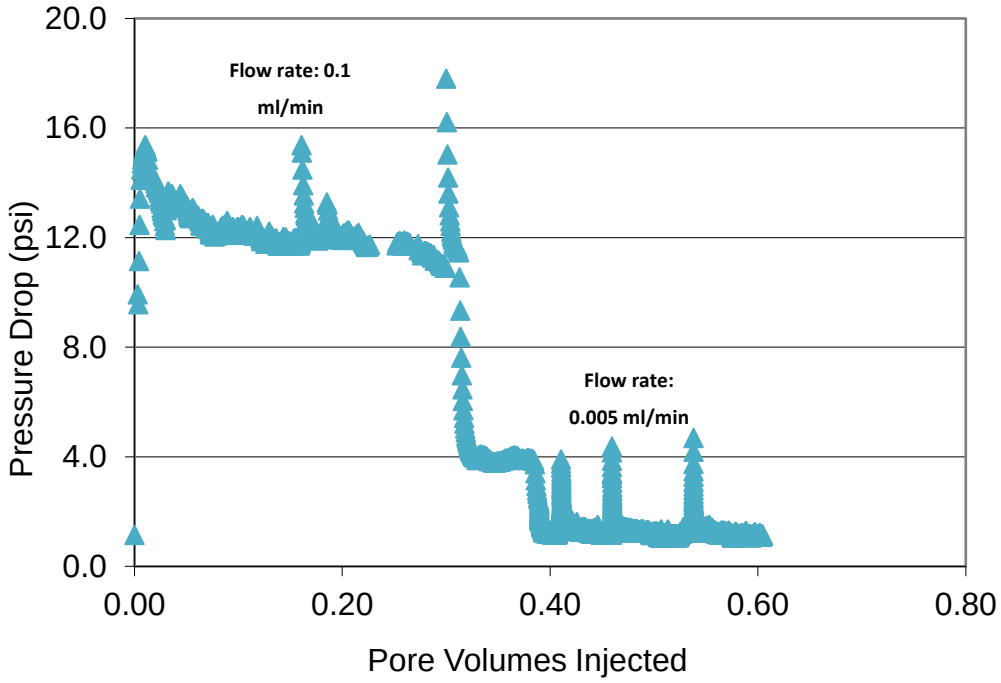

Figure 4.56 First waterflood pressure drop for FRAC-14 experiment

Second oil flood

The core was oil flooded at a constant pressure of 190 psi and a confining stress of 500 psi. 16.4 ml of water was produced and the oil saturation increased to 90%.

The confining stress was decreased to 60 psi to try to open up the fracture after the constant pressure oil flood. Oil was injected at constant rates of 0.07 and 0.09 ml/min with pressure drops of about 3.45 and 4 psi, indicating an oil permeability of about 150 md. These rates were chosen because low rates take a very long time to get to equilibrium and would have required more oil than available in the column.

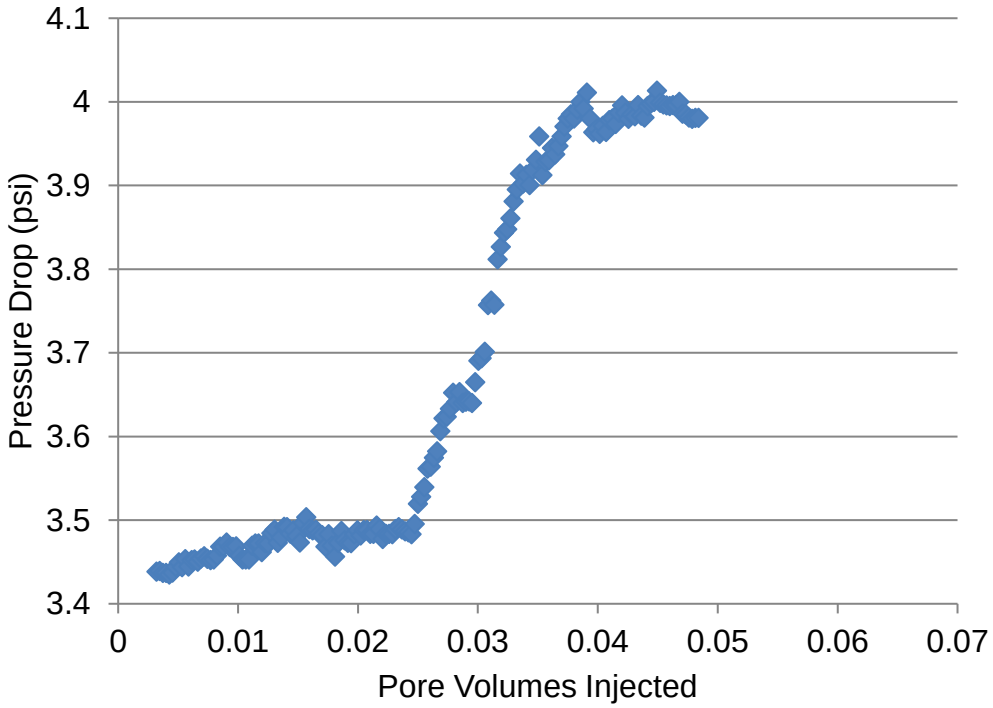

Figure 4.57 Second oil flood pressure drop for FRAC-14 experiment

Second waterflood

A second waterflood was performed after the confining stress of was reduced to 60 psi. The rate was 0.01 ml/min, and the pressure drop about 0.4 psi/ft. About 7% of the oil was recovered after 0.4 PV. The apparent permeability to water from this flood was about 4 md. The pressure drops across each section take a long time to stabilize and do not add up to the whole pressure drop.

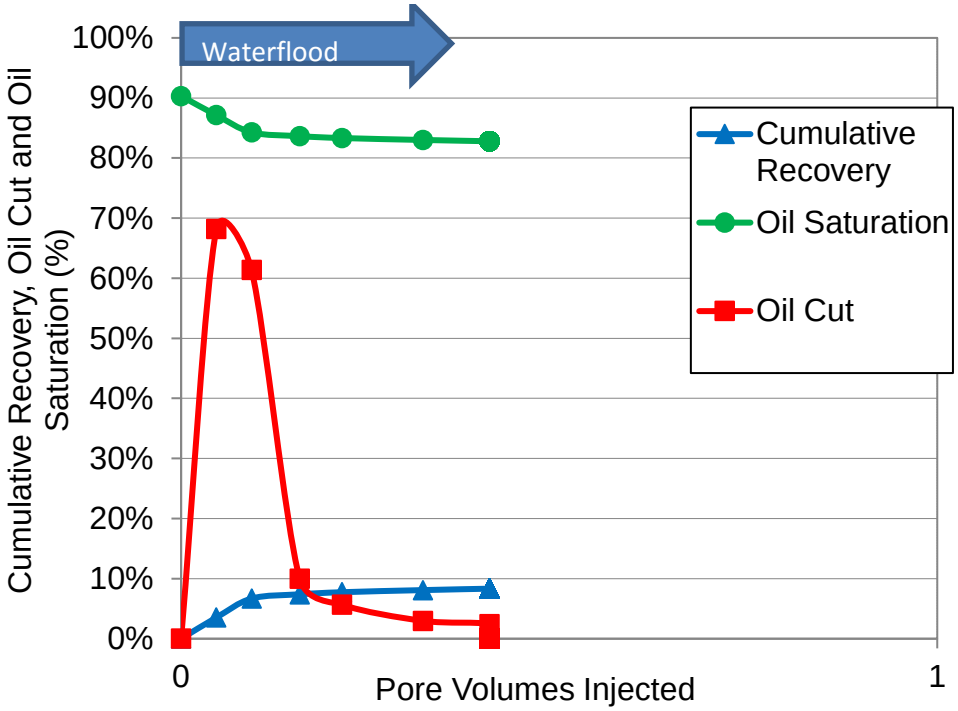

Figure 4.58 Second waterflood oil cut, recovery and saturation for FRAC-14 experiment

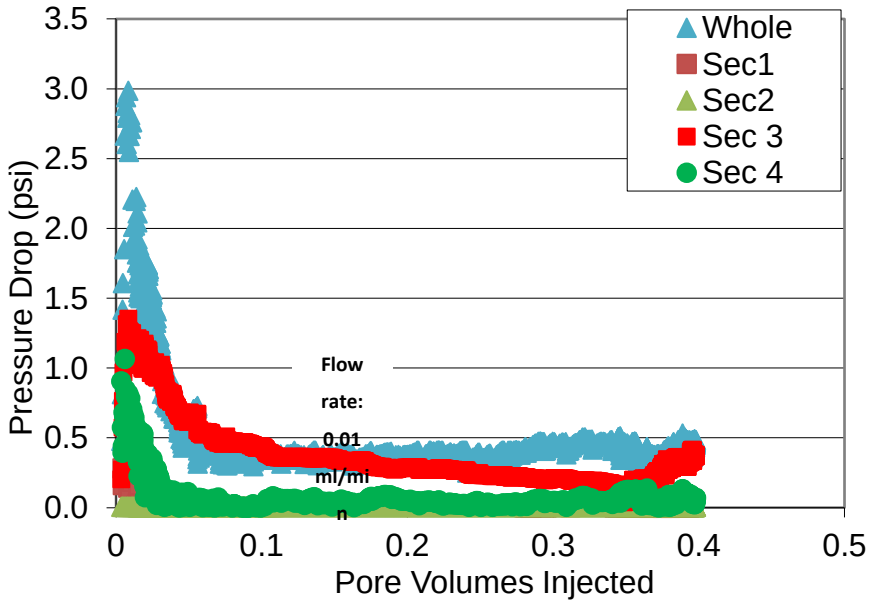

Figure 4.59 Second waterflood pressure drop for FRAC-14 experiment

Chemical flood

The oil recovery from the chemical flood can be seen in Figure 4.56. The oil recovery was 31% after 1 PV surfactant slug and 1 PV of brine drive at 0.01 ml/min. The salinity of the surfactant solution was 85,000 ppm TDS and the brine drive was 60,000 ppm. The velocity is 0.15 ft/day based on the whole core and 33 ft/day based on the fracture area. The oil solubilization ratio at 85,000 ppm is estimated to be 8.7 and the IFT between oil and the microemulsion calculated from the Huh equation is 0.004 dynes/cm.

The pressure drop at the end of the surfactant slug was about 1 psi. The pressure lines contained viscous microemulsion that had to be flushed out for accurate pressure readings at around 1.5 PV. The pressure drops along the sections did not add up to the total pressure drop during most of the flood. The pressure at the end of the brine drive was 0.25 psi compared to 0.35 psi at the end of the waterflood. This pressure drop indicates that the fracture remained open during the flood.

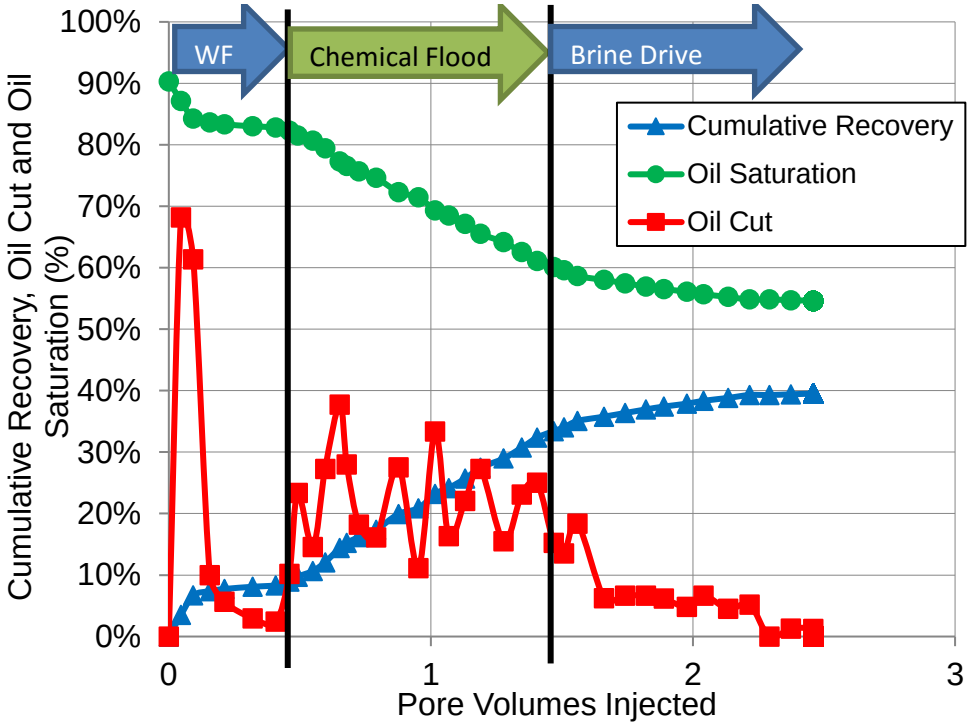

Figure 4.60 FRAC-14 oil cut, recovery and saturation

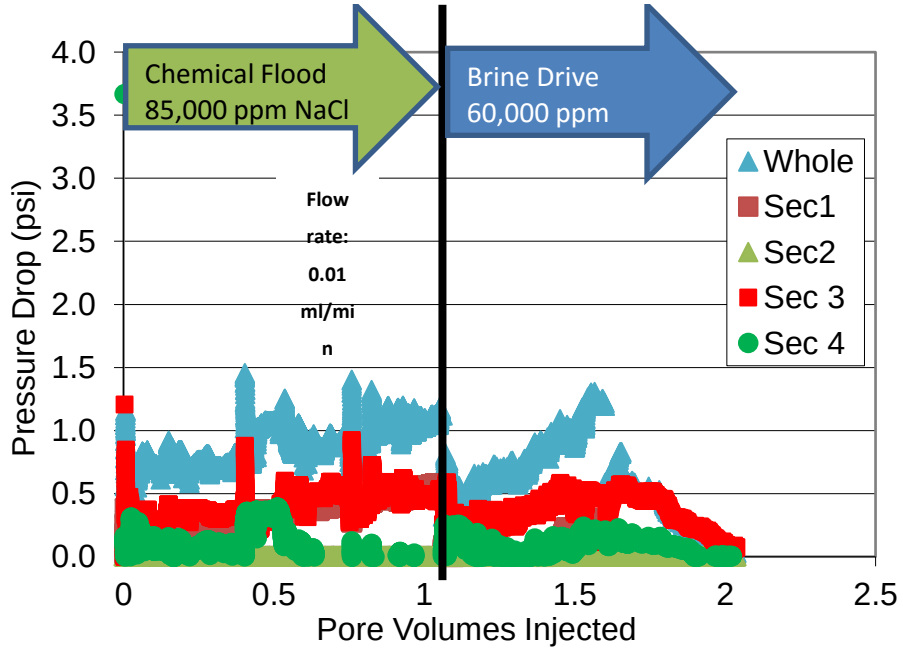

Figure 4.61 Chemical flood pressure drop

Surfactant retention

The concentration of surfactant in the effluent was measured using the hyamine titration method. The effluent surfactant concentration can be seen in Figure 4.58, which was determined using the calibration curve seen in Figure 4.59. The surfactant retention was determined using a mass balance. Since the concentration of surfactant and volume of each test tube was known, the mass of surfactant out of the core could be determined. The mass of surfactant going into the core was assumed to be 1% throughout the chemical flood. The retention was 0.07 mg/g-rock following the surfactant flood with a brine drive that included alkali. Considering the uncertainty from the minimum volume of hyamine added, 20 µL, the retention lies between 0 to 0.07 mg/g-rock. This is the lowest retention value obtained in all the corefloods.

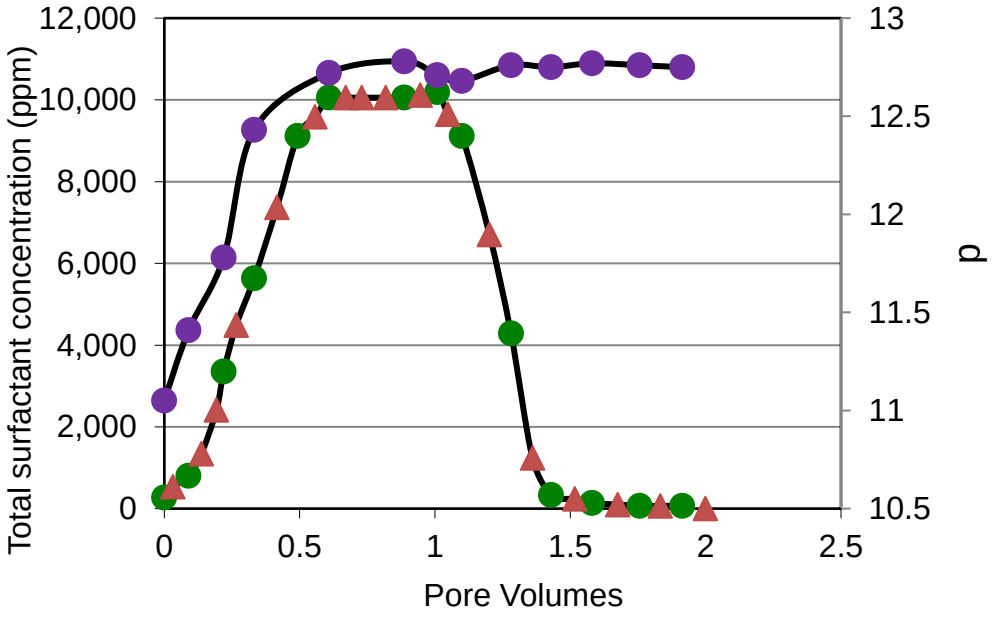

Figure 4.62 Effluent surfactant concentration and pH

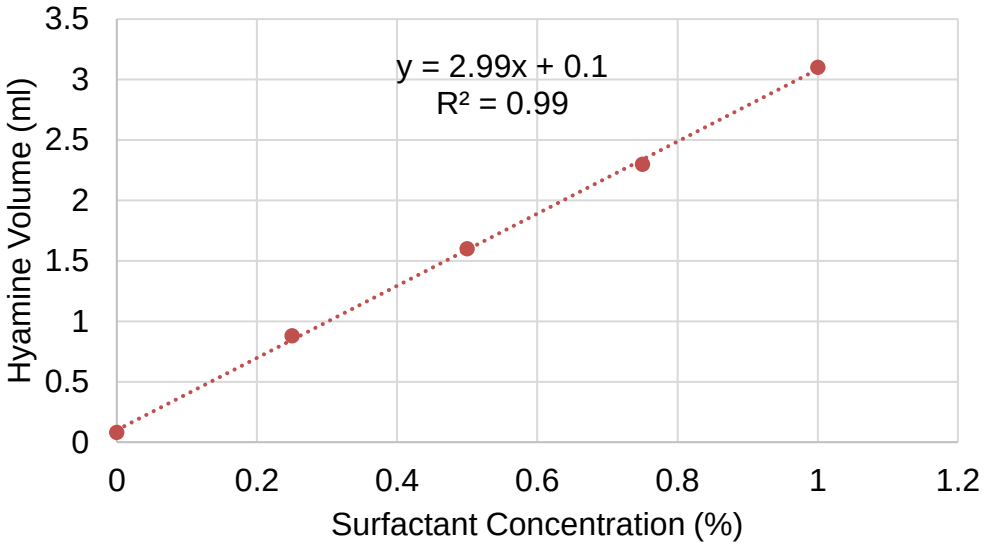

Figure 4.63 Calibration curve for surfactant concentration

4.7 Chemical Flood with a higher flow rate FRAC-15

The objective of the FRAC-15 experiment was to test the performance of a 1 PV surfactant slug and an alkali-surfactant salinity gradient at a flow rate of 0.04 ml/min in a fractured Texas Cream Limestone core. Previous FRAC experiments have showed that the oil recovery depends on the properties of the viscous microemulsion formed in-situ. This experiment was used to determine the effect of flow rate on the oil recovery. Table 4.13 shows the rock properties for the core used in this experiment.

4.7.1 Air permeability

The air permeability was measured at 1000 psi confining pressure before the core was cut. Figure 4.60 shows the pressure drop at different flow rates. The air permeability was determined to be 18 md from the intercept of permeability vs reciprocal pressure data plotted in Figure 4.61 to account for the Klinkenberg effect.

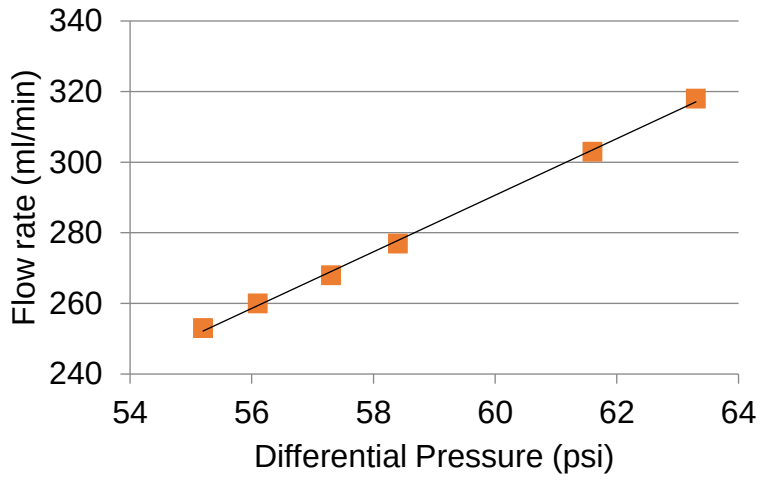

Figure 4.64 Flow rate vs differential pressure to determine rock permeability to air

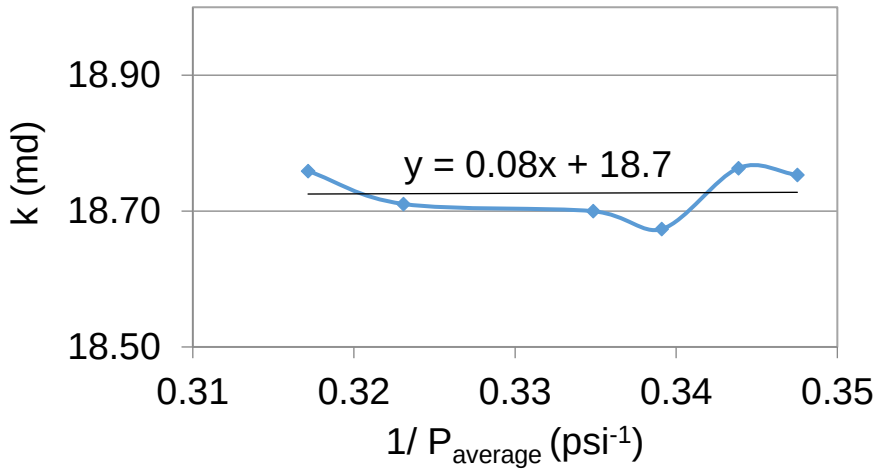

Figure 4.65 Permeability vs inverse average pressure

4.7.2 Oil saturation

The core was saturated with dead crude oil. The pore volume of the rock is 94.4 mL and porosity is 30%. The core was placed in the 78 Celsius oven and was aged for one week. The core was flooded with dead crude oil with a viscosity of 11 cp at a rate of 0.04 while the confining pressure was increased in steps. The goal was to achieve a fracture permeability on the order of 10,000 times that of the rock matrix permeability. An effective oil permeability of 350 md would have achieved this result.

The core was flooded at different rates of 0.04, 0.08, and 0.01 ml/min and the pressure drops were recorded to measure the oil permeability of the fractured core. Figure 4.62 shows the pressure drop data and Table 4.7 summarizes the oil permeability results. The core properties were calculated as follows:

$$Q = -\frac{kA}{\mu}\left(\frac{P_i - P_o}{L}\right) k = \frac{Q\mu L}{A(P_i - P_o)} = 245 * \frac{(0.04\frac{ml}{\min} * 11\text{cp} * 29.9cm)}{(11.04cm^2 * 0.8psi)} = 350md \quad (3.16)$$

$$b = \left(3\pi D k_{eff}\right)^{\frac{1}{3}} = \left(3 * \pi * 0.0375m * 0.35Darcy * \frac{9.87E^{-13}m^2}{1Darcy}\right)^{\frac{1}{3}} = 0.000049m \quad (3.17)$$

$$k_{fracure} = \frac{A_{total}k_{effective} - 2A_{matrix}k_{matrix}}{A_{fracture}} = \quad (3.18)$$

$$\frac{(11.1cm^2 * 0.35Darcy - (11.1cm^2 - 3.76cm * 0.005cm) * 0.018\,\text{Darcy}}{3.76cm * 0.005cm} = 190Darcy$$

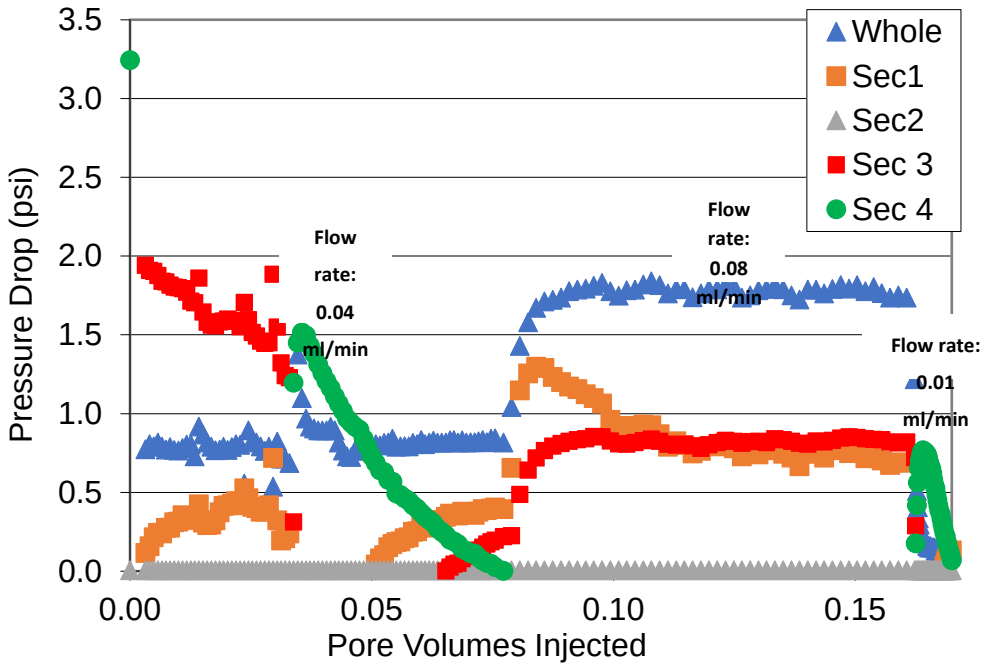

Figure 4.66 Oil flood to determine rock permeability

Table 4.7 Oil Permeability measurements at several flow rates in FRAC-15 experiment

Flow rate (ml/min)	Pressure drop (psi)	Permeability (md)	Pressure gradient (psi/ft)
0.04	0.8	350	0.85
0.08	1.8	315	1.9
0.01	0.2	390	0.2

4.7.3 Waterflood

The core was water flooded with 85,000 ppm NaCl brine at a flow rate of 0.04 mL/min, equivalent to an interstitial velocity of 0.7 ft/day based on the whole core. The oil saturation at the end of the waterflood was 93%. Figure 4.63 shows the oil saturation,

oil cut, and oil recovery from the water flood. The water flood pressure is shown in Figure 4.64. The apparent water permeability is 30 md using a pressure drop of 0.35 psi and a water viscosity of 0.433 cp. As in the single phase oil flood, the pressure drops from the sections of the core do not add up to the whole pressure drop.

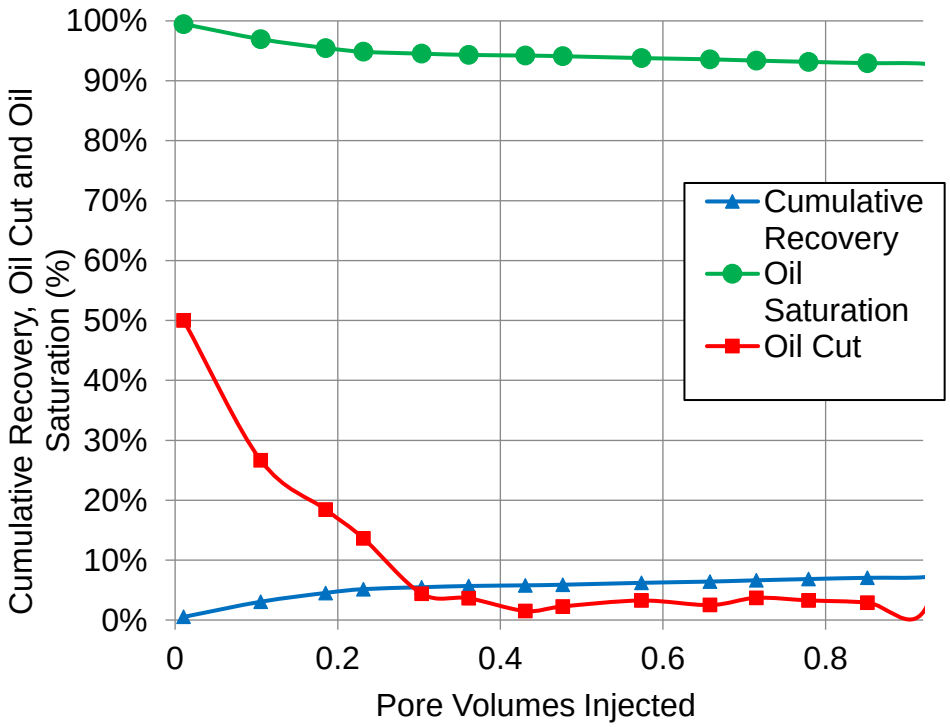

Figure 4.67 Waterflood oil cut, saturation, and recovery during waterflood

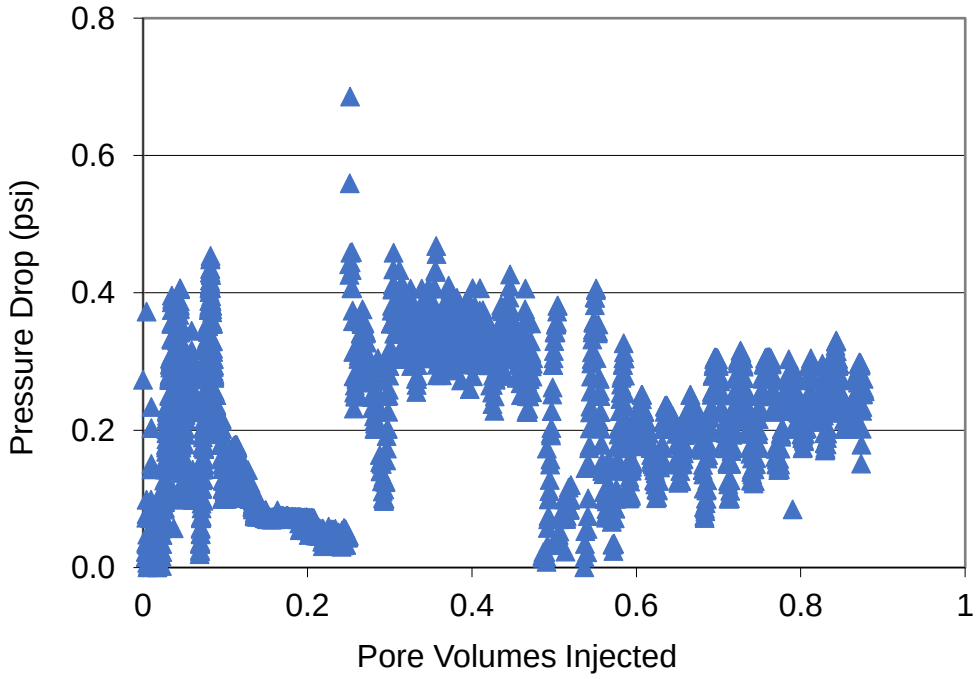

Figure 4.68 Whole pressure drop during waterflood

4.7.4 Chemical flood

The oil recovery from the chemical flood can be seen in Figure 4.65. The oil recovery was 29% after 1 PV surfactant slug with a salinity of 85,000 ppm and 1 PV of brine drive with a salinity of 60,000 ppm at a flow rate of 0.04 ml/min. This is equivalent to 0.6 ft/day based on the whole core and a porosity of 31% and 115 ft/day based on the fracture area alone. The oil solubilization ratio at 85,000 ppm is estimated to be 8.7 and the IFT between oil and the microemulsion calculated from the Huh equation is 0.004 dynes/cm. As shown in Figure 4.66, the pressure drop was the highest at the end of the brine drive.

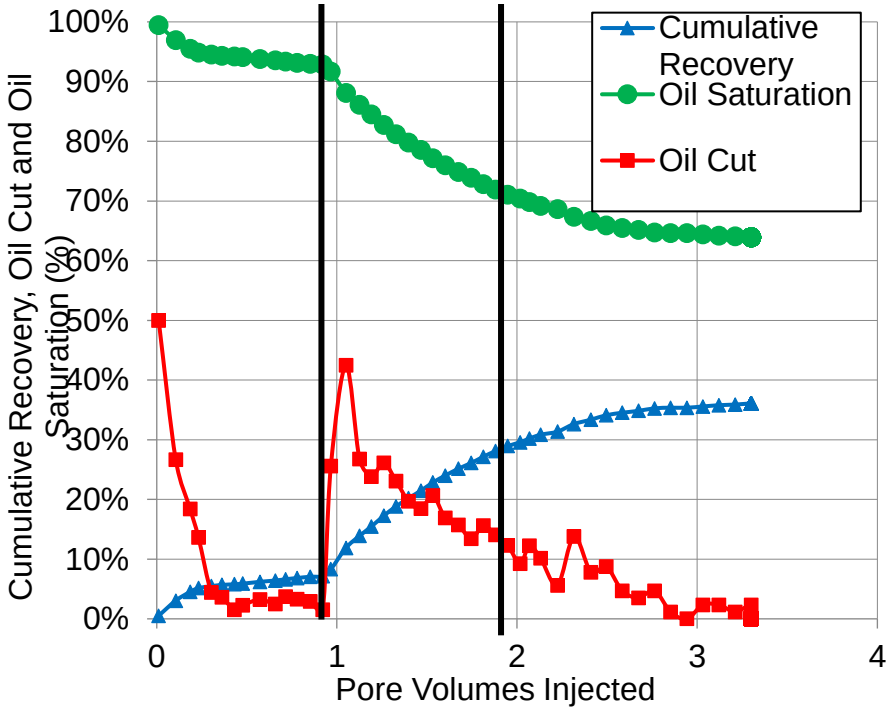

Figure 4.69 Oil recovery for FRAC-15 experiment

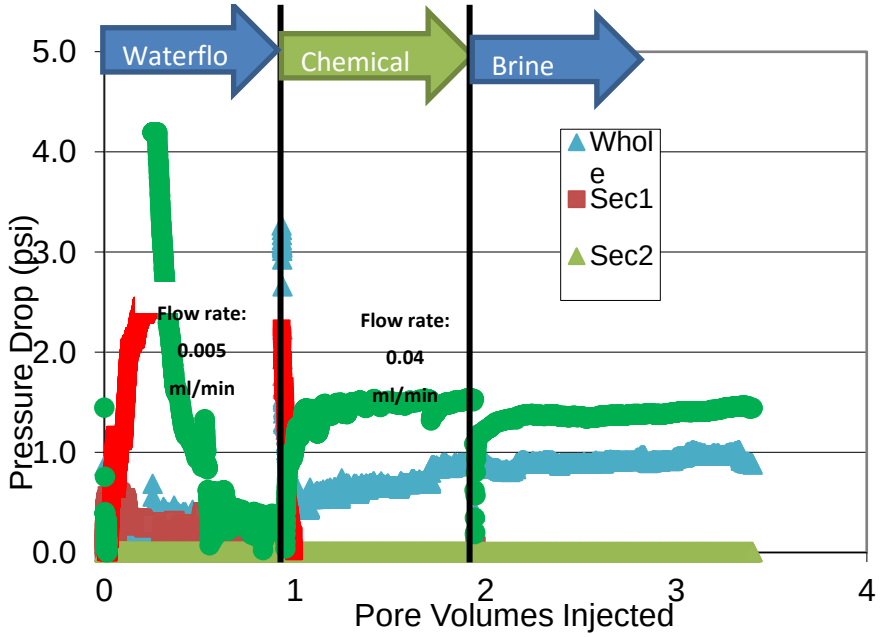

Figure 4.70 Pressure drop for FRAC-15 experiment

4.7.5 Surfactant retention

The concentration of surfactant in the effluent was measured using the hyamine titration method. The effluent surfactant concentration can be seen in Figure 4.67, which was determined using the calibration curve seen in Figure 4.68. The surfactant retention was determined using a mass balance. Since the concentration of surfactant and volume of each test tube was known, the mass of surfactant out of the core could be determined. The mass of surfactant going into the core was assumed to be 1% throughout the chemical flood. The retention calculated was 0.15 mg-surfactant/g-rock after following the surfactant flood with a brine drive that included alkali. A low bound of 0.09 mg/g-rock is obtained considering the minimum addition of hyamine of 20 µL. The retention for this experiment was higher than for a similar experiment (FRAC-13) with slower injection rate (0.01 ml/min, and 0.07 mg/g-rock rock).

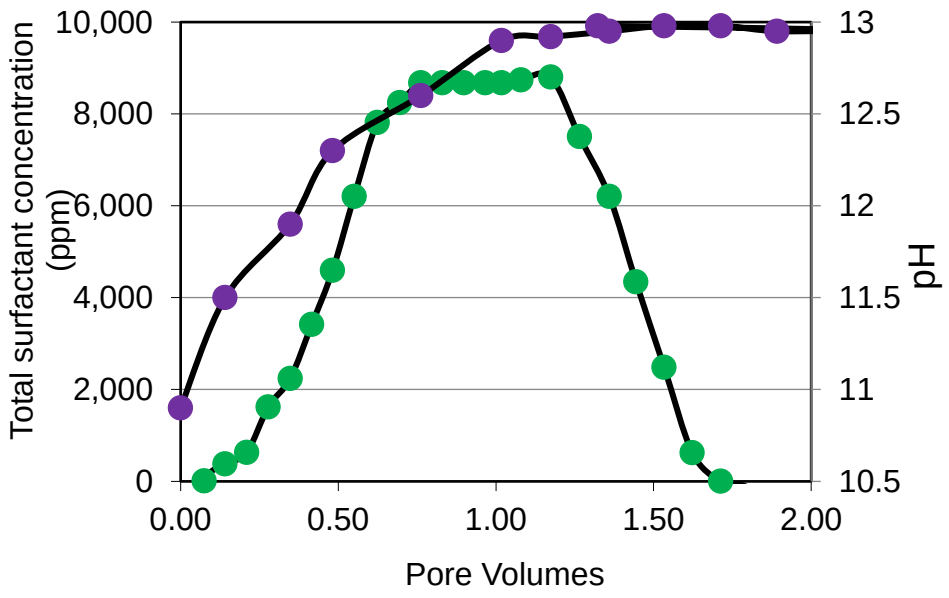

Figure 4.71 Effluent surfactant concentration and pH for FRAC-15 experiment

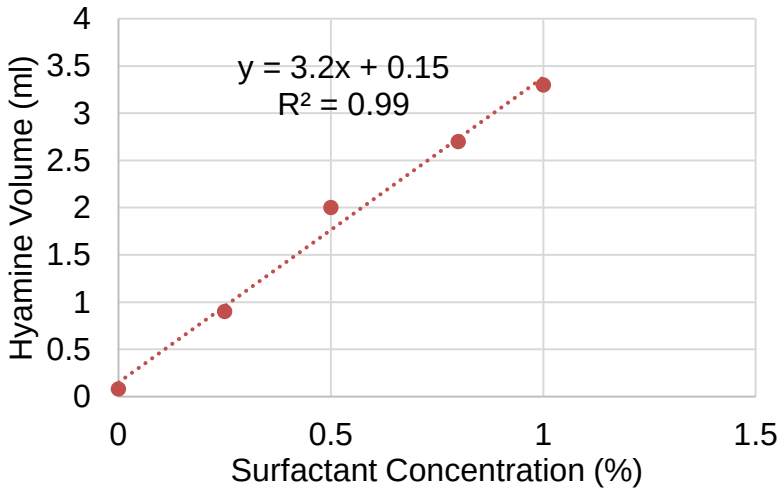

Figure 4.72 Calibration curve to determine surfactant concentration

4.8 Chemical Flood with a lower flow rate FRAC-16

The objective of the FRAC-16 experiment was to test the performance of a 1 PV surfactant slug at a flow rate of 0.005 ml/min in a fractured Texas Cream Limestone core. Previous FRAC experiments have showed that the oil recovery depends on the properties of the viscous microemulsion formed in situ. This experiment was used to determine the effect of a lower flow rate on the oil recovery. Table 4.15 shows the rock properties for the core used in this experiment.

4.8.1 Air permeability

The air permeability was measured at 1000 psi confining pressure before the core was cut. Figure 4.69 shows the pressure drop at different flow rates. The air permeability was determined to be 17 md from the intercept of permeability vs reciprocal pressure data plotted in Figure 4.70 to account for the Klinkenberg effect.

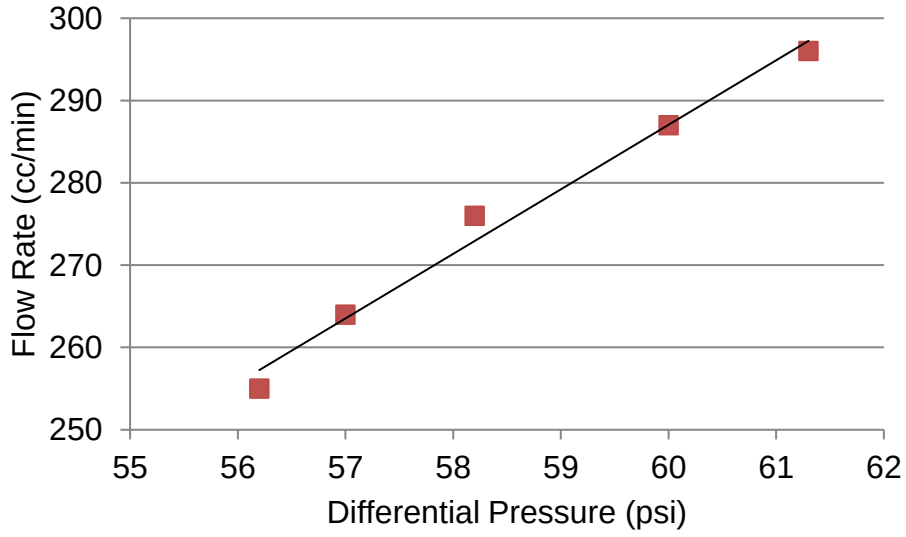

Figure 4.73 Flow rate vs differential pressure to determine rock permeability

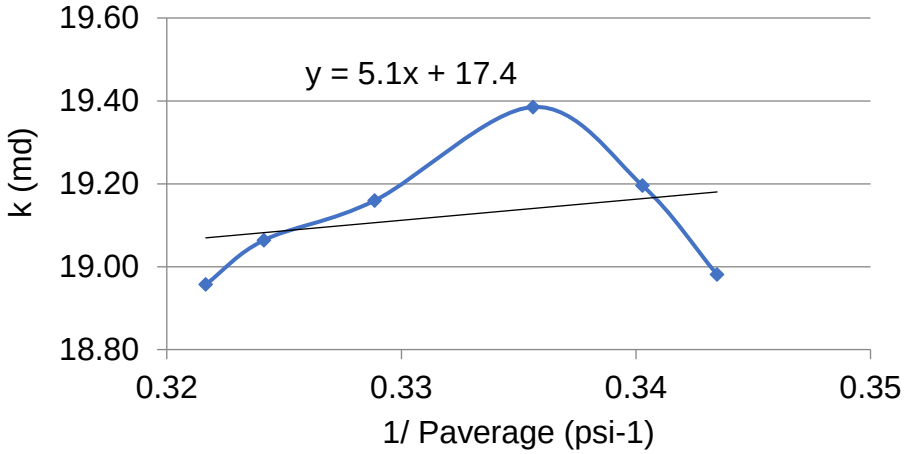

Figure 4.74 Permeability vs inverse average pressure

4.8.2 Oil saturation

The pore volume of the rock is 88 mL and the porosity is 28%. The core was aged in the oven for six days. The core was flooded with dead crude oil with a viscosity of 11 cp at rates of 0.03, 0.06, and 0.01. The goal was to achieve a fracture permeability of 200

Darcy and fracture aperture of 0.005 cm. An effective permeability to oil of 350 md would achieve this result. After increasing the confining stress in increments of 50 psi, a permeability of 320 md was achieved at 800 psi. Table 4.8 shows the calculations for this step, and Figure 9 shows the oil permeability multi-rate test. The pressures between the sections don't make too much sense as they don't add up to the total pressure. The following equations from Chapter 2 were used to calculate the permeability of the fracture:

$$Q = -\frac{kA}{\mu}\left(\frac{P_i - P_o}{L}\right) k = \frac{Q\mu L}{A(P_i - P_o)} = 245 * \frac{(0.1\frac{ml}{\min} * 11\text{cp} * 27.8cm)}{(11.1cm^2 * 2.2\,psi)} = 307md \quad (3.19)$$

$$b = \left(3\pi D k_{eff}\right)^{\frac{1}{3}} = \left(3 * \pi * 0.0376m * 0.35Darcy * \frac{9.87E^{-13}m^2}{1Darcy}\right)^{\frac{1}{3}} = 0.000047m \quad (3.20)$$

$$k_{fracure} = \frac{A_{total}k_{effective} - 2A_{matrix}k_{matrix}}{A_{fracture}} = \quad (3.21)$$

$$\frac{(11.1cm^2 * 0.307Darcy - (11.1cm^2 - 3.76cm * 0.005cm) * 0.017\,\text{Darcy}}{3.76cm * 0.005cm} = 170Darcy$$

Table 4.8 Oil Permeability measurements at several flow rates in FRAC-16 experiment

Flow rate (ml/min)	Pressure drop (psi)	Permeability (md)
0.03	0.65	311
0.06	1.4	290
0.1	2.2	307

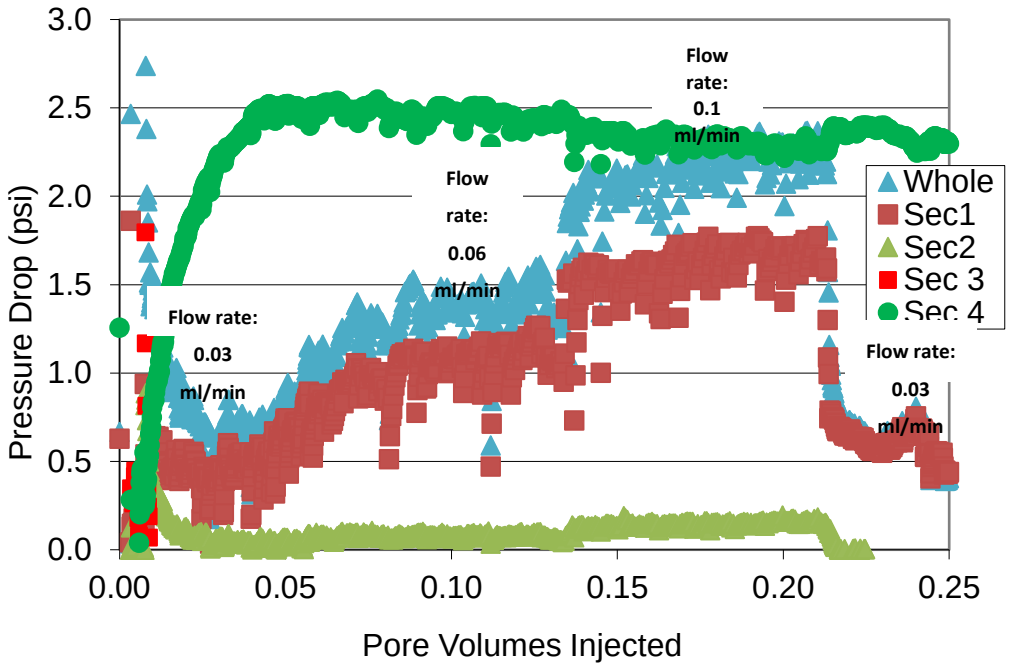

Figure 4.75 Pressure drop during oil flood for FRAC-16 experiment

4.8.3 Waterflood

Immediately after the oil flood, a waterflood of 85,000 ppm NaCl was carried out at 0.005 ml/min, the same flow rate used during the chemical flood. The oil saturation after the waterflood was 96.5%. The maximum pressure drop was 0.1 psi/ft, indicating a brine permeability of 13 md. However, the pressure gradient oscillated between 0.1 and -0.1 psi/ft, which indicates the pressure drop was too low to be accurately measured. The section pressure measurements did not add up to the total pressure drop.

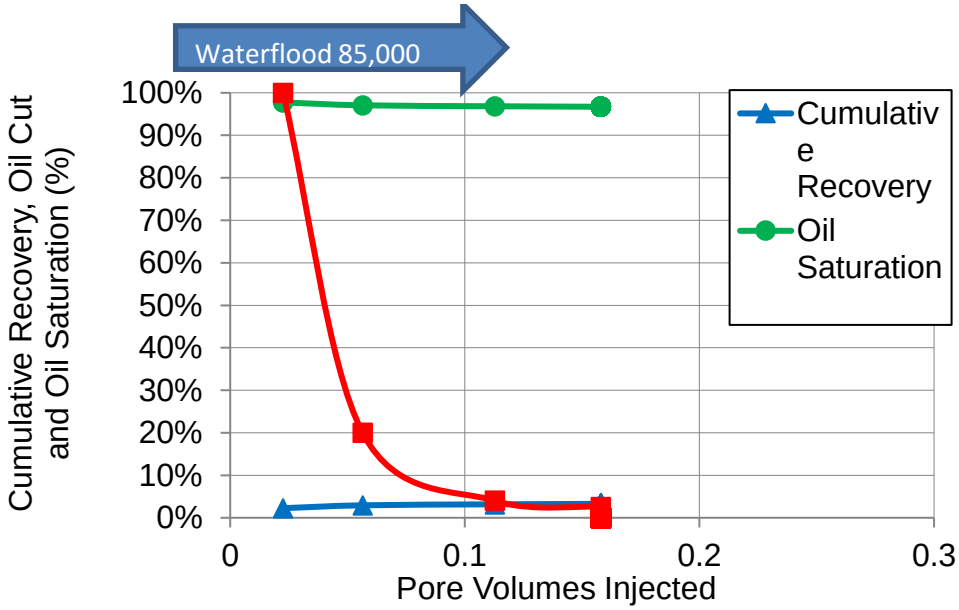

Figure 4.76 Waterflood oil cut, recovery, and saturation for FRAC-16 experiment

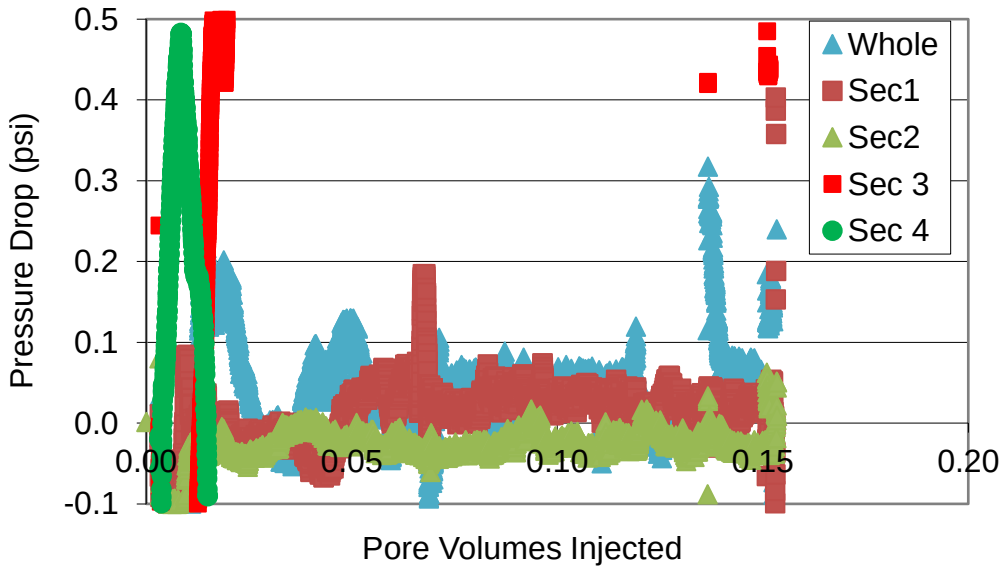

Figure 4.77 Waterflood pressure drop for FRAC-16 experiment

4.8.4 Chemical flood

The oil recovery from the chemical flood can be seen in Figure 4.74. The oil recovery was 40% after 1 PV surfactant slug with a salinity of 85,000 ppm and 1 PV of brine drive at a salinity of 60,000 ppm at 0.005 ml/min. This is equivalent to 0.1 ft/day based on the whole core and 6 ft/day based on the fracture area alone. After the chemical slug was injected, the core was shut in for 7 days. The flood was then restarted on day 8 with the brine drive. There was an abrupt increase in the oil cut to almost 70% the day the flood was restarted. The oil cut then quickly dropped to a similar value to the one before shutting in the flood.

The oil solubilization ratio at 85,000 ppm is estimated to be 8.7 and the IFT between oil and the microemulsion calculated from the Huh equation is 0.004 dynes/cm. The whole pressure drop data is scattered because collection tubes had to be sealed by a stopper and switched by hand to prevent water evaporation. During the switches, pressure was released at the outlet, which can be seen as jumps in the pressure data. The maximum pressure drop is recorded when the first tube is collected after shutting down the flood. The sectional pressure drops did not add up to the total pressure drop.

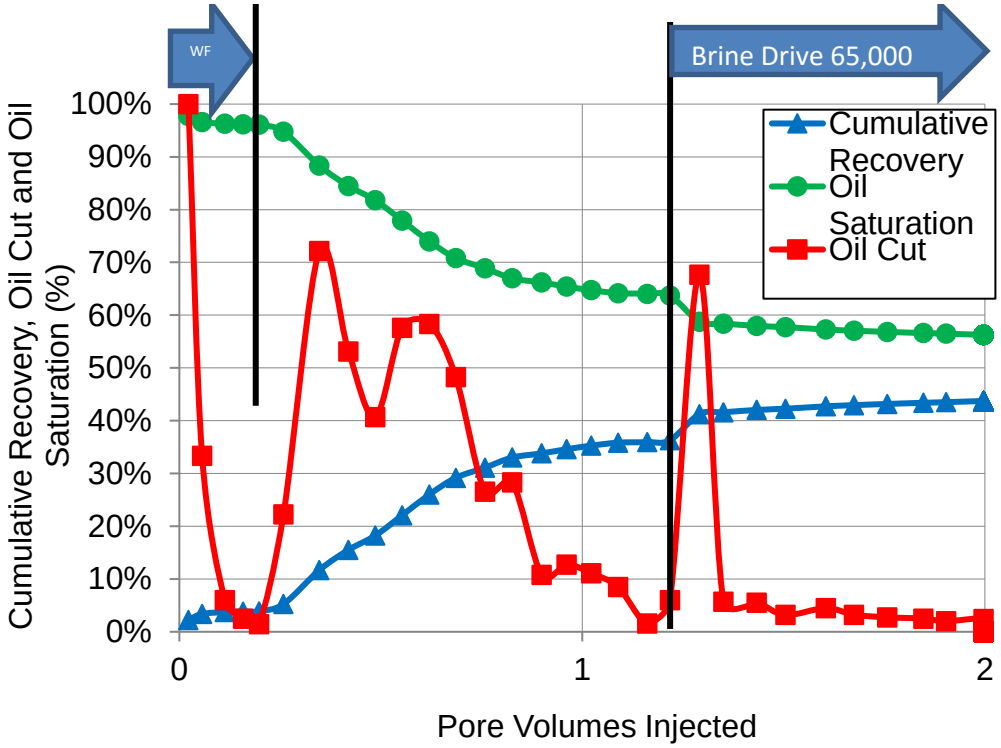

Figure 4.78 Chemical flood oil cut, recovery, and saturation for FRAC-16 experiment

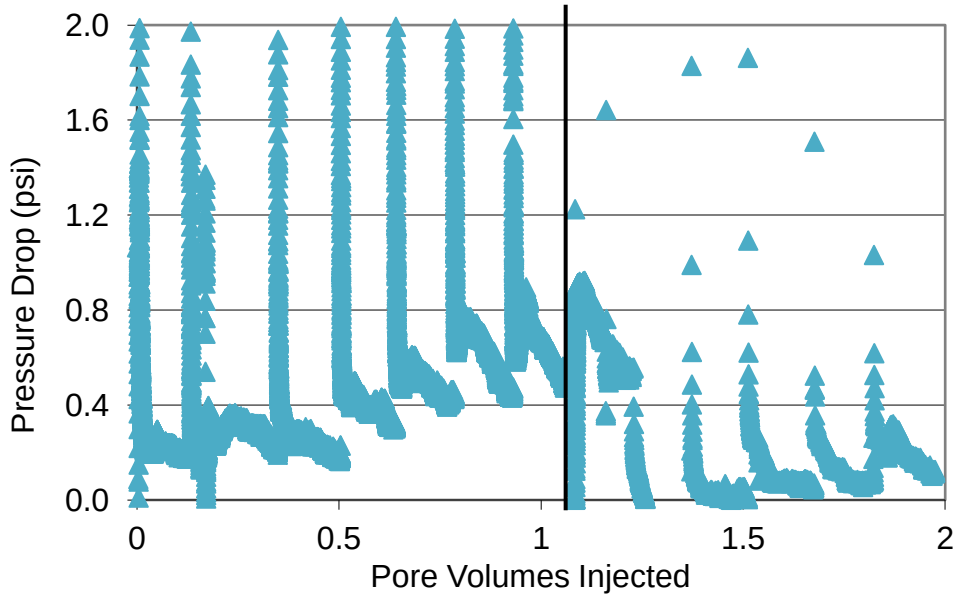

Figure 4.79 Chemical flood pressure drop for FRAC-16 experiment

4.8.5 Surfactant retention

The concentration of surfactant in the effluent was measured using the hyamine titration method. The effluent surfactant concentration can be seen in Figure 4.76, which was determined using the calibration curve seen in Figure 4.77. The surfactant retention was determined using a mass balance. Since the concentration of surfactant and volume of each test tube was known, the mass of surfactant out of the core could be determined. The mass of surfactant going into the core was assumed to be 1% throughout the chemical flood. The retention was 0.205 mg-surfactant/g-rock after following the surfactant flood with a brine drive that included alkali. With the minimum hyamine volume added, 20 µl, the lower bound for retention is 0.15 mg/g-rock. The pH remained at 12.8 during the flood and even after shutting down the flood and then re-starting.

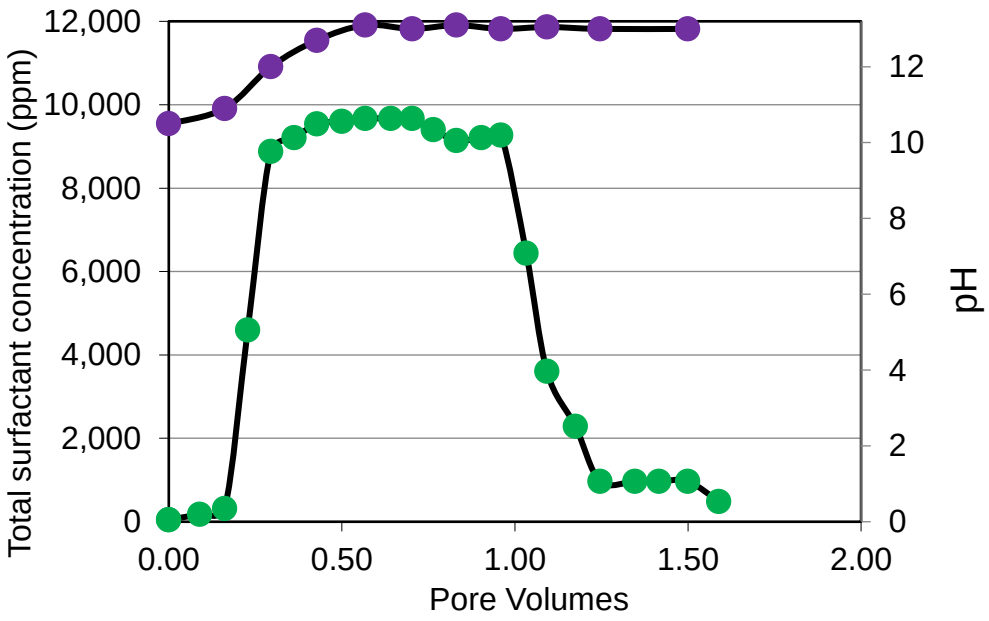

Figure 4.80 Effluent surfactant concentration and pH for FRAC-16

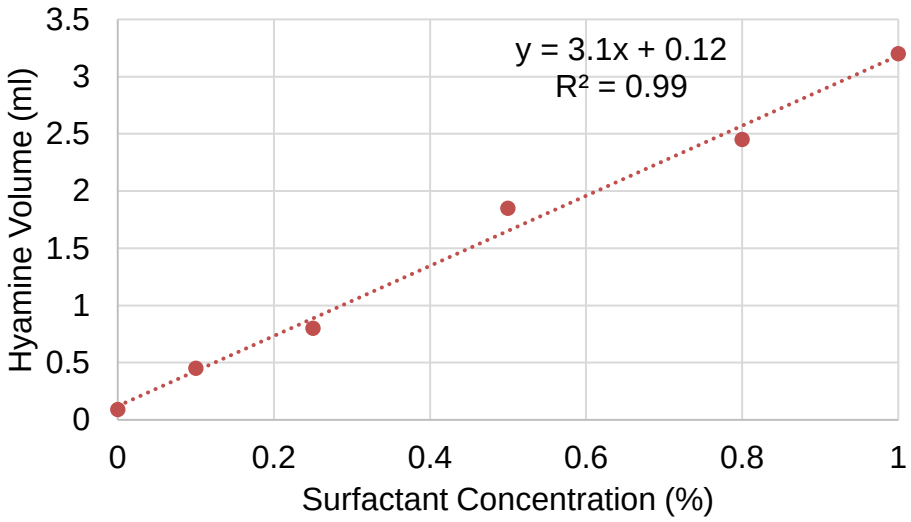

Figure 4.81 Calibration curve to determine surfactant concentration

4.9 Interpretation of the results

4.9.1 Summary of the experimental results

Table 4.9 is a summary of the experimental results.

4.9.2 General observations

Some important points to note from comparing the experiments:

- The highest surfactant retention was 0.25 mg/g-rock and the lowest was 0.07 mg/g-rock with an average value of 0.17 mg/g-rock. These low values are attributed to the high pH of NaOH used as the alkali.

- Oil recovery was low for all waterfloods when the fracture remained open. The maximum oil recovery was 9% and the minimum 4% with an average of 6.5%.

- The incremental oil recovery from the surfactant floods ranged from 29 to 40% with an average of 31%. The oil cut increased immediately after the surfactant solution was injected. The oil cut increased from 2% at the end of the waterfloods to 20-50% for the first tube of the surfactant floods.

Table 4.9 Summary of experiments

Experiment	Used spacers	Slug size (PV)	Flow Rate (ml/min)	Fracture Permeability (Darcy)	Matrix air permeability (md)	Porosity (%)	Alkali in brine drive
FRAC-09	no	3	0.01	200	32	28	no
FRAC-10	yes	3	0.01	280	30	27	no
FRAC-11	yes	1	0.01	230	28	28	no
FRAC-13	yes	0.3	0.01	200	19	30	no
FRAC-14	yes	1	0.01	100	18	29	yes
FRAC-15	yes	1	0.04	200	18	31	yes
FRAC-16	yes	1	0.005	220	14.5	29	yes

Experiment	Waterflood oil recovery (%)	Brine permeability (md)	Max pressure during chemical flood (psi)	Chemical flood Recovery (% of OOIP)	Chemical flood recovery (% of remaining oil after waterflood)	Surfactant Retention (mg/g-rock)	Total oil recovery (% OOIP)
FRAC-09	9	25	0.5	33	36	0.21	42
FRAC-10	5	60	0.45	43	45	0.25	48
FRAC-11	8	43	0.8	41	45	0.11	50
FRAC-13	6	35	0.4	32	34	0.07	39
FRAC-14	17	35	1	30	36	0.20	39
FRAC-15	7	50	0.9	29	31	0.15	36
FRAC-16	4	30	0.6	40	42	0.21	44

4.9.3 Surfactant slug size

Experiments FRAC-10, FRAC-11 and FRAC-13 had the same fracture set-up, injection flow rate, and oil recovery during the waterflood. These three experiments show the effect of surfactant slug size on the oil recovery remaining after the waterflood. The 3 PV slug used for experiment FRAC-10 resulted in an oil recovery of 45%. The 1 PV slug used for experiment FRAC-11 resulted in an oil recovery of 44%. The 0.3 PV slug used for experiment FRAC-13 resulted in an oil recovery of 30%. Using a 0.3 PV slug is the most efficient in terms of surfactant injected to oil recovered. Figure 4.78 compares the three cases.

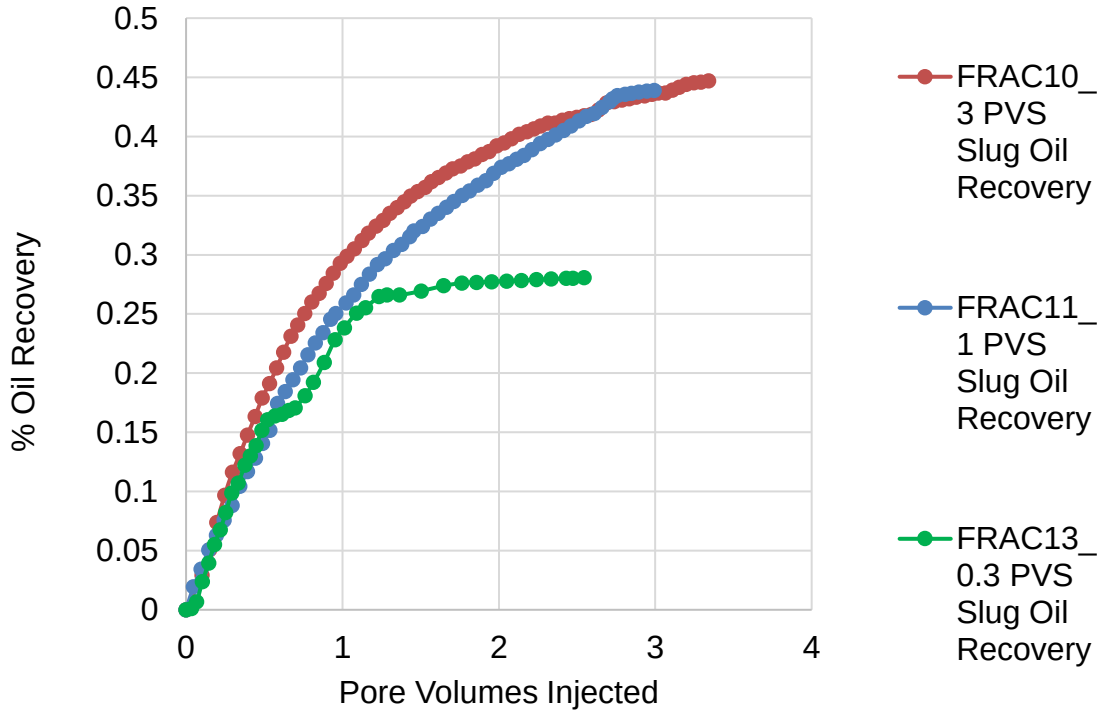

Figure 4.82 Effect of slug size on oil recovery

4.9.4 Flow rate

Experiments FRAC-11, FRAC-15, and FRAC-16 had the same fracture set-up, mass of chemicals injected and similar oil recovery during the waterflood. A lower flow rate resulted in a higher oil recovery versus pore volumes. Experiment FRAC-15 had the highest injection rate, 0.04 ml/min, and recovered 22% of the remaining oil after 1 PV. Experiment FRAC-11 had an injection rate of 0.01 ml/min and recovered 26% of the remaining oil after 1 PV. Experiment FRAC-16 had the lowest injection rate, 0.005 ml/min, and recovered 34% of the remaining oil after 1 PV. Figure 4.79 shows these results.

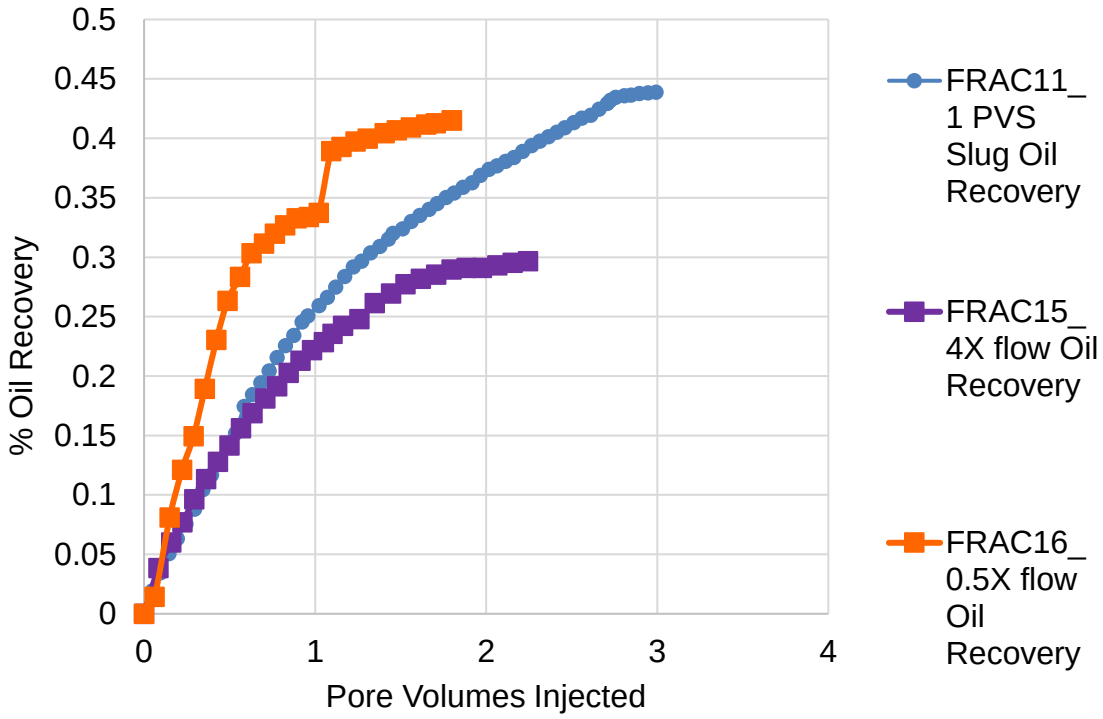

Figure 4.83 Effect of flow rate on oil recovery

4.9.5 Peak surfactant concentration

As shown in Figure 4.80, the effluent surfactant concentration broke though at about 0.15 PV and peaked between about 0.3 to 0.5 PV. This behavior suggests the possibility of recycling surfactant after it breaks through.

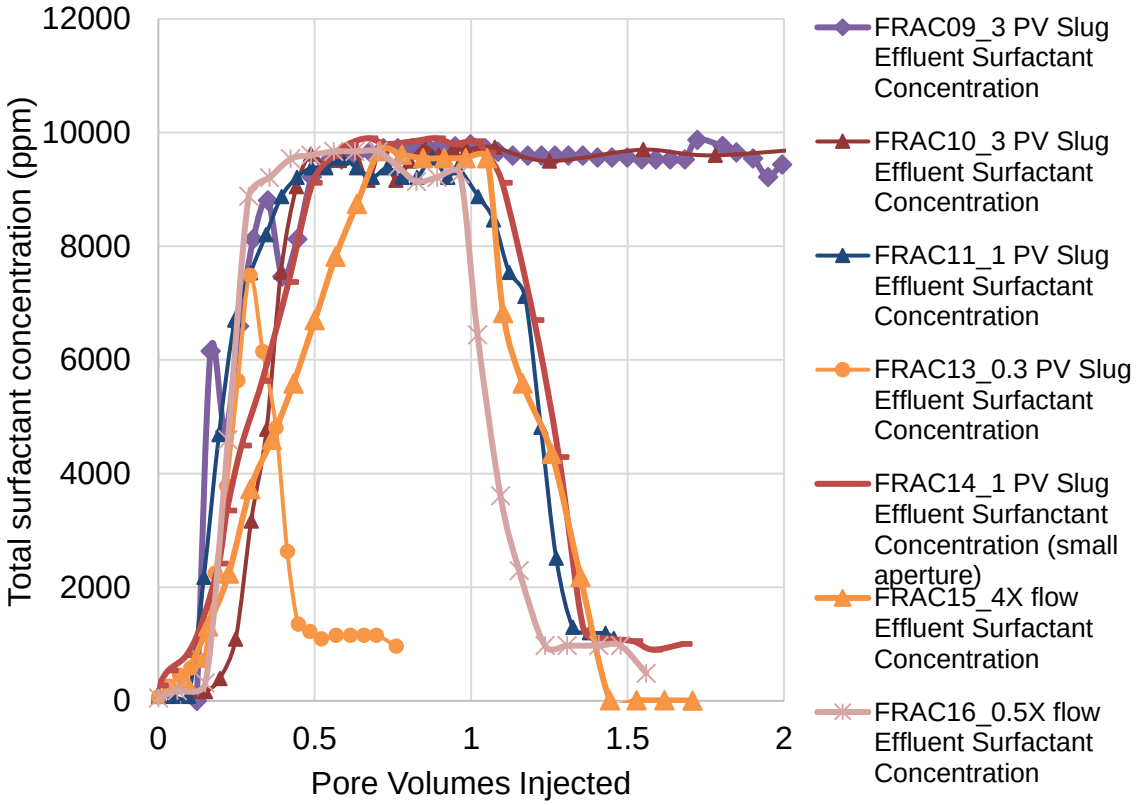

Figure 4.84 Effluent surfactant concentration

Chapter 5 Conclusions and Future Work

5.1 Conclusions

The experimental research presented in this thesis shows that viscous microemulsions formed in-situ when surfactant solution is injected can be used to significantly increase oil recovery from oil-wet fractured limestone cores using surfactant slug sizes as small as 0.3 pore volumes. Parra (2016) previously demonstrated good oil recovery in similar fractured cores with continuous surfactant injection and showed dynamic effects such as transverse pressure gradients helped explain his observations. The surfactant formulations in each case were designed to produce both ultra-low interfacial tension and wettability alteration. Alkali was used in the surfactant solutions to minimize surfactant retention. The dynamic coreflood experiments showed faster recovery than the static experiments presented by Li et al. (2017) using similar rocks, oil, and surfactants. The major difference between dynamic and static experiments is the transverse pressure gradient is greater in the dynamic experiments due to the imposed flow. The flow rate affects both the recovery efficiency and the time for the oil recovery. The main conclusions of this study are as follows:

- A new chemical formulation (SAMA-NFR-01) was developed for the new coreflood experiments. The composition is 0.5% C28-25PO-45EO-carboxylate, 0.2% C15-18 IOS, 0.3% C19-28 IOS, 20,000 ppm Na_2CO_3, 20,000 ppm Na_2SO_4, 5,000 ppm NaOH, and varying amounts of NaCl. This formulation differs from the one used in Parra (2016) because it contains no EDTA, which has a high consumption in limestone and may not be practical to use in the field. NaOH was added to minimize surfactant retention.

- Teflon spacers were found to be an effective method of maintaining an open fracture in cores under confining stress. In previous experiments by Parra (2016) the fracture was roughed manually with a sharp tool. In some of those experiments (FRAC-06) the pressure drop increased during the waterflood. This might have been due to partial closure of the fracture. Placing thin (1 mm wide) Teflon strips along the edges of the fracture prevented this from occurring. The Teflon spacers maintained the fracture open in all corefloods except FRAC-14, where the confining stress was 1,800 psi.
- Using larger amounts of surfactant produces more oil, but is less efficient in terms of oil produced over surfactant injected. FRAC-10 recovered 45% of the remaining oil using 3 PV of surfactant soluiton at 70,000 ppm (microemulsion viscosity of equilibrated sample is 0.5 cp). FRAC-11 recovered 44% of the remaining oil using a 1 PV surfactant slug with a higher salinity of 85,000 ppm (microemulsion viscosity of equilibrated sample is 30 cp), and a brine drive with a lower salinity of 65,000 ppm to provide a salinity graident. FRAC-13 recovered 30% of the remaining oil using 0.3 PV surfactant slug under the same conditions as FRAC-11.
- Designing for the formation of viscous microemulsions formed in-situ improved oil recovery. Injecting the surfactants at higher salinity (85,000 ppm) in FRAC-11 caused a viscous microemulsion to form in the core, increased transverse viscous pressure gradients and improved oil recovery (44% of oil recovered). In FRAC-10 (70,000 ppm TDS) a less viscous microemulsion recovered 45 % even though a 3 PV surfactant slug was

injected. The high microemulsion viscosity formed in-situ in FRAC-11 and FRAC-13 made the floods more efficient.

- The oil recovery at a lower flow rate was faster in terms of pore volumes injected. FRAC-15 had the highest flow rate of 0.04 ml/min and recovered 22% of the remaining oil after 1 PV. FRAC-11 had a flow rate of 0.01 ml/min and recovered 26% of the remaining oil after 1 PV of injection. FRAC-16 had the slowest flow rate of 0.005 ml/min and recovered 34% of the remaining oil after 1 PV of injection.
- It was a lot more efficient to inject a 0.9 PV surfactant slug followed by a brine drive than to inject three 0.3 PV surfactant slugs with brine drives in between following each slug. Comparing FRAC-13 to FRAC-11, where surfactant injection was continuous, it can be said that if other variables are kept the same (even the mass of surfactant injected) oil will be recovered faster with a 1 PV slug rather than three 0.3 PV slugs.
- Sodium hydroxide was effective in reducing surfactant retention in fractured Texas Cream Limestone cores. For all experiments surfactant retention was low, with a maximum of 0.25 mg/g-rock a minimum of 0.07 mg/g-rock and an average of 0.17 mg/g-rock for the seven coreflood experiments.

Wang et al. (2018), Wang (2018), Abalkhail (2018) and Maubert et al. (2016) have shown that surfactant retention can be decreased in limestone cores by using NaOH to increase the pH of the injected solution. The results in this thesis show that this is also the case for fractured limestone cores. The fractures in the experiments presented here had a permeability that was more than 10,000 times greater than the rock matrix. Even so,

the surfactant retention was low, with an average value of 0.17 mg/g-rock for the seven coreflood experiments.

The experiments used only a brine drive and no polymer after the chemical flood. The viscous microemulsions that form in-situ when the surfactant solution mixes with the oil provided an effective mobility control without the need to inject either polymer or foam. The process shows promise for enhanced oil recovery from fractured oil-wet limestone reservoirs with a high initial oil saturation because waterflood recovery is extremely low in such reservoirs. Furthermore, the low surfactant retention makes recycling the surfactant a viable option to consider.

5.2 Future work

Fractured carbonate reservoirs offer a huge potential for enhanced oil recovery. Because of their size, their properties are of great research interest. For future work, the following variables are suggested for experimentation:

- Shut-in time: Increase the time the chemical flood is shut-in to allow the rock to soak. Arbitrary choices for shut-in time would be made initially, then optimized to maximize oil recovery. For example, the core could be injected with 0.2 PV of chemicals, then allowed to soak for 2 days. Then injected again with 0.2 PV and wait for 2 more days. This would be done in cycles and the oil recovery would be observed. Stopping the flood might allow surfactant and oil more time to form a viscous microemulsion. Also, the oil cut increases dramatically (70% after restarting). From the results of FRAC-16, it is likely that increasing the time the core is shut-in increases oil recovery. The effect should be investigated. Alternatively, the shut in period can be tried at different moments of the chemical flood

process to maximize its effect. For example, shutting-in at the beginning versus after 1 PV of injection.

- Flow rate: The flow rate can be further reduced or increased to verify that a higher flow rate is detrimental to recovery efficiency. Increasing the flow rate is easier than decreasing it since the ISCO pumps cannot handle flow rates lower than 0.005 ml/min accurately. From FRAC-15 and 16, increasing the flow rate would decrease oil recovery.
- Fracture aperture: Varying the fracture aperture in multiple corefloods would allow for evaluation of the robustness of the process. The process should be effective under various conditions to be attractive. Decreasing the fracture aperture and permeability would promote crossflow. This can be done by increasing the confining stress of the core-holder. Decreasing the aperture is expected to increase oil recovery.
- Injecting microemulsion: Injecting microemulsion containing oil might improve recovery in fractured carbonates. Doing this might aid by increasing the viscosity of the injected fluid initially, maximizing crossflow, and improving sweep. From the viscosity vs concentration of oil in the microemulsion (C23) data presented in Chapter 4, microemulsions have a maximum viscosity at some oil concentration (60% in this case). Injecting a small slug (0.1 PV) might cause large transverse viscous pressure gradients which would cause a higher oil recovery.
- Inject top-down: This would negate the effect of gravity and allow for validation that transverse pressure gradients are significant and can overcome unfavorable capillary and buoyancy forces. Recovery would be

lower than injecting from the bottom because buoyancy forces are not aiding in recovery; however, floods with more viscous microemulsions would still be expected to recover more oil. Alternatively, the core could be set horizontally and the same observations could be made.

- Surfactant concentration: Lower surfactant concentrations still have low IFT above the CMC. With low surfactant adsorption, it might make sense to inject lower surfactant concentrations, but it is a complicated optimization process requiring systematic experiments.
- Using polymer: Besides the microemulsions formed in-situ, additional mobility control agents such as polymers or foams could be added and more easily adjusted for viscosity. Injecting polymer would increase crossflow and hence oil recovery. The polymer would have to be screened adequately to make sure it transports through the low permeability rock.
- Oil, rock, and chemical formulation: Optimization could be carried out to either make the process more efficient for a specific case, or more robust for various cases. The next step would be to carry out experiments in a different rock, probably Indiana limestone as Wang et al. (2018) has shown NaOH to be effective there as well. A different oil should also be used to validate the results of this thesis and Parra (2016), but this would require a new formulation since the surfactant formulation should be optimized for the specific oil, temperature and brine. Changing the oil should not change the fact that viscous microemulsions formed in-situ increase oil recovery in fractured corefloods.

- CT scanner experiments: CT images would provide insight about the fluid distributions inside the core and allow for validation of the proposed mechanism related to transverse viscous pressure gradients.

Bibliography

Abalkhail, N. (2018). *Chemical Enhanced Oil Recovery Application in a High-Temperature, High-Salinity Carbonate Reservoir*, M.S. Thesis. Austin, TX: The University of Texas at Austin.

Abbasi Asl, Y., Pope, G. A., & Delshad, M. (2010). *Mechanistic Modeling of Chemical Transport in Naturally Fractured Oil Reservoirs*. Presented at the SPE Improved Oil Recovery Symposium, Society of Petroleum Engineers. https://doi.org/10.2118/129661-MS

Adkins, S., Pinnawala Arachchilage, G. W. P., Solairaj, S., Lu, J., Weerasooriya, U., & Pope, G. A. (2012). *Development of Thermally and Chemically Stable Large-Hydrophobe Alkoxy Carboxylate Surfactants*. Presented at the SPE Improved Oil Recovery Symposium, Society of Petroleum Engineers. https://doi.org/10.2118/154256-MS

Alroudhan, A., Vinogradov, J., & Jackson, M. D. (2016). *Zeta potential of intact natural limestone: Impact of potential-determining ions Ca, Mg and SO4*. Colloids and Surfaces A: Physicochemical and Engineering Aspects, *493*, 83–98. https://doi.org/10.1016/j.colsurfa.2015.11.068

Alshakhs, M. J., & Kovscek, A. R. (2016). *Understanding the role of brine ionic composition on oil recovery by assessment of wettability from colloidal forces*. Advances in Colloid and Interface Science, 233, 126–138. https://doi.org/10.1016/j.cis.2015.08.004

Austad, T., Matre, B., Milter, J., Sævareid, A., & Øyno, L. (1998). *Chemical flooding of oil reservoirs 8. Spontaneous oil expulsion from oil- and water-wet low permeable chalk material by imbibition of aqueous surfactant solutions*. Colloids and Surfaces A: Physicochemical and Engineering Aspects, 137(1), 117–129. https://doi.org/10.1016/S0927-7757(97)00378-6

Barenblatt, G. I., Zheltov, I. P., & Kochina, I. N. (1960). *Basic concepts in the theory of seepage of homogeneous liquids in fissured rocks [strata]*. Journal of Applied Mathematics and Mechanics, *24*(5), 1286–1303. https://doi.org/10.1016/0021-8928(60)90107-6

Barnes, J. R., Dirkzwager, H., Smit, J. R., & Smit, J. P., On, An, Navarette, R.C., Ellison, B.H., and Buijse, M. A (2010). *Application of Internal Olefin Sulfonates and Other Surfactants to EOR. Part 1: Structure - Performance Relationships for Selection at Different Reservoir Conditions*, SPE 129766, presented at SPE IOR Symposium, Tulsa, OK, 2010.

Bourrel, M., & Schechter, R. S. (1988). *Microemulsions and related systems: formulation, solvency, and physical properties*. New York: M. Dekker.

BP Energy Outlook | Energy economics | BP. Retrieved September 2, 2018, from https://www.bp.com/en/global/corporate/energy-economics/energy-outlook.html

Brownell, L. E., & Katz, D. L. (1947). *Flow of Fluids Through Porous Media-Part II*. Chem. Eng. Prog., 43(11).

Bunn, R. A., Magelky, R. D., Ryan, J. N., & Elimelech, M. (2002). *Mobilization of Natural Colloids from an Iron Oxide-Coated Sand Aquifer: Effect of pH and Ionic Strength.*

Environmental Science & Technology, 36(3), 314–322. https://doi.org/10.1021/es0109141

Cauchy, A.-L. (1827). Ex. de math.

Chang, L., Jang, S. H., Tagavifar, M., & Pope, G. A. (2018). *Structure-Property Model for Microemulsion Phase Behavior*. Presented at the SPE Improved Oil Recovery Conference, Society of Petroleum Engineers. https://doi.org/10.2118/190153-MS

Chang, L., Pope, G. A., Jang, S. H., & Tagavifar, M. (2019). *Prediction of microemulsion phase behavior from surfactant and co-solvent structures*. Fuel, *237*, 494–514. https://doi.org/10.1016/j.fuel.2018.09.151

Chang, L. *Prediction of microemulsion phase behavior from surfactant and co-solvent structures.* PhD, Dissertation, The University of Texas at Austin

Chatzis, I., & Morrow, N. R. (1984). *Correlation of Capillary Number Relationships for Sandstone*. Society of Petroleum Engineers Journal, *24*(05), 555–562. https://doi.org/10.2118/10114-PA

Chevallier, E., Moreau, P., Renard, S., Tabary, R., Bazin, B., Douarche, F., & Oukhemanou, F. (2013). *Recent Progress in Surfactant Flooding in Carbonate Reservoirs*. Presented at the IOR 2013 - 17th European Symposium on Improved Oil Recovery, Saint Petersburg, Russia. https://doi.org/10.3997/2214-4609.20142634

Chilingar, G. V., & Yen, T. F. (1983*). Some Notes on Wettability and Relative Permeabilities of Carbonate Reservoir Rocks*, II. Energy Sources, *7*(1), 67–75. https://doi.org/10.1080/00908318308908076

Delshad, M., Pope, G. A., & Sepehrnoori, K. (1996). *A compositional simulator for modeling surfactant enhanced aquifer remediation, 1 formulation*. Journal of Contaminant Hydrology, *23*(4), 303–327. https://doi.org/10.1016/0169-7722(95)00106-9

Ehrlich, R., & Wygal, R. J. J. (1977). *Interrelation of Crude Oil and Rock Properties with the Recovery of Oil by Caustic Waterflooding*. Society of Petroleum Engineers Journal, 17(04), 263–270. https://doi.org/10.2118/5830-PA

Flaaten, A., Nguyen, Q. P., Pope, G. A., & Zhang, J. (2009). *A Systematic Laboratory Approach to Low-Cost, High-Performance Chemical Flooding*. SPE Reservoir Evaluation & Engineering, 12(05), 713–723. https://doi.org/10.2118/113469-PA

Fortenberry, R., Kim, D. H., Nizamidin, N., Adkins, S., Arachchilage, G. W. P. P., Koh, H. S., Weerasooriya, U., Pope, G. A. (2015). *Use of Cosolvents to Improve Alkaline/Polymer Flooding. SPE Journal, 20(02), 255–266. https://doi.org/10.2118/166478-PA*

Golf-Racht, T. D. van. (1982). *Fundamentals of fractured reservoir engineering*. Amsterdam; New York: Elsevier.

Green, D. W., & Willhite, G. P. (2018). *Enhanced oil recovery* (Second edition). Richardson, Texas, USA: Society of Petroleum Engineers.

Gupta, R., & Mohanty, K. K. (2008). *Wettability Alteration of Fractured Carbonate Reservoirs*. Presented at the SPE Symposium on Improved Oil Recovery, Society of Petroleum Engineers. https://doi.org/10.2118/113407-MS

Hirasaki, G. J., van Domselaar, H. R., & Nelson, R. C. (1983). *Evaluation of the Salinity Gradient Concept in Surfactant Flooding*. Society of Petroleum Engineers Journal, 23(03), 486–500. https://doi.org/10.2118/8825-PA

Hirasaki, George J., Miller, C. A., & Puerto, M. (2008). *Recent Advances in Surfactant EOR*. Presented at the SPE Annual Technical Conference and Exhibition, Society of Petroleum Engineers. https://doi.org/10.2118/115386-MS

Huh, C. (1979*). Interfacial Tensions and Solubilizing Ability of a Microemulsion Phase that Coexists with Oil and Brine*. Journal of Colloid and Interface Science, 71(2), 408–426. https://doi.org/10.1016/0021-9797(79)90249-2

Xie, X., Weiss, W. W., Tong, Z., Morrow, N.R. (2005). *Improved Oil Recovery From Carbonate Reservoirs by Chemical Stimulation*. SPE Journal, 10.

Jackson, A.C. (2006). *Experimental Study of the Benefits of Sodium Carbonate on Surfactants for Enhanced Oil Recovery,* M.S. Thesis. Austin, TX: The University of Texas at Austin.

Jang, S. H., Liyanage, P. J., Tagavifar, M., Chang, L., Upamali, K. A. N., Lansakara-P, D., Seerasooriya, U., Pope, G. A. (2016). *A Systematic Method for Reducing Surfactant Retention to Extremely Low Levels*. Presented at the SPE Improved Oil Recovery Conference, Society of Petroleum Engineers. https://doi.org/10.2118/179685-MS

Jenning, H. Y. J. (1975). *A Study of Caustic Solution-Crude Oil Interfacial Tensions*. Society of Petroleum Engineers Journal, 15(03), 197–202. https://doi.org/10.2118/5049-PA

Jin, M. (1995). *A Study of Nonaqueous Phase Liquid Characterization and Surfactant Remediation*. PhD, Dissertation, The University of Texas at Austin

Kamath, J., Meyer, R. F., & Nakagawa, F. M. (2001). *Understanding Waterflood Residual Oil Saturation of Four Carbonate Rock Types*. Presented at the SPE Annual Technical Conference and Exhibition, Society of Petroleum Engineers. https://doi.org/10.2118/71505-MS

Karazincir, O., Thach, S., Wei, W., Prukop, G., Malik, T., & Dwarakanath, V. (2011). *Scale Formation Prevention During ASP Flooding*. Presented at the SPE International Symposium on Oilfield Chemistry, Society of Petroleum Engineers. https://doi.org/10.2118/141410-MS

Kasha, A., Al-Hashim, H., Abdallah, W., Taherian, R., & Sauerer, B. (2015). *Effect of Ca2+, Mg2+ and SO42− ions on the Zeta Potential of Calcite and Dolomite Particles Aged with Stearic Acid*. Colloids and Surfaces A: Physicochemical and Engineering Aspects, 482, 290–299. https://doi.org/10.1016/j.colsurfa.2015.05.043

Krumrine, P. H., Mayer, E. H., & Brock, G. F. (1985). *Scale Formation During Alkaline Flooding*. Journal of Petroleum Technology, 37(08), 1,466-1,474. https://doi.org/10.2118/12671-PA

Lake, L. W., Johns, R. T., Rossen, W. R., and Pope, G. A. (2014). *Fundamentals of enhanced oil recovery* (Second edition). Richardson, Texas: Society of Petroleum Engineers.

Levitt, D., & Bourrel, M. (2016). *Adsorption of EOR Chemicals Under Laboratory and Reservoir Conditions, Part III: Chemical Treatment Methods*. Presented at the SPE Improved Oil Recovery Conference, Society of Petroleum Engineers. https://doi.org/10.2118/179636-MS

Li, Y., Pope, G. A., Lu, J., Churchwell, L., Tagavifar, M., & Weerasooriya, U. P. (2017). *Scaling of Low-Interfacial-Tension Imbibition in Oil-Wet Carbonates*. SPE Journal. doi:10.2118/179684-PA

Lu, J., & Pope, G. A. (2017). *Optimization of Gravity-Stable Surfactant Flooding*. SPE Journal, 22(02), 480–493. https://doi.org/10.2118/174033-PA

Mejia, L. (2018). *Experimental Investigation of Low Interfacial Tension Displacements in Oil-wet, Fractured Micromodels*. M.S. Thesis. Austin, TX: The University of Texas at Austin.

Nelson, R. A. (2001) *Geologic Analysis of Naturally Fractured Reservoirs*. Elsevier.

Nelson, R. C., Lawson, J. B., Thigpen, D. R., & Stegemeier, G. L. (1984). *Cosurfactant-Enhanced Alkaline Flooding*. Presented at the SPE Enhanced Oil Recovery Symposium, Society of Petroleum Engineers. https://doi.org/10.2118/12672-MS

Nelson, R. C., & Pope, G. A. (1978). *Phase Relationships in Chemical Flooding*. Society of Petroleum Engineers Journal, 18(05), 325–338. https://doi.org/10.2118/6773-PA

Winsor, P. A., *Solvent Properties of Amphiphilic Compounds*. Butterworths Scientific Publications. London, 207 S. mit zahlr. Tabb. u. Abb. Preis £ 40.—. (1956). *Fette, Seifen, Anstrichmittel*, *58*(12), 1103–1104. https://doi.org/10.1002/lipi.19560581222

Parra Perez, J. E. (2016). *Experimental investigation of viscous forces during surfactant flooding of fractured carbonate cores,* M.S. Thesis. Austin, TX: The University of Texas at Austin.

Peters, E. J. (2012). *Advanced petrophysics* (1st ed). Austin, TX: Live Oak Book Company.

Pinnawala Arachchilage, G. W. P., Spilker, K. K., Tao, E. B., Alexis, D., Linnemeyer, H., Kim, D. H., Taimur, M., Dwarakanath, V. (2018). Evaluating the Effect of Temperature on Surfactant Phase Behavior and Aqueous Stability to Forecast Optimum Salinity at High Temperature. In *SPE Improved Oil Recovery Conference*. Tulsa, Oklahoma, USA: Society of Petroleum Engineers. https://doi.org/10.2118/190249-MS

Pope, G. A., Wang, B., & Tsaur, K. (1979). *A Sensitivity Study of Micellar/Polymer Flooding*. Society of Petroleum Engineers Journal, *19*(06), 357–368. https://doi.org/10.2118/7079-PA

Pope, G. A., Wu, W., Narayanaswamy, G., Delshad, M., Sharma, M. M., & Wang, P. (2000). *Modeling Relative Permeability Effects in Gas-Condensate Reservoirs With a New Trapping Model*. SPE Reservoir Evaluation & Engineering, *3*(02), 171–178. https://doi.org/10.2118/62497-PA

Roehl, P. O., & Choquette, P. W. (Eds.). (1985). *Carbonate petroleum reservoirs*. New York: Springer-Verlag.

Sagi, A. R., Puerto, M. C., Bian, Y., Miller, C. A., Hirasaki, G. J., Salehi, M., Thomas, C. P., Kwan, J. T. (2013). *Laboratory Studies for Surfactant Flood in Low-Temperature, Low-Salinity Fractured Carbonate Reservoir*. Presented at the SPE International Symposium on Oilfield Chemistry, Society of Petroleum Engineers. https://doi.org/10.2118/164062-MS

Sanaei, A., Delshad, M., & Sepehrnoori, K. (2018). *Study of Scale Formation During ASP Pilot in a Middle Eastern Carbonate Reservoir.* In SPE Improved Oil Recovery Conference. Tulsa, Oklahoma, USA: Society of Petroleum Engineers. https://doi.org/10.2118/190169-MS

Seethepalli, A., Adibhatla, B., & Mohanty, K. K. (2004). *Physicochemical Interactions During Surfactant Flooding of Fractured Carbonate Reservoirs*. SPE Journal, 9(04), 411–418. https://doi.org/10.2118/89423-PA

Shah, D. O., Schechter, R. S., & American Institute of Chemical Engineers (Eds.). (1977). *Improved oil recovery by surfactant and polymer flooding*. New York: Academic Press.

Solairaj, S., Britton, C., Kim, D. H., Weerasooriya, U., & Pope, G. A. (2012). *Measurement and Analysis of Surfactant Retention*. Presented at the SPE Improved Oil Recovery Symposium, Society of Petroleum Engineers. https://doi.org/10.2118/154247-MS

Sondi, I., Bišćan, J., Vdović, N., & Škapin, S. D. (2009). *The electrokinetic properties of carbonates in aqueous media revisited*. Colloids and Surfaces A: Physicochemical and Engineering Aspects, 342(1), 84–91. https://doi.org/10.1016/j.colsurfa.2009.04.012

Standnes, D. C., & Austad, T. (2000). *Wettability alteration in chalk: 2. Mechanism for wettability alteration from oil-wet to water-wet using surfactants*. Journal of Petroleum Science and Engineering, 28(3), 123–143. https://doi.org/10.1016/S0920-4105(00)00084-X

Standnes, D. C., Nogaret, L. A. D., Chen, H.-L., & Austad, T. (2002). *An Evaluation of Spontaneous Imbibition of Water into Oil-Wet Carbonate Reservoir Cores Using a Nonionic and a Cationic Surfactant*. Energy & Fuels, 16(6), 1557–1564. https://doi.org/10.1021/ef0201127

Statistics | World - Total Primary Energy Supply (TPES) by source. Retrieved September 2, 2018, from https://www.iea.org/statistics/?country=WORLD&year=2015&category=Key%20indicators&indicator=TPESbySource&mode=chart&categoryBrowse=false

Stegemeier, G. L. (1977). *MECHANISMS OF ENTRAPMENT AND MOBILIZATION OF OIL IN POROUS MEDIA*. In Improved Oil Recovery by Surfactant and Polymer Flooding (pp. 55–91). Elsevier. https://doi.org/10.1016/B978-0-12-641750-0.50007-4

Tagavifar, M., Herath, S., Weerasooriya, U. P., Sepehrnoori, K., & Pope, G. (2016). *Measurement of Microemulsion Viscosity and Its Implications for Chemical EOR*. Presented at the SPE Improved Oil Recovery Conference, Society of Petroleum Engineers. https://doi.org/10.2118/179672-MS

Tagavifar, M., Sharma, H., Wang, D., Jang, S. H., & Pope, G. (2018). *Alkaline/Surfactant/Polymer Flooding With Sodium Hydroxide in Indiana Limestone: Analysis of Water/Rock Interactions and Surfactant Adsorption*. SPE Journal. https://doi.org/10.2118/191146-PA

Upamali, K., Liyanage, P. J., Cai, J., Lu, J., Jang, S. H., Weerasooriya, U. P., & Pope, G. A. (2018). *New Surfactants and Co-Solvents Increase Oil Recovery and Reduce Cost*. In SPE Journal. Tulsa, Oklahoma, USA: Society of Petroleum Engineers. https://doi.org/ 10.2118/179702-PA

Walker, D., Britton, C., Kim, D. H., Dufour, S., Weerasooriya, U., & Pope, G. A. (2012). *The Impact of Microemulsion Viscosity on Oil Recovery*. Presented at the SPE Improved Oil Recovery Symposium, Society of Petroleum Engineers. https://doi.org/10.2118/154275-MS

Walsh, M. P., & Lake, L. W. (2003). *A generalized approach to primary hydrocarbon recovery* (1st ed). Amsterdam; Boston: Elsevier.

World Bank. (2016). *Monitoring Global Poverty: Report of the Commission on Global Poverty*. The World Bank. https://doi.org/10.1596/978-1-4648-0961-3

World Population Prospects: The 2017 Revision | Multimedia Library - United Nations Department of Economic and Social Affairs. Retrieved September 2, 2018, from https://www.un.org/development/desa/publications/world-population-prospects-the-2017-revision.html

Zapata, V. J., & Lake, L. W. (1981). *A Theoretical Analysis of Viscous Crossflow*. Presented at the SPE Annual Technical Conference and Exhibition, Society of Petroleum Engineers. https://doi.org/10.2118/10111-MS

Zeltner, W. A., & Anderson, M. A. (1988). *Surface charge development at the goethite/aqueous solution interface: effects of CO2 adsorption*. Langmuir, 4(2), 469–474. https://doi.org/10.1021/la00080a039

Zhang, R., & Somasundaran, P. (2006*). Advances in adsorption of surfactants and their mixtures at solid/solution interfaces*. *Advances in Colloid and Interface Science*, *123–126*, 213–229. https://doi.org/10.1016/j.cis.2006.07.004